Premotor and Motor Cortex and Visually Guided Grasp

A Methodological and Experimental Study of Local Field Potentials in the Cortex of the Awake, Behaving Macaque Monkey.

Rachel Lucy Spinks

Institute of Neurology
University College, London

Submitted for PhD
March 2005

Supervisor: Professor R.N. Lemon

ProQuest LLC
789 East Eisenhower Parkway
P.O. Box 1346
Ann Arbor, MI 48106-1346

Abstract

When we reach for and grasp an object, we must transport our hand to the correct location, shape it appropriately and subsequently grasp the object with an appropriate amount of force. This involves a complex series of neuronal computations to process the visual properties of the object, generate a desired action, and to finally relay instructions to the musculature of the hand and arm to execute the action. The premotor and primary motor cortices constitute an important part of this pathway.

In the macaque monkey, the premotor cortex (F5) is known to receive visual and visuomotor information concerning the properties of graspable objects from the anterior intraparietal region (AIP). A strong reciprocal connection links F5 to the primary motor cortex (M1), from which the major descending output to the hand and arm muscles originates. This thesis is a study of local field potentials recorded in M1 and F5 during the performance of a reach to grasp task in the macaque monkey, and investigates their relationship to the task and to each other during two phases of the task; the observation of the object to be grasped, and the execution of the grasp.

This study required the development of sophisticated techniques for the accurate localisation of recordings and for chronic recordings to be made with multiple electrodes in the two different cortical areas simultaneously. The use of MRI to aid localisation, and the use of an antimitotic solution that retards dural growth and thus allows long term multielectrode recordings are also described and validated.

Contents

List of Figures

Abbreviations

5FU - 5-Fluorouracil

ADL - Antidromic Latency

AIP - Anterior Intraparietal Area

CM - Corticomotoneuronal

CMA - Cingulate Motor Area

CST - Corticospinal Tract

ED - Euclidean Distance

EEG - Electroencephalogram

EMG - Electromyogram

ERD - Event Related Desynchronisation

ERS - Event Related Synchronisation

F5 - Rostral Ventral Premotor Cortex

HAPEX - Hydroxyapatite Polyethylene

HPR - Home Pad Release

ICMS - Intracortical Microstimulation

LFP - Local Field Potential

LIP - Lateral Intraparietal Area

M1 - Primary Motor Cortex

MEG - Magnetoencephalogram

MIP - Medial Intraparietal Area

MRI - Magnetic Resonance Imaging

PRR - Parietal Reach Region

PT - Pyramidal Tract

PTN - Pyramidal Tract Neuron

SD - Standard Deviation

SE - Standard Error

SMA - Supplementary Motor Cortex

VIP - Ventral Intraparietal Area

Declaration of Conjoint Work

The work to be presented in this thesis is my own original work completed without assistance, apart from the following:

1. Critical stages of surgical procedures were performed by Prof. R.N.Lemon.
2. The experimental work was performed in collaboration with Prof. R.N.Lemon and members of his research group, both academic and technical.
3. Some of the data analysed in Chapter 3 (monkey M24) was collected during a previous experiment by Prof. R.N.Lemon and the members of his team.
4. Assistance with software programming was received from Drs A. Jackson and T. Brochier.
5. MRIs were aquired with the assistance of Mr. D. MacManus, NMR Group, ION.
6. Post-mortem histology was performed by Mr. J. Dick, Sobell Department, ION.

Acknowlegements

I would like to acknowledge and thank the following people for their assistance and friendship over the last 6 years, without whom this thesis would not have been possible. Firstly, Professor Roger Lemon, who has always supported, advised, and taught me with great knowledge, kindness, enthusiasm and belief that I would get there in the end.

All members of the Lemon lab have contributed their time and skills generously, and have made work a great place to be. Expert technical help from Sam Shepherd, Helen Lewis, and Nora Philbin was invaluable, as was the support and assistance from Dr. Stuart Baker, Dr. Alessandra Umilta, Prof. Daniel Wolpert, Gita Prabhu, and Ben Townsend. Special mention and thanks must go to Dr. Thomas Brochier for continual support on a long project and to Dr. Andrew Jackson for never ending help, friendship and patience, even after moving 3000 miles away.

I would also like to thank the many people in the Sobell Department who have made this possible with their time and help – Dr. Chris Seers, Debbie Hadley, Julie Savvides, Kully Sunner, Ed Bye and Victor Baller. Gratitude is also due to David MacManus and Dr. Robin Richards for their collaborations and suggestions.

Finally, I would like to pay tribute to those who have supported me in so many other ways – my parents, John and Sylvia Spinks who always encouraged me to follow my dreams, my sister Katherine (the first, but hopefully not the last, Dr. Spinks), my friends, and lastly my husband James Reynolds for his love, patience, support, laundry service and always being there for me. Thank you.

Chapter 1. Introduction

1.1 Visuomotor Co-ordination

Humans move under continuous sensory guidance. The motor behaviour of primates has become increasingly dominated by vision (Passingham, 1982). When we wish to make skilled hand movements to achieve a specific, desired outcome, for example, to grasp a cup of tea or a pen, we must firstly know and comprehend where the object is located. This requires the visual system to see, locate and identify the object. To act on it, we must either move our arm, or possibly even our whole body to an appropriate location so that the hand can be transported to the object. In this way, initial visual stimuli lead us to move in order to perform all sorts of everyday actions.

Most skilled hand movements require this type of visual input, and therefore need a large degree of visuomotor co-ordination. Even after the hand reaching movement has been initiated correctly towards the location of the object, there are still many factors to be taken into account. To grasp an object accurately, the object's physical properties such as the size, orientation, surface texture, likely weight etc. must be observed and encoded such that the hand is pre-shaped and the arm stabilised appropriately before contact is even made with the object. This is all achieved under visual guidance. In this example, until contact with the object is made, visual information and past experience of grasping similar objects are all that we have to base our action upon. Once the visuomotor transformations have taken place for an accurate reach and grasp, proprioceptive and tactile feedback can assist in the action, but up to that point, the control of reaching and grasping are purely visuomotor.

Feedback on the success of the action allows us to improve our performance on the next occasion that a similar action is required. Visual and proprioceptive feedback are used to update internal inverse models that allow feed-forward planning and control of movements (Kawato *et al.*, 1987; Wolpert *et al.*, 1995).

The co-ordination between the visual and motor systems is thus crucial for prehension; co-ordination between different parts of the motor system is also important. A carefully synchronised action of many muscles and joints, occurring in a very short time frame, is required to orientate the arm and wrist correctly for succesful reaching, to shape the fingers for the upcoming grasp, and to provide stability to the more proximal arm and trunk muscles. This is a complex process, involving multiple areas of the brain's motor network in a highly co-ordinated fashion, to bring about the desired action.

1.2 Action and Perception

When we see a familiar object in our environment, not only do we know where it is, we also immediately know what it is, and what interest it may be to us. This visual perception of an object enables us to make a decision about whether we wish to act upon it. In this way, the visual input provides information on both 'what' and 'where' an object is. The visual processing may be linked to a motor output, or it may not, depending on the percept.

It has long been hypothesised (Ungerleider & Mishkin, 1982) that the 'what' and the 'where' functions of visual processing are effectively mapped onto diverging streams of output from the visual cortex; the 'what' stream (which carries information on visual attributes such as the size, shape, orientation, colour of an object) moving ventrally to the inferotemporal cortex and the 'where' stream (carrying location information)

progressing dorsally to the posterior parietal cortex. In this schema, the ventral and dorsal streams are essentially separate. More recent work has suggested that the dorsal stream and the ventral stream interconnect and both have an important influence on visuomotor control (Boussaoud *et al.*, 1990), suggesting that the two streams are not as separate as first thought. An alternative classification of the two streams was therefore put forward by in a series of papers (summarised in Milner & Goodale, 1995), suggesting that instead of simply 'where' and 'what', the dorsal and ventral streams instead correspond to perceptual representation and visuomotor control, that is to say that they process incoming visual information in a parallel fashion for different purposes. This places more emphasis on the output of the two streams, rather than on the inputs to them. For visuomotor control (the dorsal stream) this means that not only is the visual location of the object encoded, but also the beginnings of the motor output that is needed to act upon it.

The projection from the visual cortex to the posterior parietal cortex is only the beginning of the pathway that causes a visual stimulus to lead to a specific motor output, and represents the first of several transformations that underpins the visuomotor coordination system we need to reach for and grasp an object.

1.3 Anatomical Substrates for Hand Movements under Visual Control

There are three main contributors to the brain motor network: the cerebral neocortex, the basal ganglia and the cerebellum. Visuomotor control predominantly involves multiple cortico-cortical loops and a cortico-cerebellar pathway.

The cerebral motor cortex is located in the frontal part of the brain, anterior to the central sulcus, and is defined as the agranular region of the frontal lobe. It contains anatomically

and functionally distinct sub-divisions, such as the primary motor cortex (M1), the premotor cortex (PM), and the supplementary motor area (SMA). Other cortical areas involved include the posterior parietal cortex, in particular the anterior intraparietal area (AIP), but also the ventral intra parietal area (VIP). The main sub-cortical parts of the motor system are the cerebellum and the basal ganglia. The brain's output to the musculature of the hand and arm is via descending motor pathways which contain both direct and indirect projections to the hand motorneurones, located in the cervical enlagement (C7 to Th1).

1.3.1 Cortical Structures and Connections Involved in Visuomotor Control

In early experiments designed to elucidate pathways for visuomotor control of the hand, it was demonstrated that split brain monkeys were able to reach successfully for objects, but were then unable to shape the hand appropriately unless vision was available to the hemisphere contralateral to the hand (Brinkman & Kuypers, 1972; Brinkman & Kuypers, 1973). This suggested that visual to motor transformations are conducted via intra-hemispheric projections. It was later shown by Moll & Kuypers (1977) that damage to parieto-frontal connections in monkeys caused lasting apraxia-like deficits of visually guided grasping movements, demonstrating the importance of these projections. Since these early lesion studies, the circuits involved in visuomotor grasp have been studied extensively.

The main areas which are involved are shown in Figure 1.1, (figure and legend taken from the review by Rizzolatti *et al.* in 1998). This shows the anatomy and body part representations present in the frontal motor areas and the parietal cortex (including the unfolded intraparietal areas) that are involved in visuomotor control. The sections below detail the cortico-cortical connections to the different subdivisions of the parietal and

frontal motor areas. For reasons of space, I have not included the major thalamic projections to all these areas which convey important pallidal and cerebellar inputs to them.

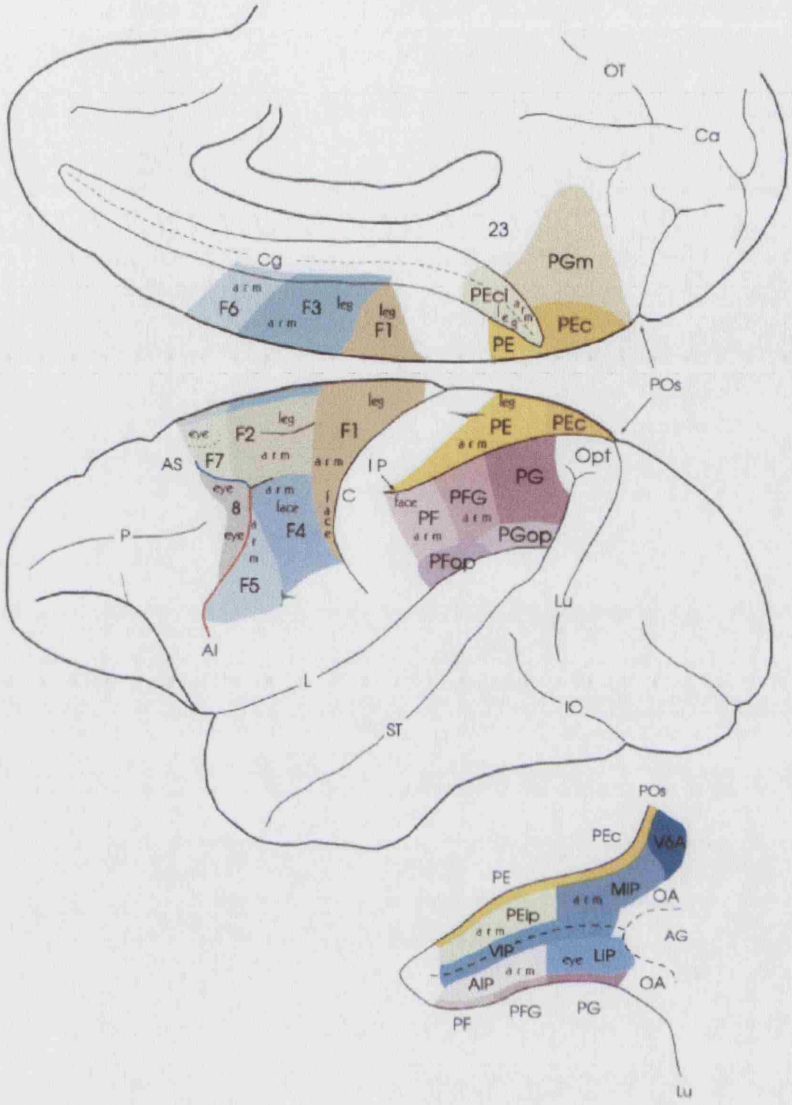

Figure 1.1 Mesial and lateral views of the macaque brain showing the cytoarchitectonic parcellation of the agranular frontal cortex and of the posterior parietal cortex. Motor areas are defined according to Matelli et al. (1985, 1991). All parietal areas except those buried within the intraparietal sulcus are defined according to Pandya & Seltzer, 1982. The areas located within the intraparietal sulcus (IP) are defined according to physiological data and are shown in an unfolded view of the sulcus in the lowest part of the figure. On the basis of the available data, the various body-parts representations are reported. In the prefrontal cortex the frontal eye field (FEF) is also defined according to physiological criteria. The superior arcuate sulcus (AS), the inferior arcuate sulcus (AI) and the inferior precentral dimple are drawn in blue, red and green, respectively. AG, annectant gyrus; C, central sulcus; Ca, calcarine fissure; Cg, cingulate sulcus; IO, inferior occipital sulcus; L, lateral fissure; Lu, lunate sulcus; OT, occipitotemporal sulcus; P, principal sulcus; POs, parieto-occipital sulcus; ST, superior temporal sulcus.

1.3.2 Posterior Parietal Cortex.

In the macaque monkey, the posterior parietal cortex is formed by two lobules, the superior and the inferior parietal lobules. It contains multiple arm, leg and face representations, and both lobules receive somatosensory and visual inputs. In the intraparietal sulcus between the two lobules, there are four areas that can be identified – these are the lateral, medial, ventral and anterior intraparietal areas (known as LIP, MIP, VIP and AIP respectively). On the surface of the superior parietal lobule is area PE, and on the convexity of the lower parietal lobule is area PF. These areas contribute to various parieto-frontal circuits which make up the basic elements of the cortical motor system (fully reviewed by Rizzolatti *et al.*, 1998).

1.3.1.1.1 Anterior Intraparietal Area

The anterior intraparietal area (AIP) receives input projections from the visual cortex via several higher processing visual areas, such as the parieto-occipital area and the middle temporal area (MT) as well as from lower visual cortical areas such as visual area 3A. Neurons in AIP show selective activation to a wide variety of stimuli, both motor and visual, in particular visually guided hand manipulation tasks. In one study, Sakata *et al.* (1995) used a task that involved either object grasp or object fixation in the light or dark to elucidate the properties of the neurons (using an apparatus very similar to that used for experiments described later in this thesis). They found that AIP neurons could be purely motor, purely visual or visuomotor in their response. When cells showed visual and motor proporties, these properties matched, suggesting that these neurons play an important role in matching the pattern of hand movement to the visuo-spatial characteristics of the object to be manipulated. In a later study, the same group reported that the visual reponses of the neurons could be selective also for the shape, size and

orientation of the objects to be grasped, as well as selective for the shape of the grasp and hand orientation, suggesting that the dorsal pathway via AIP is concerned with the aspects of object form that are relevant to the visual control of movement (Murata *et al.*, 2000). They were not concerned with the position of the object in space (Taira *et al.*, 1990) showing that the cells are concerned with hand and finger movements and not more proximal reaching movements.

Anatomical studies have shown that AIP has a strong reciprocal connection with the ventral premotor area, F5, in particular the anterior bank (Matelli *et al.*, 1986; Luppino *et al.*, 1999). This functional loop will be discussed later.

1.3.1.1.2 Medial Intraparietal Area

In area MIP, neurons respond to both visual and somatosensory stimuli (Colby & Duhamel, 1991). It is part of the parietal reach region (PRR, which also incorporates area V6A) that has been shown to encode parameters of an intended movement (Snyder *et al.*, 1997) and more specifically, to specify the target location for an upcoming reaching movement (Batista & Andersen, 2001) and it does this predominantly in eye centred co-ordinates (Batista *et al.*, 1999). It is therefore different to area AIP with respect to the reach-to-grasp movement: it mostly represents the reach, rather than the grasp, and is predominantly active during instructed delay periods of the task. It has rich connections with other parietal areas, including a reciprocal connection to V6A (Caminiti *et al.*, 1999) and to VIP (Lewis & Van Essen, 2000). Frontally, it projects to the ventrorostral part of frontal motor area, F2 (Matelli *et al.*, 1998; Caminiti *et al.*, 1999). This MIP-F2 circuit is thought to use somatosensory and visual information for planning and controlling arm movements (Rizzolatti *et al.*, 1998).

1.3.1.1.3 Ventral Intraparietal Area

This area is in the fundus of the intraparietal sulcus. Neurons in VIP are either purely visual, or visual and tactile - the visual neurons are often selective for stimuli moving in a preferred direction, or for a location that is a particular distance from the face (Colby *et al.*, 1993), and the bimodal neurons tend to have visual and tactile receptive fields that correspond with one another (Bremmer *et al.*, 1997). VIP receives inputs from visual areas such as MT and MST (Bremmer *et al.*, 2002; Boussaoud *et al.*, 1990) and from somatosensory areas PEc and PFG (Seltzer & Pandya, 1986). It projects to area F4 in the frontal motor cortex (Matelli *et al.*, 1994). It is likely that the function of this loop is to encode the peripersonal space and to therefore transform the location of an object into an appropriate reaching movement towards that location (Rizzolatti *et al.*, 1998).

1.3.1.1.4 Area PE

Area PE is located in the superior parietal lobule and is usually considered as a higher order somatosensory area which is mostly concerned with proprioceptive information. It does not receive visual inputs (Caminiti *et al.*, 1996), and many of its neurons encode arm location in body-centred co-ordinates (Lacquaniti *et al.*, 1995). It is not therefore strictly part of the visuomotor grasp process. It is connected to the primary motor area, M1 and it is thought that this circuit is involved in skeletomotor transformations which provide M1 with information on the position of body parts that is needed for controlling their movements (Rizzolatti *et al.*, 1998).

1.3.2 Frontal Motor Areas

At the light microscope level, the motor areas of the frontal lobe these areas appear to lack a granular layer IV. The region is bounded caudally by the central sulcus and

rostrally by the arcuate sulcus. Originally, the area was simply divided into two cytoarchitectonic regions by Brodmann, areas 4 and 6, but this has subsequently been revised repeatedly, and it is now accepted that there are at least 7 subdivisions. These are distinct from one another when examined microscopically and have different interconnections and functions. There are thought to be several premotor areas, instead of the one classical premotor area that was originally thought (Dum & Strick, 2002), including the dorsal and ventral premotor cortices (labelled and subdivided as F2/F7 and F4/F5, respectively in Fig. 1.1), and the dorsal, rostral and ventral cingulate motor areas found below the supplementary motor area (SMA, or F3 in Fig. 1.1) and pre-SMA (F6). The classical primary motor cortex, usually called M1, is labelled as F1 in Fig. 1.1.

The nomenclature that will be used in this thesis is predominantly as redefined by Matelli *et al.* (1985, 1991). The most commonly used exception will be M1 for the primary motor area; otherwise, usage will be F5 for the rostral ventral premotor cortex, F4 for the dorsal part of the ventral premotor cortex and F2 for the dorsal premotor cortex (Luppino & Rizzolatti, 2000).

1.3.1.2.1 F2 – Dorsal Premotor Cortex

Area F2 (the dorsal premotor cortex) contains somatotopic representations of leg and arm movements (Kurata, 1989; Dum & Strick, 1991; He *et al.*, 1993; Godschalk *et al.*, 1995). Neurons recorded in F2 show complex properties – they encode attributes of intended reaching movements such as direction during an instructed delay period in a reaching task (Crammond & Kalaska, 1994; Crammond & Kalaska, 1996). Motor responses are much greater in a visually guided reach than in a memory guided one (Mushiake *et al.*, 1991) suggesting a role in the planning of visuomotor reaching tasks.

There is some evidence of representation of distal arm movements (He *et al.*, 1993; Dum & Strick, 2005) but not specifically of hand movements. There is a strong projection to and from the parietal cortex, principally to area MIP, and also to PEc and PEip. As has already been described, area MIP is part of the parietal reach region and represents both visual and somatosensory information. This loop is thought to utilise somatosensory and visual information to plan, and control arm movements, such as the reach, by monitoring and controlling hand position during the transport phase of a reach-to-grasp, when the hand is moving towards its target (Rizzolatti *et al.*, 1998). F2 has a strong reciprocal connection with F5 (Dum & Strick, 2005) and also projects to the spinal cord directly, to both upper and lower cervical segments (Dum & Strick, 2002), allowing it to modulate reaching both by direct influence on the spinal mechanisms and via its interconnections with other motor areas.

1.3.1.2.2 F3 – Supplementary Motor Area

Area F3 is a subdivision of the traditionally described supplementary motor area and is also known as 'SMA proper'. F3 is located in the caudal part of SMA, on the mesial surface of the frontal lobe. Neurons in F3 respond to mostly to somatosensory rather than visual stimuli, and mostly to active movements (Rizzolatti *et al.*, 1996; Tanji & Shima, 1994). They are often responsive to a sequence of multiple movements performed in a particular order, that is to say, when there is temporal organisation (Tanji & Shima, 1994; 1996). There are also neurons that discharge specifically for the interval between movements in a sequence (Shima & Tanji, 2000). Neuronal responses to actions involving multiple joint articulations are often observed, most usually those involving the forelimb (Luppino *et al.*, 1991). F3 receives its major input from area PEci, a parietal area in the cingulate sulcus which contains a complete somatosensory

map of the body (Murray & Coulter, 1981) and contains neurons which, although usually insensitive to visual stimuli, play a role in interactions between gaze angle and hand position (Ferraina *et al.*, 1997). It is suggested that the parietofrontal circuit involving F3 and PEci controls motor activity in a global way, perhaps with a role in postural adjustments needed for movements (Rizzolatti *et al.*, 1998).

1.3.1.2.3 F4 – Ventral Premotor Cortex (Dorsal)

Area F4, the dorsal sector of the ventral premotor cortex is particularly connected with area VIP. As previously stated, the function of this loop is to encode the peripersonal space and to transform the location of an object into an appropriate reaching movement towards that location (Rizzolatti *et al.*, 1998). The area was extensively studied by Fogassi *et al.* in 1996. They found that neurons in F4 were either unimodal (either somatosensory or very occasionally visual) or bimodal (both) in their responses to sensory stimuli. They had receptive fields that were located in peripersonal space, and in most cases the visually reponsive neurons discharged preferentially to stimuli directed towards the tactile receptive field, and these receptive fields are predominantly encoded in body-centred co-ordinates (Graziano *et al.*, 1994). Neurons show somatotopical organisation - the axio-proximal movements are represented caudally, the distal movements are represented near the arcuate sulcus, the mouth field is located laterally, and the hand field medially (Gentilucci *et al.*, 1988). Microstimulation in F4 produces predominantly proximal movements (Gentilucci *et al.*, 1989). F4 is also connected strongly with F3 (Luppino *et al.*, 1993) and to M1. This, combined with the reciprocal connection to area VIP, suggests that F4 is mostly involved with the production of reaching movements.

1.3.1.2.4 F5 – Ventral Premotor Cortex (Rostral)

Area F5 has many connections, in particular to AIP, and to M1. It is sometimes subdivided into two sectors, the anterior bank area and the convexity, and it is with the anterior bank that the majority of AIP connections are made (Matelli *et al.*, 1994). Microstimulation of F5 can evoke hand, digit and mouth movements, showing that it contains representations of these hand and mouth movements (Rizzolatti *et al.*, 1988; Hepp-Reymond *et al.*, 1994). Studies of neurons in F5 have shown that it appears to have a dual role. Most neurons fire predominantly in relation to goal directed hand movements, such as grasping, holding, tearing etc., but many may also respond to visual stimuli. Grasping neurons are the most common of the different 'motor' neurons, and many are further classifiable by the type of grasp, i.e. precision grip, whole hand prehension, finger prehension, etc. However, the visual stimuli that they respond to are of two kinds – some neurons, especially those located in the anterior bank, respond to the visual presentation of graspable objects, when the prehension of the object would require a grasp of the type encoded by that neuron. These neurons have been designated as 'canonical' neurons. Other neurons, located on the convexity of the precentral cortex close to the arcuate sulcus, respond when the monkey observes hand actions performed by another individual, when the action matches the motor behaviour encoded by the neuron. These remarkable neurons have been designated as 'mirror' neurons, and these have been the subject of intense further research in both monkeys and humans (Arbib *et al.*, 2000; Kohler *et al.*, 2002; Grezes *et al.*, 2003; Ferrari *et al.*, 2003; Rizzolatti & Craighero, 2004).

The coding of co-ordinated actions by F5 neurons, rather than simple individual movements has led to the suggestion that F5 may store motor schema, or a 'vocabulary' of motor behaviours (Rizzolatti & Gentilucci, 1988).

1.3.1.2.4.1 Canonical Neurons

The behaviour of the canonical neurons suggests that F5 plays a crucial role in the visuomotor transformations neccesary for the successful grasp of objects. Reversible inactivation studies have confirmed this, by demonstrating that after an injection of muscimol into the anterior bank of F5, monkeys showed deficits in the preshaping of the hand during the reach of a reach-to-grasp task (Fogassi *et al.*, 2001) and were only able to shape the hand appropriately after contact with the object was made and tactile input could be used. The anterior bank has the strongest connection with AIP, and when AIP was inactivated, again, the major deficit was in hand preshaping (Gallese *et al.*, 1994). The reaching component of the task was accomplished succesfully, suggesting that the circuit provides the monkey with the capacity to extract the 3D properties of an object and to transform them into an appropriate hand shape to grasp it.

1.3.1.2.4.1 Mirror Neurons

Mirror neurons were first described in 1996 by Gallese *et al.*, and show very similar motor properties to the canonical neurons, but have the ability to encode goal directed actions performed by another individual. The visual presentation of an object is not sufficient. The actions that are encoded are most commonly grasping, placing and manipulating objects, and some neurons are highly specific in their responses. More recently, mirror neurons have been shown to not only respond to the observation of an action, but also to the sound of certain congruent actions, such as the breaking of a

peanut shell (Kohler *et al.*, 2002). They have also been shown not to require full vision of the action, that is they respond even when the final part of an action (when the hand grasps or places the object) is hidden (Umilta *et al.*, 2001). Mouth mirror neurons have been described which discharge in resonse to the observation of mouth movements by an experimenter (Ferrari *et al.*, 2003), showing that the vocabulary of actions represented in F5 is large and not restricted to the hand.

The interpretation of the mirror neuron results has been that their discharge generates an internal representation of the external action, whether seen, heard or inferred. This representation is believed to be used for two main purposes – action understanding, and action imitation. The imitation function is poorly developed in monkeys and it is subject to debate whether monkeys can imitate actions at all, but in humans it is highly evolved. It is the action recognition function that has generated most interest. Having a representation of an action that is accessed when a similar action is observed allows us to interpret and give meaning to the actions of others. Interpretations of the mirror neuron system have gone as far as to suggest that it could form the basis for the experiential understanding of the actions of others and thus underly many aspects of social cognition in humans (Gallese *et al.*, 2004).

F5 receives input from part of the parietal reach region, area V6A (Caminiti *et al.*, 1999). It also has a rich anatomical connection with area AIP (Matelli *et al.*, 1994). Both areas contain a representation of distal arm movements, and respond to the presentation of 3D objects. Inactivation of either area leads to disruption of the monkey's ability to correctly transform object characteristics into an appropriate grasp, whilst leaving the reaching movement unaffected (Gallese *et al.*, 1994; Fogassi *et al.*, 2001). It is therefore thought that the AIP-F5 circuit plays a crucial role in the

transformation of object properties into appropriate hand movements (Jeannerod *et al.*, 1995).

In the macaque monkey, F5 has corticospinal projections to the midcervical levels of the spinal cord but not to the low cervical motor nuclei that innervate hand and finger muscles (He *et al.*, 1993). It has a major output to the primary motor area, M1 (Dum & Strick, 1991; Dum & Strick, 2002; Dum & Strick, 2005). It is possible therefore that its influence on distal movements is mediated via the M1 projection, rather than directly (Cerri *et al.*, 2003; Shimazu *et al.*, 2004).

1.3.1.2.5 M1 – Primary Motor Cortex

The primary motor cortex is the largest of the motor areas, and it is also possibly the most richly connected. It is characterised by containing large numbers of pyramidal neurons in an expanded layer V, including the giant pyramidal cells (Betz cells), whose axons project to a large variety of subcortical structures. The sub-cortical projections from M1 all arise from layer V and VI, including the axons of the corticospinal tract. It is estimated that 10-20% of M1 pyramidal cells axons project to the spinal cord (Porter & Lemon, 1993). All of their axons pass through the medullary pyramidal tract from which they can be identified as pyramidal tract neurons (PTNs). The corticospinal tract (CST) represents the largest descending motor pathway in the primate brain.

M1 receives inputs from multiple cortical areas, both frontal and parietal, as well as from subcortical structures via the thalamus. Microstimulation of M1 has shown that M1 has a complex organisation. This organisation was originally thought to be a rather strict somatotopic map of motor outputs It is now considered that whilst there is strict mapping of body parts (area maps of leg, arm, face), the intra-areal mapping is much

more complex, with considerable intermingling of different limb parts (e.g. digits, wrist, elbow, etc.) (Penfield & Rasmussen, 1952; Andersen *et al.*, 1975; Donoghue *et al.*, 1992; Lemon, 1988; Schieber, 2001).

Neurons in M1 respond to a wide range of somatosensory and kinaesthetic stimuli and especially passive and active joint motion (Fetz *et al.*, 1980; Porter & Lemon, 1993). Visual stimulation also produces responses in a small proportion of neurons (Wannier *et al.*, 1989).

Early work showed that M1 neuronal discharge correlated with muscle force in a simple wrist extension-flexion task (Evarts, 1968). Later work showed that the activity of populations of M1 neurons could encode the direction of a centre-out reaching task (Georgopoulos *et al.*, 1982), and that this activity could also encode a combination of both force and direction in a similar task (Kalaska *et al.*, 1989). Posture and the geometry of reaching movements also influence the discharge of some M1 neurons (Scott & Kalaska, 1997). M1 is clearly highly modulated by reaching movements and its physical parameters, and many of its properties have been described as 'muscle-like', reflecting its executive motor function (Todorov, 2000).

The precision grip task has also been used extensively to study M1 neurons (Muir & Lemon, 1983; Bennett & Lemon, 1996; Baker *et al.*, 2001; Baker *et al.*, 2003). Neurons often modulate their discharge during the task, showing higher firing rates whilst squeezing the levers than than during the maintenance of a steady hold, i.e. during the dynamic phase of the task rather than the static (Smith *et al.*, 1975; Baker *et al.*, 2001). Neuronal discharge varies with the force required for the precision grip, as well as the rate of change of force. The force-firing rate relationship is not invariant and is modulated by context (Hepp-Reymond *et al.*, 1999). In a visually cued reach-to-grasp

task, the discharge of M1 neurons was highly modulated during the reach and grasp, and was highly dependent on the object grasped (Mason *et al.*, 2002).

From the parietal cortex, the major input is from area PE (Brodmanns area 5) (Fig.1.1), which is a higher order somatosensory area which is mostly concerned with the analysis of proprioceptive information, and can encode the position of the arm in space (Lacquaniti *et al.*, 1995). This connection is thought to provide M1 with information on the location of the body parts necessary for the control of limbs (Rizzolatti *et al.*, 1998) and as such contributes to the postures needed for grasp. The parietal projection from PE does not contain visual information.

M1 receives input from at least six of the premotor areas (Dum & Strick, 2002) and also the cingulate motor areas (Dum & Strick, 2005). These include F2, F3, F4 and F5. Visuomotor information mostly reaches M1 via these connections rather than directly (Pandya & Kuypers, 1969), suggesting that the higher order processing has already been performed by the premotor areas, before information reaches M1. The densest projections from the premotor cortex to M1 arise from F2 (PMd) and F5 (PMv, Ghosh *et al.*, 1987; Dum & Strick, 2005). The connection to F5 is reciprocal (Dum & Strick, 2005). These main interconnections are shown in Figure 1.2, redrawn from Dum & Strick, 2005.

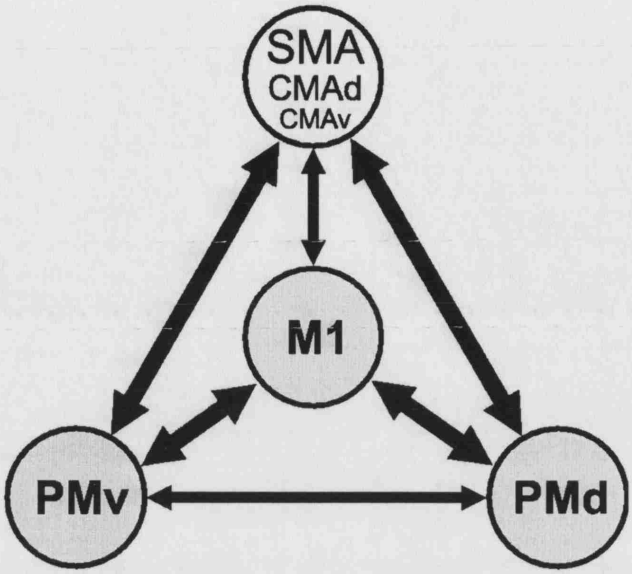

Figure 1.2 Frontal lobe network for hand movements. The size of the arrows indicates the relative strength of an input. Shaded circles indicate motor areas on the lateral surface. Un-shaded circles are motor areas on the medial wall.

1.3.3 Descending Pathways for Motor Control

When making a reach-to-grasp movement, the many circuits and connections allowing visuomotor transformations lead finally to command signals to the motoneurones supplying the musculature of the arm and hand. The main pathway for this is the corticospinal tract (figure 1.3). Much of this projection arises from the motor cortex. Around 60% of all CST fibres arise from the frontal lobe, and injection tracer studies have revealed that of these, approximately 49% of corticospinal neurons originate from M1, 4% from the premotor areas, 18% from the supplementary motor areas, 21% from the cingulate motor areas, and the remaining 7% from precentral areas (Dum & Strick, 1991). The values vary somewhat depending on the cervical level at which the injections were made, showing that different areas project predominantly to different levels and to different regions of the spinal cord. The number of fibres that make up the pyramidal

tract is large, over 400,000 in the macaque and over 1 million in humans (Porter & Lemon, 1993). Across species, there is a strong correlation betwwen the number of fibres and bodyweight. The majority of fibres are small (92% are <4μm in humans).

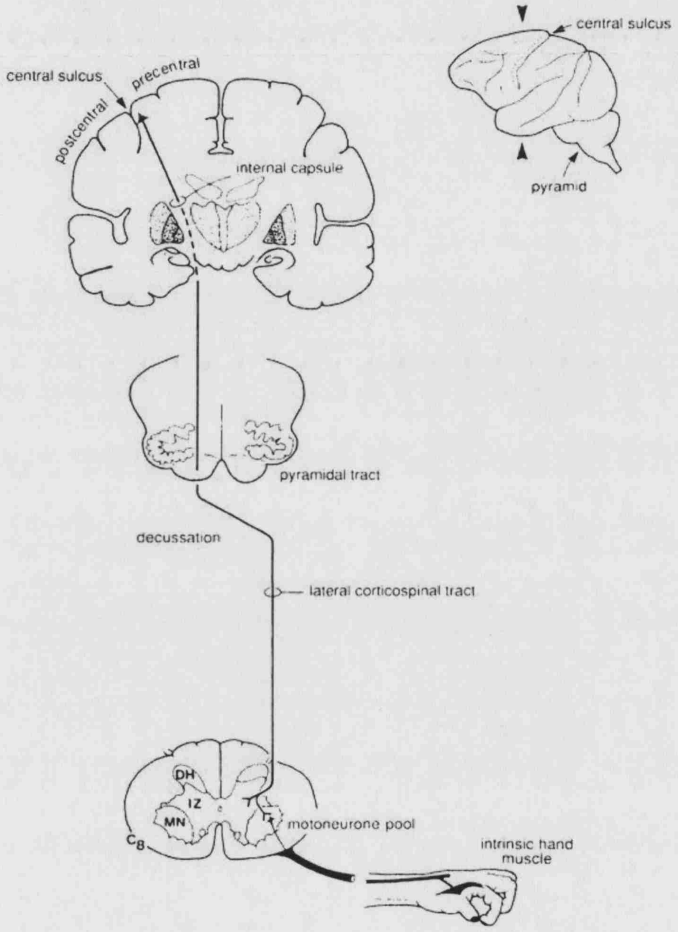

Figure 1.3 The corticospinal pathway in the macaque monkey. Diagram includes the monosynaptic projection from M1 to the contralateral spinal motoneurons via the pyramidal tract.

Fig. 1.3 shows that from the cortex, the corticospinal tract passes through the internal capsule, and descends ipsilaterally through the brain stem until the pyramidal decussation at the caudal end of the medulla. It then descends as the lateral corticospinal tract before making extensive connections within the spinal grey matter at all spinal levels. Some axons make a monosynaptic connection to the spinal motoneurons. Those

cells giving rise to these projections are referred to as cortico-motoneuronal cells. They probably make up only a small component of the entire CST projection. There is considerable branching of corticospinal axons at all levels of the neuraxis, including the spinal cord, such that a single cell may contact many motoneurons leading to facilitation of activity in multiple muscles (Shinoda *et al.*, 1981). The CST also makes numerous connections in the dorsolateral intermediate zone of the contralateral cord, and to the ventromedial part of the intermediate zone both contralaterally and ipsilaterally (Porter & Lemon, 1993). The corticospinal projection therefore permits the motor cortex to influence both individual muscles and groups of muscles simultaneously. This allows the co-ordinated activations of different muscles neccesary for accurate reach-to-grasp movements. The CST does not act alone in its influence on movements. The rubrospinal tract and propriospinal system also contribute to the generation of movements, although in the primate, they are of lesser importance for cortical control than the corticospinal tract (Lemon *et al.*, 2004).

Both M1 and F5 (among other premotor areas) contribute projections to the corticospinal tract. They are therefore ideally placed to execute a planned action. However, compared with other premotor areas, corticospinal outputs from F5 are few in number and do not project as far as the cervical enlargement, where motor nuclei supplying hand muscles are located, but terminate at midcervical levels (He *et al.*, 1993; Galea & Darian-Smith, 1994). It is has been shown that stimulation in F5, although not eliciting always direct movements, facilitates the motor response to stimulation in M1 (Cerri *et al.*, 2003) and that some motor effects evoked from stimulation in F5 are mediated by its inputs to M1 (Shimazu *et al.*, 2004), suggesting that it is via this F5 to M1 projection that F5 exerts its influence on motor actions.

1.4 Rationale for Thesis

The M1-F5 circuit is of crucial importance for visuomotor grasp. Inactivation of F5 leads to deficits in preshaping of the hand during a reach-to-grasp task - the reach is unaffected, and after contact with the object is made, grasp can be performed with tactile feedback. This M1-F5 interconnection is rich, and it is likely that it is via M1 that F5 exerts its influence on the motor output rather than directly via the CST. The anatomy of this reciprocal connection has been well-studied, as have the two areas in isolation. However, no simultaneous study of the function of M1 and F5 during a reach-to-grasp task in the awake, behaving monkey has been published. It is not sufficient to know what each area does to establish its functional relationship to motor behaviour. Simultaneous multiple electrode recordings are an important way to show how the areas interact during a behavioural task, in order to fully understand how this stage of the visuomotor reach and grasp is executed. Such a study is described in this thesis.

Achieving simultaneous recordings in two specific areas of the cortex with multiple microelectrodes is not a trivial challenge. It is crucial that stable recordings can be made from accurately located electrodes. Recent developments have permitted these criteria to be fulfilled. The use of structural magnetic resonance imaging (MRI) has led to accurate individualised maps of the cortex to be produced for each monkey in the study. MRI also enables the customised head restraint devices that are neccesary for stable neuronal recordings to be manufactured and fitted perfectly to the individual monkey without any surgical invasion prior to implantation, a significant improvement in both scientific terms and animal welfare. These uses of MRI will be discussed in Chapter 2.

The repeated insertion of multiple micro-electrodes through the dura and into the cortex of a monkey requires the mainintenance of a thin, unscarred dura to limit damage to both

the cortex and to expensive microelectrodes. With repeated surgical intervention it is possible to keep a dura penetrable for only a limited time. In order to make the long-term recordings described in this thesis, and for all the other ongoing projects in this laboratory, a new method of reducing dural scarring has been developed. Without this, it would not have been possible to record the amount or type of data presented in Chapters 4, 5 and 6. The evaluation of this new method is described in Chapter 3.

Having established accurate, simultaneous multiple microelectrode recordings in M1 and F5, it has been possible to examine the relationships between M1, F5 and a visuomotor reach-to-grasp task. The background and methods for this study are described in Chapter 4. The local field potentials (LFPs) recorded from multiple sites in both M1 and F5 have been studied and found to contain oscillations in the beta frequency range. These oscillations were task dependent, and varied according to the stage of the task and the object that was involved. The relationship of the power of these oscillations in the beta frequency range to the task in each area is examined in Chapter 5. The relationship between M1 and F5 oscillations during the task is evaluated in Chapter 6. Chapter 7 will discuss the results and issues arising from them.

The studies described in this thesis have helped to understand both the function and M1 and F5 during a visually-guided grasp, and the importance of the interaction between these two keys areas of the cortical motor network.

Chapter 2. Uses of MRI for the Guidance of Neurophysiological Recordings and Manufacture of Implants.

2.1 Introduction

The successful study of the cerebral cortex of the awake, behaving monkey using chronic recording techniques requires a considerable degree of technical achievement. Two of the most important requirements are that firstly, the head of the monkey must be restrained firmly and comfortably so that stable recordings can be made, and secondly that recording chambers must be accurately located above the desired cortical tissue at a suitable angle for access. Both of these can be greatly facilitated by the use of Magnetic Resonance Imaging, or MRI. This permits an accurate picture of each monkey's head to be obtained allowing the visualisation of both the brain and skull. From this image, techniques have been developed to improve both the quality of the head restraint implant itself and the fit to the skull in order to achieve stable head restraint. The same scan can be used to generate accurate brain maps for individual monkeys to facilitate the precise location of recording chambers and to establish the macroscopic structure of the cortex within each recording chamber. This has led to a significant improvement in the quality and accuracy of chronic recordings in this laboratory. The non-invasive nature of the MRI means that, compared to previous approaches, less surgery is required in order to ensure the success of our recording methods; this is a significant improvement in practice and leads to improved well-being for each animal. The extended use of MRI techniques has therefore improved both the quality and efficiency of our recordings and has led to improved animal welfare and data collection which has aided both my own studies and others from this laboratory.

2.2 Methods.

2.2.1 Scan Procedures

Parts of our original MRI methodology has been described previously (Baker *et al.*, 1999b). The procedure for each scan was as follows. Anaesthesia was induced with 10mg.kg^{-1} ketamine i.m. (Ketaset, Fort Dodge Ltd.) and maintained with 2-2.5% isofluorane in 50:50 O_2:N_2O, using an open circuit. Long (c. 3m) plastic tubes were used to connect the animal to the anaesthetic trolley which had to be kept a safe distance from the MRI scanner. In later scans, anaesthesia was induced and maintained with a combination of ketamine and medetomidine (Dormitor, Pfizer Ltd.). 15 mg/kg i.m. Ketamine:Dormitor (mixed 80:1 by weight) was reversed with atipamezole hydrochloride (4 mg/kg i.m., Antisedan, Pfizer Ltd.) at the end of the scan.

In order to assess the level of anaesthesia, respiration rate and end tidal pCO_2 were monitored throughout the scan using a small capnograph/oximeter (Model V9004 Capnograph, Burtons). ECG was monitored using the scanner's integral system via four surface electrodes placed and taped securely onto three limbs and the chest. Once stable anaesthesia was achieved, the monkey's head was fixed into a non-metallic stereotaxic frame. This was made in house using a combination of Perspex and Plexiglass. As with a surgical stereotaxic frame, it contained atraumatic eye bars and ear bars. However, in this case, the bars were machined to have a small hollow core which ran the length of the bars. These holes were filled with oil (either vegetable cooking oil, or a from a vitamin capsule such as cod liver oil). This oil yields high contrast in MR images and allows their position on the final scan to be determined. The oil is sealed in with a small nylon screw to prevent leakages or the introduction of air. A capsule of cod liver oil or vitamin E is taped to the inferior, posterior right side of the head. This acted as a marker

bead to ensure that left and right were easily distinguishable on the scan. Once in the frame, the monkey was then wrapped warmly in plastic bubble wrap, towels and veterinary fleece and placed on a heated wheat bag. This prevented loss of body heat whilst the scan was in progress. This was especially important as the MRI scanner room must be deliberately kept at a low temperature. The monkey was then transferred to the scanner table, and positioned such that the head was as straight as possible in the scanner. The anaesthetic trolley and monitoring equipment were placed as far away from the scanner as possible and in a position where the screens could be seen from the scanner control room. The scan was then performed.

A GE Medical Systems Signa Horizon 1.5 Tesla system, with two 3 inch circular receiver coils in a phased array configuration and using spin echo (2D) to establish the positioning of the head and set up the gradient echo (3D volume) which was used during data acquisition. Two gradient echo scans are usually performed; firstly a lower resolution scan of the whole head for which the voxel dimensions are 0.7 mm^2, and secondly a higher resolution scan of the upper surface of the brain and skull, voxel dimensions 0.4 mm^2. Each scan takes approximately 12 minutes. After scanning, the monkey was returned to the operating theatre, removed from the stereotaxic apparatus and anaesthesia discontinued. Once recovery commenced, the animal was placed in a recovery cage and monitored until it had recovered enough to be returned to the home cage.

2.2.2 Scan Data Processing

The scans were obtained and stored in GE Signa native format for initial inspection to verify successful scanning. Using a Sun workstation, these were then converted to Analyze files, a standard industry format. These consist of an image file containing the

scan in combined slice format, and a header file which has the detailed information of the scan, such as voxel size, slice thickness, resolution, etc. These Analyze files were then transferred to a PC for further conversion and processing.

The software used for image processing is 3D Workstation (R.Richards, Medical Graphics, UCL). The 3D Workstation software allowed on screen manipulation of the scan. Although best efforts were always made to place the monkey into the scanner aligned squarely to the scanner, usually there was a small error which meant that the scan was not in perfect stereotaxic alignment. This can be seen in Fig. 2.1. Two slices are shown from a typical, initial scan, in this case of monkey M40, a male rhesus macaque. The ear bars can clearly be seen in A, although one is slightly thinner than the other, indicating a small height discrepancy. However, the eye bars appear in a different slice, shown in B. This slice is 4 slices from slice A, a total of 2.8 mm apart.

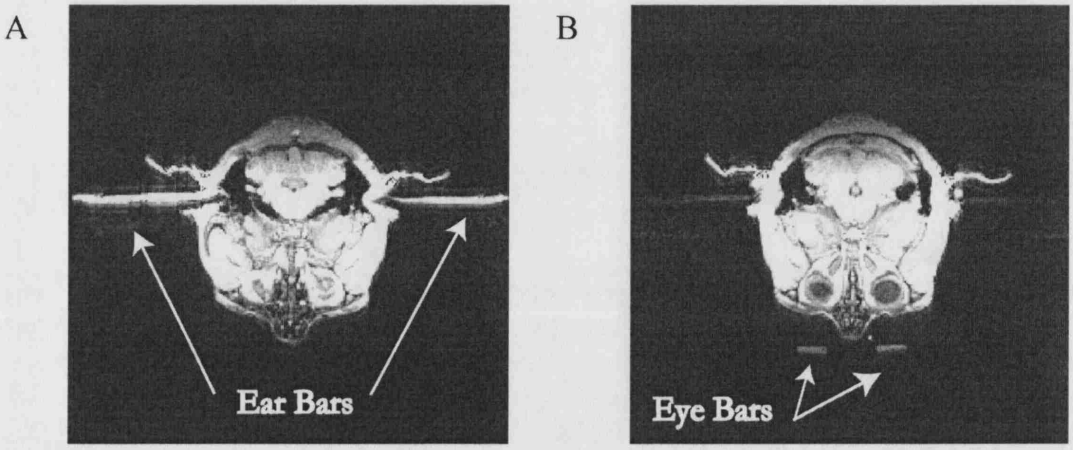

Figure 2.1 Coronal slices A. Showing ear bars. **B.** Showing eye bars.

Using the 3D Workstation software, the scan was rotated laterally to ensure the ear bars were in the same horizontal plane. It was then rotated forwards or backwards such that the eye bars are set to the same horizontal plane as the ear bars; all are then designated

as having a height of zero. Once the scan has been aligned in stereotaxic space it was resampled to produce new orthogonal slices in stereotaxic planes. Using the eye and ear bars which are visible in the scan, a stereotaxic zero point was set. This is a point located in the midline, halfway between the tips of the ear bars. The three planes that pass orthogonally through this point were used as references for stereotaxic measurements. These planes are referred to as Medial-Lateral (M-L), Anterior-Posterior (A-P) and Height (H). Figure 2.2 shows slices taken in these planes of the rotated images. The blue lines represent the planes, and can be seen to intersect at stereotaxic zero in every slice.

Once the necessary rotations of the image set had been calculated, these rotations were repeated on the high resolution scan (which does not in itself contain the eye and ear bars, being solely of the upper surface of the brain and skull). In this way, the two scans for each monkey are aligned in stereotaxic space.

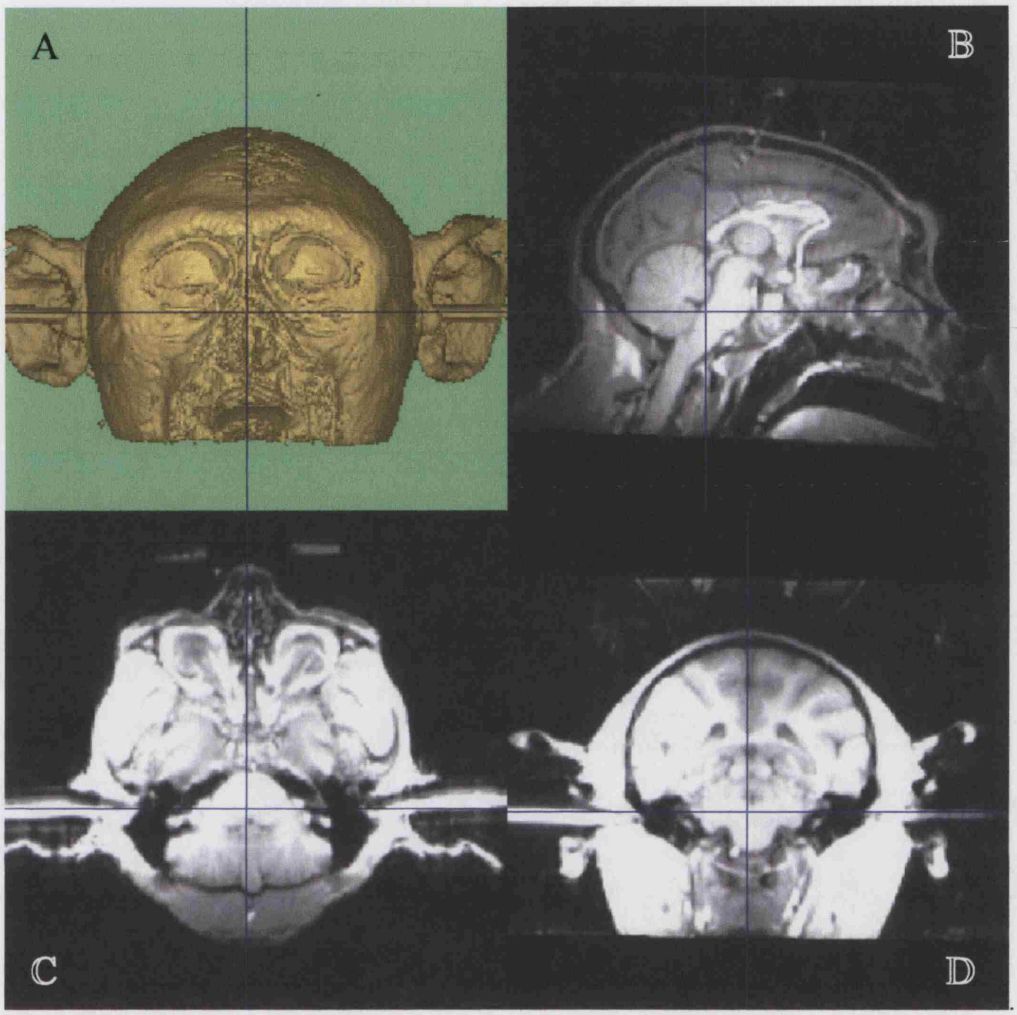

Figure 2.2 Realigned scan. A. Surface reconstruction of the can. **B.** Sagittal Slice at the midline, M-L zero. **C.** Coronal slice at height zero (ear and eye bar place). **D.** Transverse section at A-P zero.

2.3 Uses of the MRI Scan

2.3.1 Head Restraint Design and Manufacture

2.3.1.1 Introduction

Once a naïve monkey has reached an adequate level of training on the task to be considered suitable for to be used for chronic recording, the monkey must be prepared for surgery to implant a head restraint system, and later on, recording chambers over the

cortical sites of interest. The head restraint is necessary to allow stable chronic recordings of single neurons with extracellular microelectrodes. In our laboratory, we use the Thomas Recording Microdrive system to insert multiple microelectrodes through the dura into the cortex. The microdrive is not fixed directly to the chamber or head in anyway; it is therefore imperative that the head is fixed securely to the primate chair system, onto which the drive is mounted. This ensures that there is no movement between the two, which would lead to instability of the neuronal recordings, and potentially damage to both the cortical tissue and to the electrodes themselves which are very fragile.

Over many years, a head restraint system has been developed in this laboratory, based on that originally described by Lemon (1984). This approach allows the firm attachment of a headpiece to the skull, which is stable and relatively healthy over extended periods of time. In brief, the method involved a custom made stainless steel ring for each monkey with 3 upright M6 bolts by which the monkey could be attached to the recording rig. The implant was affixed to the skull by use of custom made steel bolts. This steel headpiece was manufactured to fit the individual monkey by taking an impression of its skull using a dental acrylic polymer. The monkey was anaesthetised and placed in a full metal stereotaxic frame. An incision would be made down the midline from the orbitofrontal ridge to the nuchal line on the posterior aspect of the skull, and the skin and muscle reflected to reveal the calvarium. Once exposed fully, the dental compound is pushed onto the skull and left to set, and once cured, removed to produce an impression of the skull. The muscle and skin would then be pulled up back over the skull, and sutured in layers to close the wound. The monkey was then allowed to recover, and the stitches would be removed 8-10 days later, sometimes under sedation

if necessary. The impression taken would then be used to create a 'plaster of paris' 'positive' model of the skull, onto which the stainless steel ring could be shaped during manufacture. Using this technique to create an accurate impression of the skull surface meant that the monkey would be anaesthetised at least once, and would be left with scarred skin and muscle on the scalp, even with the most careful of surgical techniques. The monkey would have to recover from the surgery and the stress involved, which has a negative impact on welfare and also on the progress of training the monkey whilst it recovers from the procedure.

However, with the use of MRI, a full picture of the skull can be captured non-invasively. A technique has been developed in which the scanned images are used to produce a 3-dimensional model of both the skull surface and the underlying brain surface, allowing us to omit the invasive surgery described above. The method has been developed in collaboration with Robin Richards from the Medical Physics Department at UCL.

2.3.1.2 Methods.

The 3D Workstation software allows visualisation of areas of interest through editing of the slices. This involved designating areas to be retained or removed from each slice of the data set. By editing the coronal slices to 'remove' the scalp from above, and the brain from below, the skull can be clearly seen in a 3D reconstruction. The software used a Houndsfield threshold detector to determine boundaries between areas of higher and lower contrast. This accurately separated the skull (low contrast) from the scalp, dura, cerebrospinal fluid and brain (higher contrast) around it.

This computer-generated view of the skull was used to take stereotaxic measurements of landmarks such as the coronal suture and bregma. These were later used to guide the surgeon when placing recording chambers. Most importantly, it was also used with a

Stratasys FDM 3000 rapid prototyper machine, which effectively acted as a 3-dimensional printer. It used fused deposition modelling to create a full size model of the skull from an ABS plastic polymer, built up in layers according to the editing in the scan provided to the machine. This skull model was therefore a perfect replica of the monkey's skull, and was created without any invasive procedures. The monkey was of course anaesthetised for the scan, but without any surgical interference, and therefore recovered immediately from the procedure, which only took approximately 2.5 hours in total from start to finish, and only approximately 1-2 hours of light anaesthesia. A typical edit and model manufactured from the edit is shown in Figure 2.3. Pencil marks used to design the headpiece for this monkey can be seen on the plastic model in 2.3C and also the intended location for the chamber for neuronal recordings in M1 and F5. The coronal suture of the skull can also be seen clearly in the screen picure of the skull (Fig. 2.3A). This landmark is particularly useful during surgery.

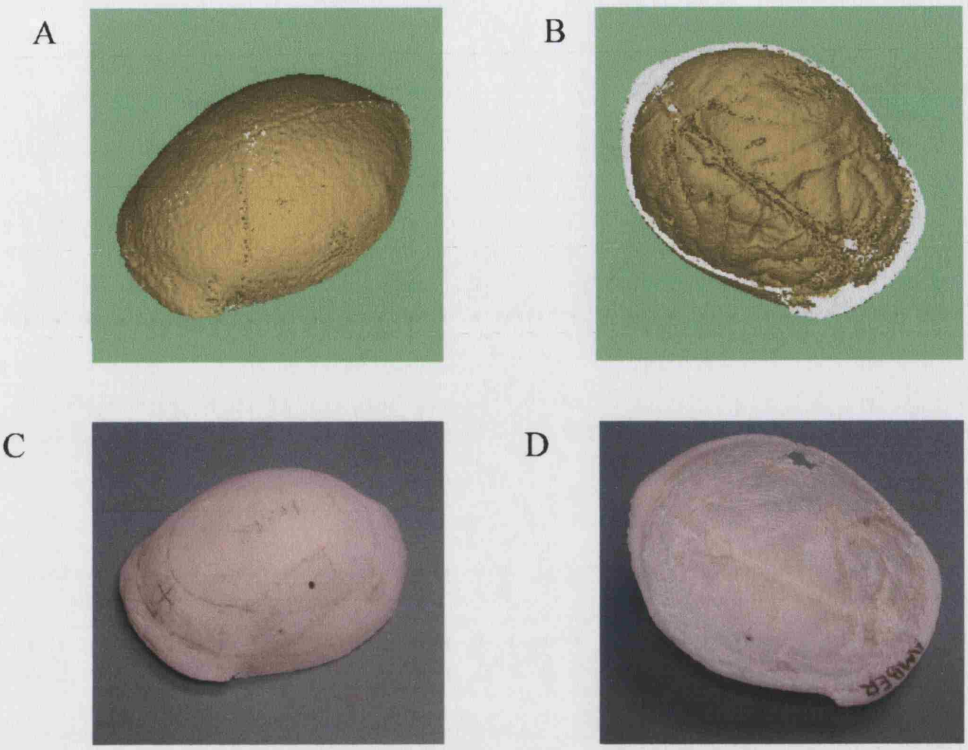

Figure 2.3 Plastic skull mound A. Screen shots of computerised edit of skull outer surface and **B.** Skull inner surface. **C.** Photograph of outer surface of plastic skull model made from the edit in A. and **D.** Model inner surface.

2.3.1.3 Conclusions.

The use of MRI in this way represents a significant advance on our previous technique of taking a skull impression directly, requiring the surgical invasion of the head. It reduced the trauma for the animal, reduced the total number of surgeries it must undergo to be prepared for recording, interfered less with the training of the animal by eliminating the recovery time previously needed, and avoids a second anaesthesia for removal of sutures. It also meant that the monkey's head remains untouched surgically prior to the actual implant of the headpiece. As a result, the implant surgery is performed on healthy, unscarred tissue which leads to improved recovery from the implant surgery and better acceptance of this implant. The use of the scans in this way is now standard procedure in our laboratory.

A further use of this software and scan is currently being investigated. To date, the headpieces have been manufactured from stainless steel to fit the moulds produced using the MRI, as described. However, a new form of headpiece is being trialled. This is manufactured from a material called HAPEX (hydroxyapatite polyethylene) supplied by Professor Elizabeth Tanner of the Department of Biomaterials, Queen Mary, University of London. This is a hard plastic material which is 'bone-friendly'. Hydroxyapatite is chemically similar to the mineral phase of bone, and is therefore bioactive – when implanted in contact with bone, new bone will grow up to the HAPEX and will epitaxially bond with the surface, providing a strong bond between the HAPEX with a shear strength of up to 10Mpa (Tanner *et al.*, 1990). It is nearly modulus matched to bone, having a stiffness of 3.7Gpa, compared to 7-25Gpa for cortical bone (Bonfield, 1988). Being plastic, it is also MRI compatible. The computer based skull representation and the custom software can be used to program a CNC milling machine. This has enabled a block of HAPEX to be milled with a surface impression of the skull of a specific monkey. This block was then hand machined to produce a smooth ring implant of similar design to the previous stainless steel ring, with an inner surface which was a perfect match for the upper surface of the skull, and an outer surface which was contoured to leave three mounds with 3 tapped, threaded holes (where bolts may be placed at a later date) and a thinner ring between the mounds (Fig. 2.4)

Figure 2.4 HAPEX headpiece. Viewed from the front, left aspect. The three mounds where the uprights will be inserted can be clearly seen, along with a fixation hole located close to the anterior mound, used to bolt the headpiece to the skull.

It is lighter in weight, and significantly more biocompatible than steel. It is also MRI compatible, potentially allowing further scans to taken place after the implant, for example to verify locations of recording chambers if needed. The HAPEX headpiece is currently being tested in monkey M40. Under anaesthetic, (protocol as before) the ring was surgically affixed to the skull with titanium bolts using the same method as for the steel headpieces. The skin was then pulled up entirely over the implant and sutured. After leaving the implant to integrate and bond with the bone for a period of 2 months, the skin above the mounds and the grub screws were removed, and three upright bolts were fitted. The top of the mounds and the uprights therefore now protude through the skin and may be used to head fix the monkey securely. This headpiece is currently in use for head fixation, although its strength and suitablility for neuronal recordings have yet to be established. If proven to be successful, this method will allow perfectly fitting, biocompatible headpieces to be made, all from the MRI scan. Its biocompatibility should ensure total acceptance of the implant by the monkey and by its succesful integration

with the bone, should provide optimum stability for head fixation and stable neuronal recordings.

MRI is therefore of great use alongside other technologies for the design and manufacture of head restraint devices, leading to improved implants, animal welfare, and greater stability of neuronal recordings.

2.3.2 Sulcal Maps of the Cortex

2.3.2.1 Introduction

A second use of the MRI scan was in the production of an individual cortical sulcal map for each monkey. When performing neuronal recordings, it is crucial to locate the recording electrodes as accurately as possible both in terms of the point of penetration of the cortical surface and the angle of approach. This is complicated by the variability between animals in sulcal geometry and in the stereotaxic location of the different cortical areas. Structural MRI allowed an individual map to be constructed for each monkey, and measurements of both distances and angles to be taken to greatly improve the accuracy of chamber placement and angle of electrode approach. Another issue is the variability of the bony structures used to position the monkey into the stereotaxic apparatus. This could affect the stereotaxic readings for a given monkey if not taken into account. Many laboratories simply use standard neuroanatomical atlases to guide their recordings (as described in Martin & Bowden, 2000), combined with very large recording chambers so that more of the brain can be seen to guide electrode placement. These give predicted coordinates of neuroanatomical features in stereotaxic space for a 'standard' monkey. However, given the potential for different positioning of the brain due to variability in cranial features, even if the brain conformed to predicted maps, the

stereotaxy may not be accurate. In order to verify the importance and relevance of using MRI for individual maps as opposed to relying on standard stereotaxic atlases, a systematic approach was used to measure the differences. A survey of 10 monkeys that were scanned in the course of our work has been undertaken, comparing the individualised maps with standard atlases and with each other. In this way, it was possible to assess the variability between monkeys, and to ascertain if this variability appeared to be related to the size or sex of the monkey concerned, or to the species (both male and females, and *M. mulatta* and *M. fascicularis* were studied).

2.3.2.2 Methods

The same scans were used as for the previously described procedure. In this case, instead of editing skin and brain to leave the skull, a slice by slice edit was performed to remove the skull and scalp to leave a surface rendering of the cortex. This rendering clearly showed the sulci, gyri, and may even show superficial blood vessels. A typical rendering is shown in Fig. 2.5. Here, the top of the skull has been removed, revealing the upper surface of the brain.

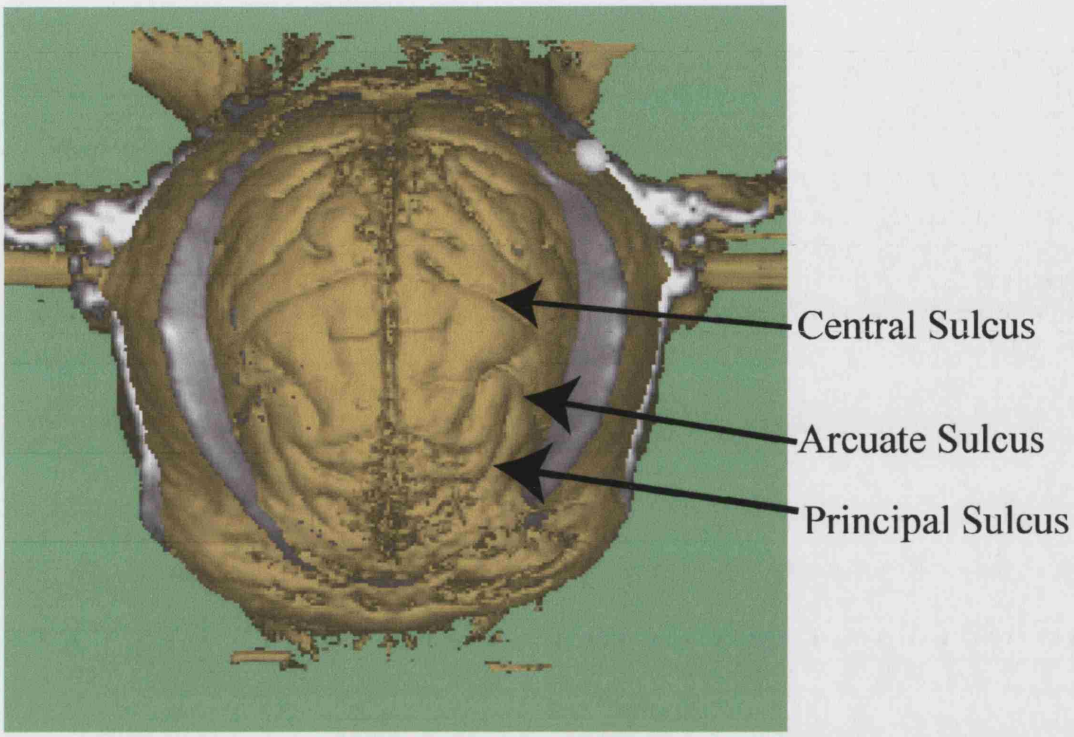

Figure 2.5 Surface rendering of brain. View from above the top of the head, nose pointing downwards.

This gives a general idea of the typical morphology of the brain as revealed in the scan. The features of most interest to our laboratory are those which can be used to determine location of the motor areas of the cortex, as this is usually where recordings are made. These are the central sulcus, the arcuate sulcus, the spur of the arcuate (if it is present), and the midline. These were therefore chosen to represent the anatomy of the brain for further assessment.

Using the 3D Workstation software, measurement markers were placed along these features of interest, as shown in Fig. 2.6.

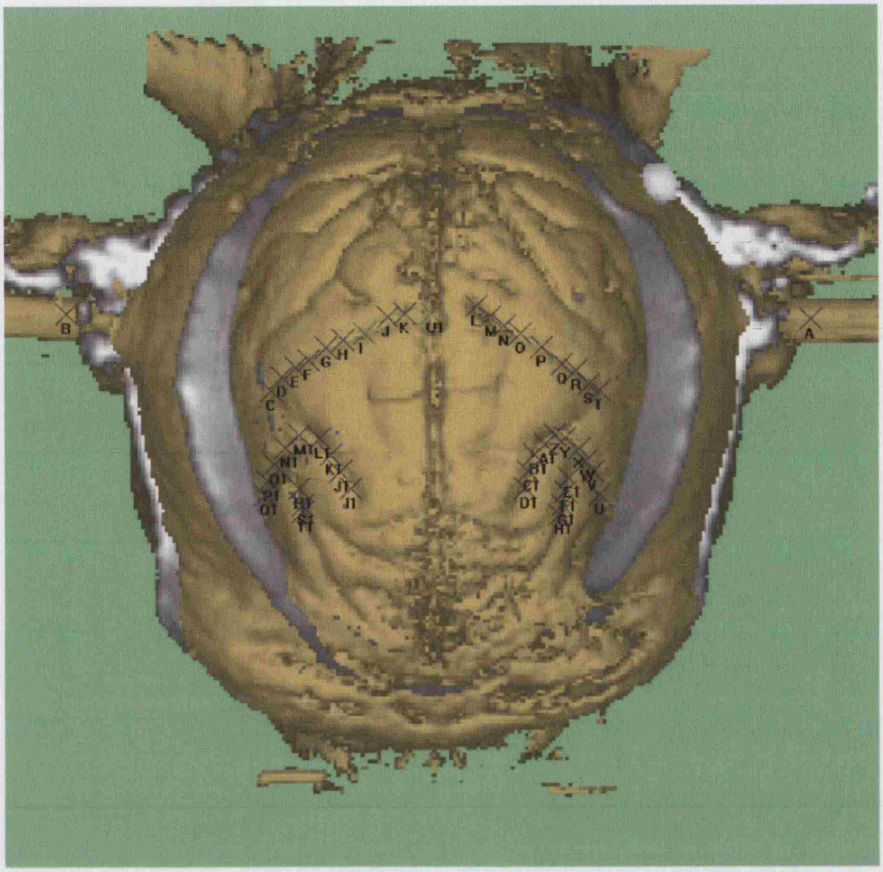

Figure 2.6 Placing of markers on features of interest. Here, the central, arcuate and principal sulci, and the ear bars have been marked at regular intervals with crosses, the locations of which can be extracted.

These markers were set in stereotaxic coordinates which were then be extracted and plotted to create a 'cortical map' which was specific to that particular monkey. This was used to identify potential sites for future chamber placement and entry points for neurophysiological recordings. Markers can also be related to skull features such as the coronal suture, to provide geographical landmarks which were particularly useful when making craniotomies for chambers.

In similar fashion, the MRI scan was also used to guide the placement of chronically implanted pyramidal tract or cerebral peduncle electrodes as required for the individual monkey and study.

Data from 10 monkeys were used for this study, and comparisons with standard stereotaxy made using Martin and Bowdens Stereotaxic Atlas (within Martin & Bowden, 2000). This atlas also contains software templates for the standardised brains that can be 'warped' to fit.

2.3.2.3 Results

2.3.2.3.1 Typical Cortical Maps

Typical maps of the central and arcuate sulci derived from MR images are shown in figures 2.7, 2.8 and 2.9. *In vivo* measurements are also shown; these were taken from the animal whilst in the stereotaxic frame during a surgery to implant a recording chamber. Large blood vessels may be seen through the dura which tend to overly the sulci, and measurements of these were made. Post-mortem measurements were also taken stereotaxically from the post-fixed brain tissue; after transcardiac perfusion with 3% paraformaldehyde, the head was removed, and mounted into the same sterotaxic frame as was used during surgery and measurements taken. Data in Fig. 2.7 was obtained from monkey M34 (*M. mulatta,* female).

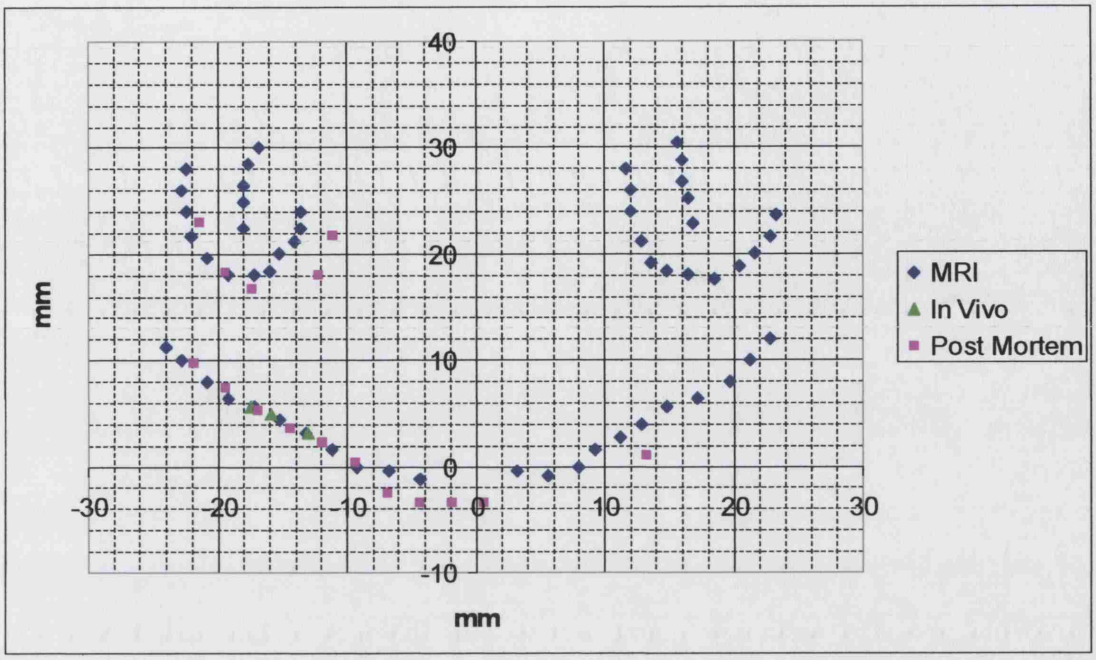

Figure 2.7 Cortical measurements of central and arcuate sulcus in M34.

It can clearly be seen that precise measurements for the location of cortical motor areas can be made from the MRI derived map. The accuracy of the map was verified by both the *in vivo* data and post mortem data which showed that in this case, the MRI data was highly accurate. Post mortem measurements can be subject to significant distortion due to the fixtives used for perfusion, although no significant distortion was noted in this case.

A further example is shown below in Figure 2.8. Data from M38 (*M. mulatta,* female) are presented. It can be seen that the MRI and *in vivo* data were quite well matched, to within 1 mm, although in this case the post-mortem data did not match so well. It appears similar in morphology but inaccurate in the A-P dimension. In this case, the brain tissue was noted as swollen, which may account for the discrepancy.

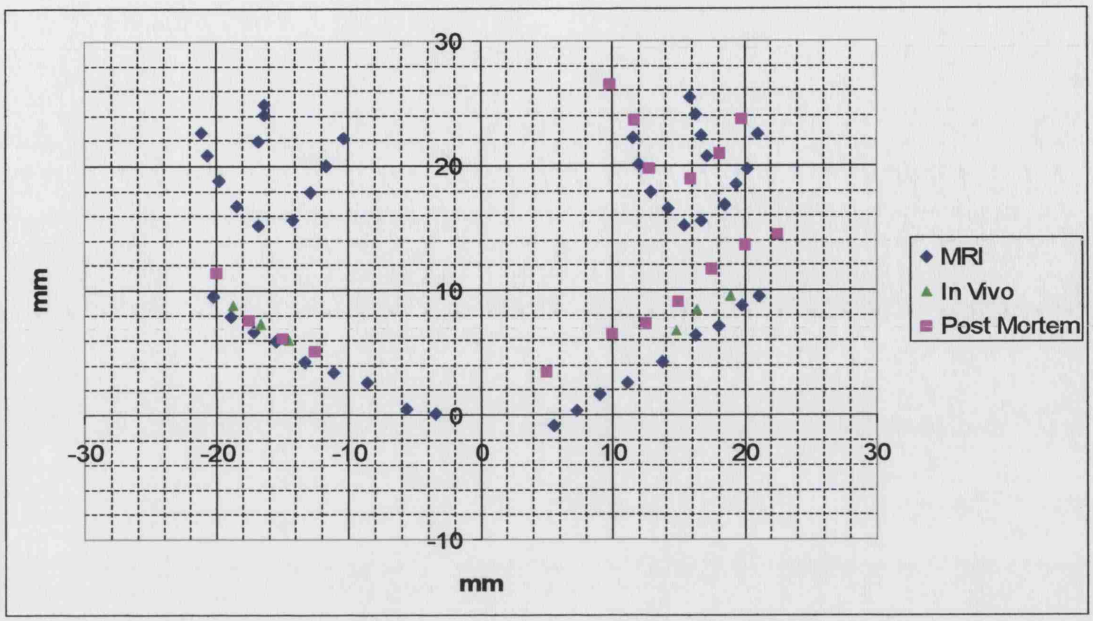

Figure 2.8 Cortical measurements of central and arcuate sulcus in M38.

A final example is shown in Figure 2.9.

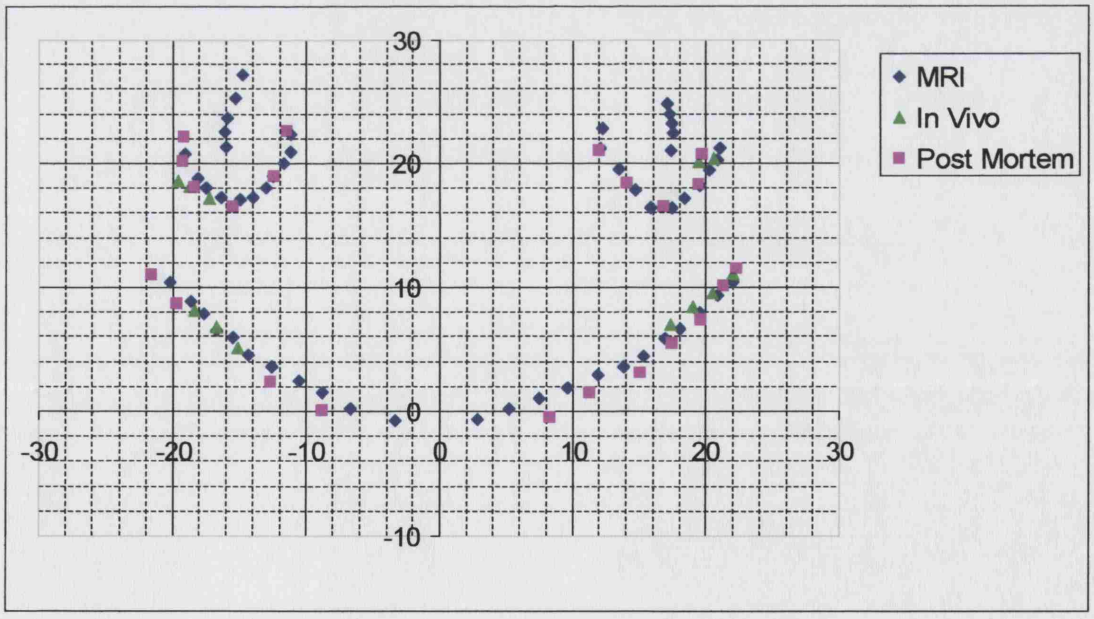

Figure 2.9 Cortical measurements of central and arcuate sulcus in M37.

In this case, the MRI, *in vivo* and post mortem data are all closely matched.

In all cases, there was a high degree of accuracy between the MRI derived measurements and those taken *in vivo*. The post mortem data were more variable, due to the varied distortion effects that the brain fixatives may have had.

2.3.2.3.2 Comparison of Maps between Monkeys.

The variability in different monkeys can be seen by plotting all the data together. This is shown in Figure 2.10. Here, measurements from 8 female rhesus monkeys are shown, including the three shown in figures 2.7, 2.8 and 2.9.

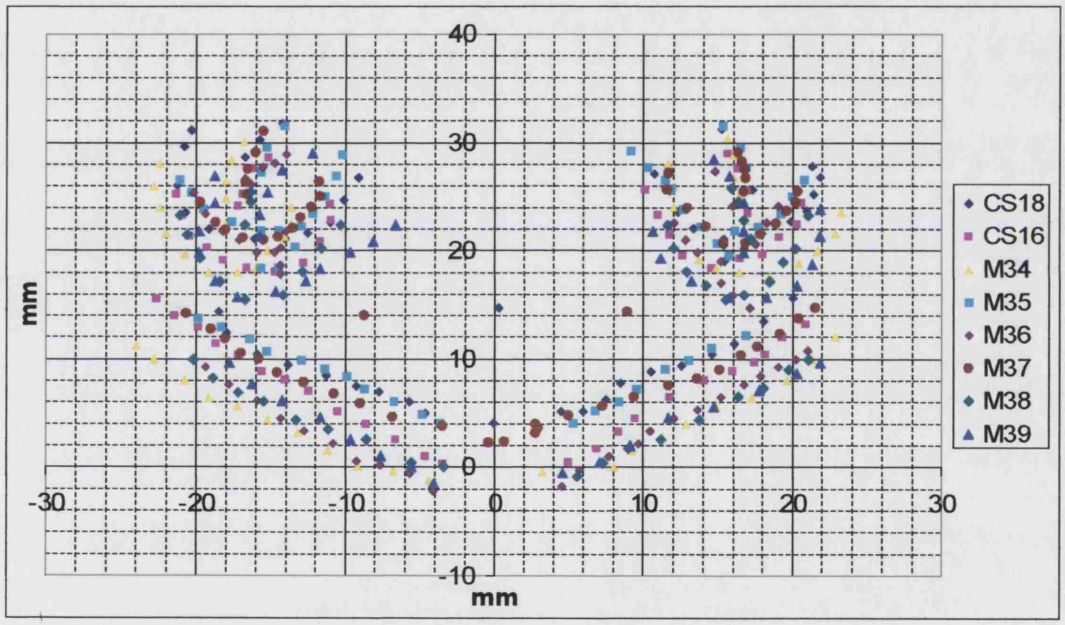

Figure 2.10 Chart to compare measurements of 8 monkeys.

It can be seen that there is considerable variability from one monkey to another when looking at their MRI derived maps, particularly in the A-P dimension where there is a range of more than 6 mm from one monkey to another, suggesting that to have relied purely on standardised atlas measurements for these monkeys would have led to inaccurate placing of recording chambers.

2.3.2 Comparison with standard data.

Martin & Bowden (2000) published stereotaxic data obtained from young adult males, weight range 3.4-3.6 kg. A template is provided for a typical brain. Although the data were compiled from measurements from *Macaca fascicularis*, it is claimed that their data is comparable with other published atlases for other species, and that there is sufficient degree of topological homology among macaques (except *M. nemestrina*) to use data from their atlas across species. Scaling factors are suggested for different species, based on other published atlases, for the targetting of upper brain stem landmarks, and an expected discrepancy is calculated. For three rhesus monkey atlases the absolute discrepancies are 0.4 mm, s.d. 0.3mm (Clarke & Henderson, 1920), 0.5 mm, s.d. 0.3mm (Olszewski, 1952), and 0.4 mm, s.d 0.4 mm (Snider & Lee, 1961), suggesting that the standard templates should be accurate to within a millimetre or two.

Three edited scans were compared with the standard template provided. The three scans compared with this standard were as follows; M40, male *M. mulatta*, aged 3, weight, 4.3 kg, M34, female *M. mulatta*, aged 6, weight 7.7 kg, and CS12, male, *M. fascicularis,* aged 4, weight 3kg. These are shown below.

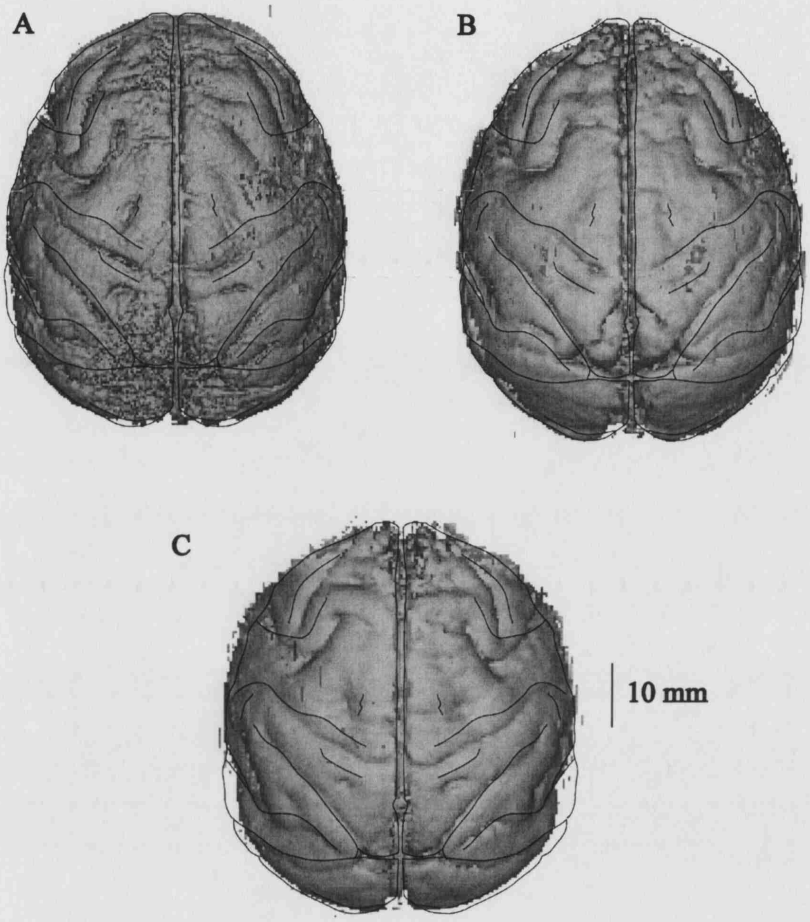

Figure 2.11 Scanned brain images compared to standard templates. A. M40 (male, rhesus, 4.3 kg) **B.** M34 (female, rhesus, 7.7 kg). **C.** CS12 (male, fascicularis, 3 kg). The template is shown as black lines.

The brain images are 'top down' views of the brain produced by the MRI software. The template was 'morphed' to fit the brains by superimposing the template, and then stretching or compressing it in the M-L and A-P dimensions to match the length and width of the brain image, using image software (Adobe Illustrator v10, Adobe Systems Inc.). It can clearly be seen that in these three cases, the template is not a very good match for the brain, despite being aligned stereotaxically in each case and the template being morphed to match the brain. In Fig. 2.11A, the monkey was of the same sex and

approximate weight as the 'standard' (although a different species) and very few of the sulci matched. The central suclus was more posterior on M40, and the arcuate sulci were a long way posterior and also more medial than those of the template. Interestingly, M34, shown in 2.11B was perhaps a better match to the template, despite being female, a different species, and much larger than the template standard monkey. The central sulci were well matched, although the arcuate sulci were also more posterior and medial than the template. In both cases, the more posterior parts of the brain appear better matched than the anterior. In the third case (Fig. 2.11C), the monkey scanned was of the same species, sex and weight to the standard sample monkey featured in the atlas, and although the fit was better than for either rhesus monkey, it was still not exact. The spur of the arcuate sulcus for example was approximately 5 mm more posterior than would be predicted.

It can clearly be seen that for these three monkeys, relying on the template to guide the positioning of recordings in the motor cortex may have led to significant errors. This was particularly true for the two rhesus monkeys. The ventral premotor area F5 would be predicted to be more anterior than it actually is, potentially leading to recordings anterior to the arcuate sulcus being performed by mistake. One possible explanation for the discrepancy could be the positioning of the brain. In the previous figures, the scanned brains have been orientated stereotaxically by their external landmarks, as would be the case during surgery to mount recording chambers. However, the standard templates were orientated differently. After mounting in a stereotaxic frame, a lateral ventriculogram was obtained to reveal the anterior and posterior commissures, and the cranium was rotated about the ear bars until the bicommissural line (i.e. the line between the anterior and posterior commissures) was horizontal, creating the coronal zero plane.

The angle of rotation was not mentioned. A similar approach is used in many human stereotaxic procedures. To examine the possibility that it is the rotation that caused the discrepancy, the commissures were identified on the MRI scan of M40, and the scan rotated in the same way as the standard, in this case, 6° (nose rotating upwards). The upper surface was then compared to the template again, which can be seen in Figure 2.12.

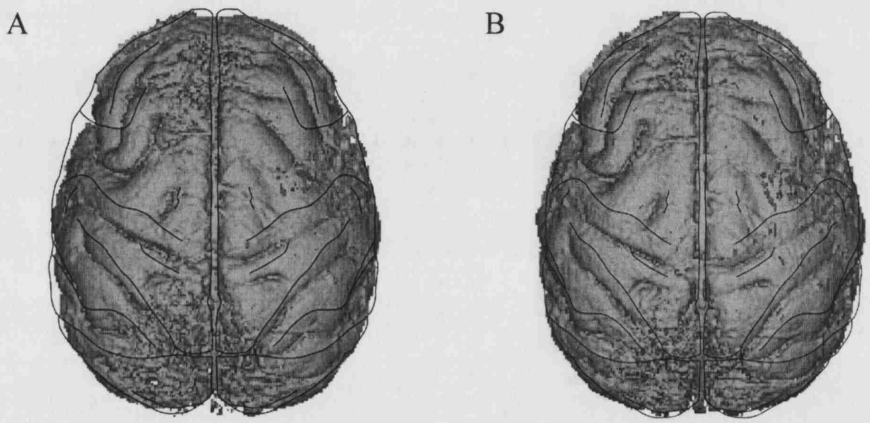

Figure 2.12 Comparison of templates. A. To ear-eye bar zeroed coronal plane and **B.** To commissural line zeroed coronal plane.

Although this slightly improves the fit, it certainly does not account for the mismatch. It seems therefore that for this case at least, the template and the anatomy are not well correlated, despite the subjects being of similar age, weight, and the same sex. One explanation may be that the atlas is derived from post mortem tissue which has been fixed. As was shown earlier, this may lead to differences in measurements, even within the same animal, so comparing post mortem tissue atlases to *in vivo* brains will always have a potential source of error.

The template used above is only one feature of the atlas. Sophisticated warping techniques and a far more extensive set of templates and images are available to locate

structures accurately in the imaged monkey. The above comparisons are not intended to suggest that the atlas is irrelevent or wrong, merely to illustrate that using an atlas alone for a monkey of any size, sex and species may lead to errors. If MRI scanning techniques are available, the atlas and software allows the warping of the images to identify structures not visible in MR images. It also suggests scaling factors for brain stem locations. However, little mention of superficial cortical features, like the sulci, is made. This may be because traditionally, large recording chambers have been used by many laboratories, which enable visualisation of the superficial landmarks by which electrode placement may be guided. However, large chambers have their disadvantages, and may have a negative impact on the welfare of the monkey. Smaller chambers are only possible and useful if accurately placed and the results show that MRI is a valuable tool for achieving this, in particular when recording in the frontal cortex, where brain-atlas discrepancies appear to be largest.

2.4 Conclusions

MRI is a valuable tool for the neurophysiologist wishing to make accurate, stable recordings in the awake, behaving monkey. Its use has several advantages to assist in the manufacture of ever-improving head restraint devices, to locate recording chambers accurately and to guide recordings within those chambers. Refinement of techniques leads to improved well-being for the monkey and to accurate and precise data collection for the experimenter.

Chapter 3. The Problem of Dural Scarring: a Solution Using 5-Fluorouracil.

3.1 Introduction

3.1.1 The Dural Scarring Problem

Multiple microelectrode methods are increasingly being used in awake, behaving monkey studies. In many approaches, this involves the use of relatively fine and fragile electrodes. For example, the Thomas multielectrode system (Thomas Recording Ltd; Eckhorn & Thomas, 1993) uses up to 16 independently moveable electrodes; they are made of platinum-iridium (Pt-Ir) and insulated with quartz glass. These microelectrodes are very fine, with an external shaft diameter of only 80μm, and during transdural penetration, dural thickening can cause them to buckle and break.

When the dura mater is first exposed at surgery, in preparation for single unit recording, it is usually thin, unscarred, and free of any covering tissue, and therefore it is possible to penetrate it with fine electrodes. As the inflammatory wound-healing response begins, scar tissue forms, and the dura thickens. At first, this tends to be a filamentous growth, which subsequently becomes fibrous and vascularised. Conventional tungsten or Pt-Ir microelectrodes typically have a shank diameter of 150μm, and are still able to penetrate this type of growth successfully (Lemon, 1984). In contrast, the thickened dura is almost impenetrable to the more delicate (and expensive) Thomas electrodes within two weeks. The ratio of broken electrodes to successful penetrations becomes high and costly. Furthermore the quality of recordings is diminished because difficult penetrations cause excessive dimpling of the dura, and pressure-induced spreading depression in the underlying cortex. In order to continue with further recording, the dura must be stripped

of this growth. This usually requires a general anaesthetic. These surgeries interrupt the routine of chronic recording and adversely affect the performance of the monkey on the behavioural task, as well as its general well being.

A well-tested method has been established to suppress the growth of connective and scar tissue above the exposed dura, and to reduce the vascularity of this tissue in the recording chamber. This involves the topical application of a solution of 5-fluorouracil (5FU) to the exposed dura. 5FU is an antimetabolic, antimitotic agent that reduces tissue growth by interfering with the enzyme reactions essential for nucleic acid synthesis, thus preventing mitosis, and therefore the division and proliferation of cells.

3.1.2 History of 5FU Use

The first use of a single five minute application of 5FU in sponges to prevent scarring after ocular surgery in humans (Smith *et al.*, 1992) was based on the discovery that short, five minute applications of 5FU caused long term fibroblast growth arrest in culture with minimal cell death (Khaw *et al.*, 1992a; Khaw *et al.*, 1992b). This was subsequently confirmed in an aggressive model of scarring after surgery to create a new outflow channel to drain aqueous fluid out of the eye to reduce intraocular pressure. *In vivo* the treatment was found to have focal long term effects on fibroblast proliferation without overt toxicity (Khaw *et al.*, 1993a; Khaw *et al.*, 1993b). Single five minute applications have also subsequently been shown to prevent cell mediated collagen contraction *in vitro* (Occleston *et al.*, 1994) and in models of tendon scarring after injury (Akali *et al.*, 1999; Khan *et al.*, 1997; Moran *et al.*, 2000). An adapted version of this single treatment in combination with heparin has also been shown to significantly reduce retinal scarring in a human trial without any detectable retinal toxicity (Asaria *et al.*, 2001; Kon *et al.*, 1998).

Antimitotic solutions are already used in many clinical situations, for example ophthalmic surgery for conditions such as glaucoma (Khaw & Migdal, 1996) and strabismus (Andreo *et al.*, 1997). It is also used in chemotherapy regimes for a range of solid tumours including breast and colorectal cancers (Cunningham & Coleman, 2001) and as a topical treatment for non-melanoma skin cancers such as basal cell and squamous cell carcinomas (Nguyen & Ho, 2002).

It is therefore believed that the topical use of 5FU may be expected to safely act to retard the growth of dural scar tissue with minimal risk to the individual. The actions of 5FU on the dura have been investigated by assessing its effects on the quality and yield of single neuron recordings in the awake, behaving monkey. By using 5FU to control dural scarring and solve the 'tough dura' problem, it is now possible to record continuously for periods of up to three months before having to perform a surgery to strip the dura. 5FU has improved the success rate of the penetrations and decreased the rate of breakage of electrodes, thus reducing the cost and increased the efficiency of each experiment. Any deleterious effects 5FU might have on the underlying cortex have been investigated and none were found. This method therefore offers significant refinement to and reduction of animal procedures, as well as more efficient data capture.

A brief description of these methods has been previously published (Baker *et al.*, 1999b), and fully published (Spinks *et al.* 2002).

3.2 Methods

3.2.1 5-Fluorouracil

5-Fluorouracil (Faulding Pharmaceuticals Plc.) is a potent anti-mitotic agent. It is supplied in aqueous solution in 10 ml vials (250 mg, 25 mg/ml). According to the manufacturers, when given systemically in chemotherapy, it can cause side effects including diarrhoea, nausea, vomiting, alopecia, dermatitis, nail pigmentation changes, blood disorders and ECG changes. If used in pregnancy, it may be teratogenic. It is therefore essential that it is handled carefully for the safety of both experimenter and animal. Vials should be kept in a locked cupboard, and protective clothing (lab coat, disposable mask and gloves) must be worn during use. After use, the solution itself and the fluids used to flush it away are disposed of via the laboratory sink, washed down with copious amounts of tap water. Syringes, needles, cotton wool, gloves and masks used are disposed of into clinical waste for incineration.

3.2.2 Recording Chamber

Our recording methods have been described previously (Baker *et al.*, 1999b; Baker *et al.*, 2001). The procedure for each monkey was as follows. Briefly, during a surgical procedure, a small craniotomy (typically 10 mm in diameter) was made above the area from which recordings were to be taken, and a stainless steel chamber was implanted. Chamber position was guided by a previous MRI scan. The chambers have a rather shallow lower section (height only 3.5 mm) that was seated into the surrounding bone so that the upper surface of the chamber (with the lid detached) was about 5 mm from the dural surface. The lid was designed to give additional height to the chamber when it was sealed so that the entire craniotomy could be protected and bathed in sterile saline when

the chamber was closed and filled through holes in the lid. The shallow chambers allow easy access to the dura both during the initial surgery, and later during the recording period whilst the monkey was awake and headfixed.

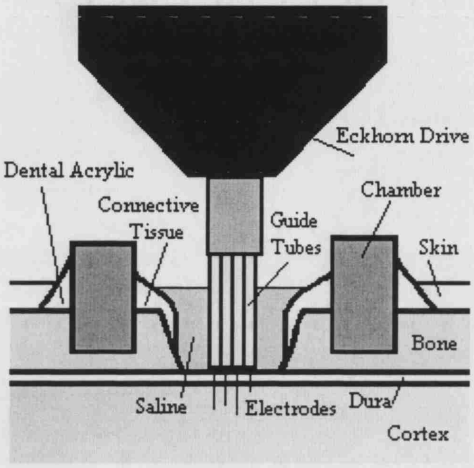

Figure 3.1 Schematic diagram to show the arrangement of the chamber and Thomas Recording multiple electrode drive during recording.

3.2.3 Preparation for Recording

At the beginning of each recording session, the small area of the chamber to be recorded from had to be prepared for electrode penetration. After opening the chamber, any superficial connective and loose agranular tissue that had accumulated was removed under a binocular microscope using gentle suction applied to a fine glass sucker (tip diameter around 1.5 mm), together with a pair of fine watchmakers forceps and a fine, 90°, 6mm corneal hook. This was not normally painful to the animal and the monkeys did not usually show any signs of discomfort whilst clearing this small area. Once the chamber was prepared, the electrodes could be inserted and the recording session commenced. The mechanical mounting of the electrode drive wass such that the entry of electrodes through the dura could be examined directly under a binocular microscope.

This, along with the monitoring of the electrode alignment and electrophysiological activity from the electrode tip, revealed any excessive dimpling of the dura by the electrode.

3.2.4 Removing Excess Fibrous Tissue

This tissue was removed after most recording sessions with the objective of clearing a new area of dura in preparation for the next session. Once the electrodes and drives had been removed, a local anaesthetic cream (EMLA, Astra Pharmaceuticals Ltd.) was applied so as to cover the exposed dura and connective tissue and this was left in place for five mins; the cream was then aspirated and the chamber flushed with sterile saline. This application helped to minimise any discomfort felt by the monkey during contact with the dura. The use of local anaesthetic is most often necessary when working close to a large dural blood vessel (e.g. middle meningeal artery). Dural nociceptive fibres are known to be positioned predominantly close to such vessels (Wolff, 1963).

Under microscopic examination, fibrous tissue was removed from the chamber using gentle suction, the corneal hook, straight watchmaker's forceps and a pair of miniature opthalmic surgical scissors. It was often necessary to peel back layers of fibrous tissue that can accumulate above the dura. Even when treated with 5FU, this tissue can be very robust and tough enough to prevent electrode entry. However, it is rather avascular, and there was little blood loss during the removal procedure. Once the translucent blue-white appearance of the underlying dura had been revealed by removing the fibrous layers above it, there was no need to continue stripping off any further layers, since this may result in tearing of the dura. Once the dura had been stripped of the new growth and the dura could be clearly seen, it was flushed and all fluid aspirated. In this way, a chamber is prepared for treatment with 5FU.

3.2.5 Treatment with 5FU

Sufficient 5FU solution to cover the exposed dural area was drawn up using a syringe and hypodermic needle from the container. The exact amount required varied, depending on the depth, size and angle of the chamber, but a typical quantity was 0.5 ml in a circular chamber of internal diameter 12 mm, depth 5 mm from the surface to the dura. If the chamber was at an angle, a small piece of sterile cotton wool was placed in the chamber to soak up and distribute the 5FU, as it was important that the solution covers the entire dura and other tissue within the chamber. The 5FU was then applied carefully to the dura, ensuring in particular that there was no spillage onto the skin surrounding the chamber. The solution of 5FU was left for five min for optimal suppression of tissue growth, as is common practice for its use in wound healing after ophthalmic surgery (Wilkins *et al.*, 2000; Merriman *et al.*, 2001). After this time, the 5FU was removed from the chamber using the glass sucker. The chamber was then thoroughly flushed with a large volume of sterile saline which was also aspirated to a safe container; typically ~30 ml was used direct from a sterile infusion bag. The chamber was then closed and the monkey returned to its home cage. 5FU was never applied at the beginning of a recording session, but used at the end of the session, immediately after the excess connective tissue had been removed.

3.2.6 Frequency of Use

The first application of 5FU was made on the day of the chamber surgery when the dura was first exposed. After this, three times per week was sufficient to maintain successful suppression of growth - it has been shown that a single dose of 5FU causes suppression of fibroblast proliferation for 3 or more days after application (Merriman et al. 2001).

3.2.7 Safety Procedures

In addition to the safety precautions referred to above, additional measures were taken to ensure that 5FU only came into minimal contact with dura and connective tissue in the chamber. The exposure time in the chamber was restricted (5 mins) and most importantly, a thorough flush of saline was used to completely remove it. It was also important to try to reduce the risk of 5FU crossing the dura during application. For example, if after several months of recording in the same chamber, repeated 'picking' or 'stripping' of the dura caused a minor tear or herniation of the dura, the 5FU protocol was stopped until it had healed. This usually took around one week. Although there is no known toxic effect of 5FU on the central nervous system, these measures seemed prudent to avoid the risk of unnecessary uptake, which could lead to unwanted actions or systemic side effects.

3.3 Results

Observations were gathered over a 6-year period, from 10 monkeys, and from a total of 33 chambers implanted on these monkeys. Typically, the period of active recording within a chamber was around 15-30 weeks, and 5FU was applied throughout this period.

3.3.1 General Observations

No behavioural problems resulting from the application of 5FU were observed, nor any neurological deficits that might have arisen, for example, from damage to motor cortex. None of the known side effects listed by the manufacturer were observed. The topical doses and concentration of the 5FU used are respectively smaller and lower than those used routinely in trabulectomy surgery, where there is topical application to the eye and supplementary injections where needed (Mora *et al.*, 1996). The use as described here

was therefore well within current safety margins for humans. The treatment appeared to be more effective in some animals than in others. Prior to using 5FU, infections occurred occasionally within chambers. Since using the 5FU protocol, there was not a single occurrence of infection in a chamber. This was probably due to 5FU suppressing any potential bacterial proliferation.

3.3.2 Electrophysiology

The use of 5FU causes no detectable deterioration in the quality of the either single neurone or local field potential (LFP) data during the recording period in a given area. Initial recording data from a given chamber was qualitatively the same as that obtained towards the end of the recording period in that chamber, which was often 3 or more months later - after at least 35-40 applications of 5FU.

To make a quantitative assessment of any effects of 5FU on the electrophysiology of the primary motor cortex (M1), data recorded in two adult purpose-bred monkeys (*M. mulatta*) was compared. Both monkeys had been trained to perform a precision grip task, and recordings were made from M1. Neurons were identified antidromically as pyramidal tract neurons (PTNs) by stimulation of the medullary pyramidal tract (biphasic current pulse, each phase 0.2 ms duration; see Baker et al., 2001). At the sites from which PTNs were recorded, the threshold for evoking hand or finger movements by repetitive intracortical microstimulation was determined (rICMS: 13 biphasic pulses at 300 Hz pulse, each phase 0.2 ms duration, with a cycle period of 1Hz).

In the control monkey (M24), recordings were made with conventional single-electrode techniques, using glass-insulated Pt-Ir electrodes. A total of 68 PTNs were recorded in 48 separate sessions from the right hemisphere (chamber 1); this took 20 weeks in all; subsequently a further 60 PTNs were recorded in a further 43 sessions from the left

hemisphere (chamber 2) and this took 23 weeks. In the second monkey (M36), 5FU was routinely used in the cortical chamber throughout the recording period. In this monkey, a total of 154 PTNs were recorded in 30 sessions from the right hemisphere (chamber 1) and this took 12 weeks. A further 196 PTNs were recorded in 55 sessions from the left hemisphere (chamber 2) and this took 22 weeks. Thus in M24 the average yield of PTNs was 1.4 per session (128/91), compared to 4.1 in M36 (350/85), and the yield was 3.0 PTNs per week in M24 vs. 10.3 in M36. These figures confirm the major increase in the yield of neuronal data using a multiple vs. single electrode technique. They also demonstrate that PTNs were commonly encountered in cortex immediately beneath 5FU-treated dura.

Four different criteria were investigated: the antidromic latency, threshold and depth of identified PTNs, and repetitive intracortical microstimulation (rICMS) thresholds. Data was compared from M24 (no 5FU) with M36 (5FU). For M36 comparisons were also made between data collected during the first (early) and second (late) half of the recording period from a given chamber.

3.3.2.1 Antidromic Latencies

The antidromic latency (ADL) of a PTN covaries negatively with the size of neuron (Humphrey & Corrie, 1978). If 5FU, for example, selectively damaged large pyramidal neurons, one would expect to see an increase in the mean ADL after treatment with 5FU. As Figure 3.2 shows the distribution of ADLs was, in fact, unaffected by use of 5FU. The range of ADLs in PTNs recorded in the two untreated chambers of M24 were 0.6-5.2 ms and 0.6-4.2 ms respectively, while for the 5FU treated chambers in M36, the ranges were 0.7-3.9 ms and 0.4-4.4 ms. The mean antidromic latency was significantly shorter in the 5FU-treated animal than in the control (1.2 ± 0.7 ms vs. 1.6 ± 1.3 ms, $P<$

0.01, t-test). The mean values are highly skewed by the higher proportion of slow PTNs (ADL > 2.0 ms) that were targeted in the M24 study (see Bennett & Lemon, 1994). In M24 these comprised 22%, but only 8% in M36. When the distribution of fast PTNs (ADL < 2.0 ms) only was compared, there was no significant difference (mean ADL 1.1 ± 0.3ms in both monkeys). In M36, there was no significant difference between the mean ADL for early *vs.* late recording periods in either of the chambers (mean 1.2 ± 0.6 ms, n=83 PTNs vs. 1.4 ± 0.5 ms, n=71) for chamber 1 and (mean 1.3 ± 0.9 ms, n=96 vs. 1.1 ± 0.6 ms, n=100) for chamber 2 (see Figure 3.2).

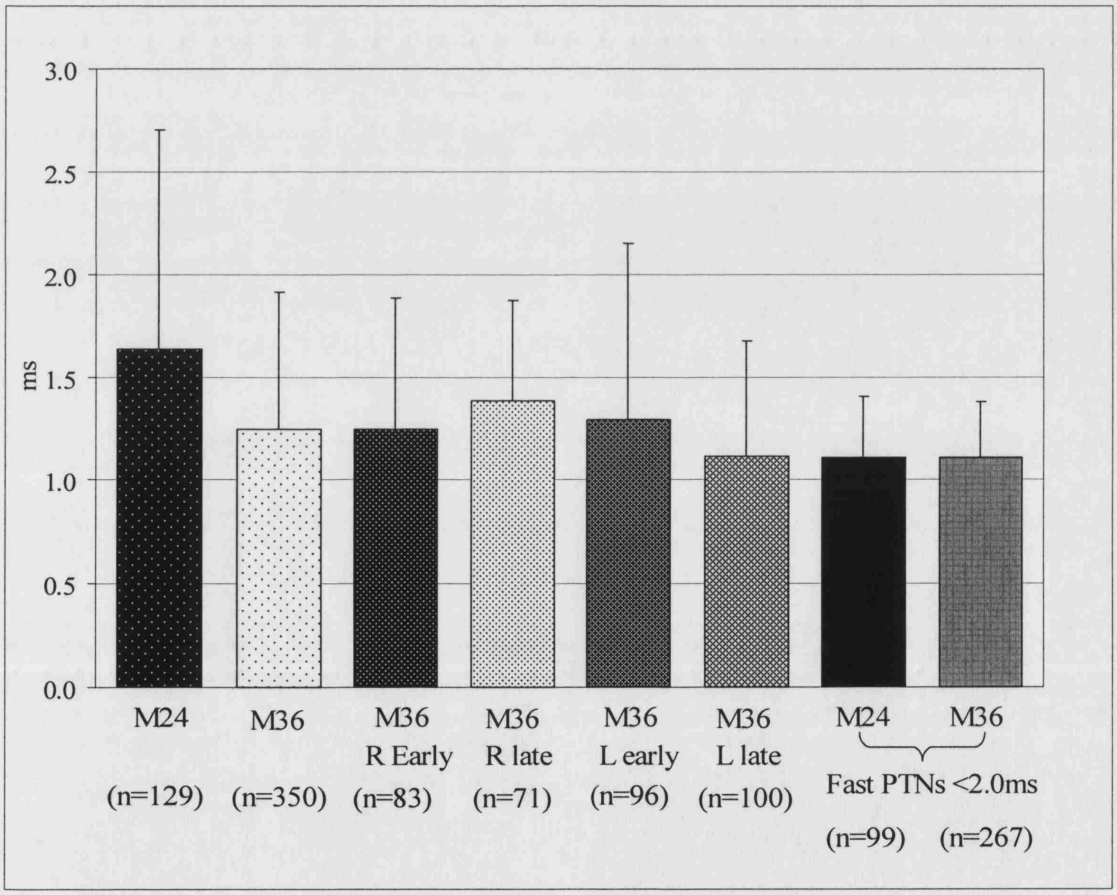

Figure 3.2 Mean antidromic latency (±SD). Data is shown from 2 monkeys, and for the early and late parts of recording in both M36 hemispheres. A further comparison is made between the two monkeys for 'fast' PTNs with ADLs of <2.0 ms.

3.3.2.2 Antidromic Thresholds of PTNs

The antidromic threshold of a given PTN is influenced both by the size of the axon and the precise location of the PT stimulating electrodes relative to the axon (Lemon, 1984). If 5FU damaged PTNs in any size-dependent manner, the mean antidromic threshold might be affected. However, in neither animal was there any significant correlation between ADL and antidromic threshold, and it is therefore questionable whether such damage would have been detected by a change in threshold.

3.3.2.3 Depths of PTNs

If 5FU damaged the cortex it might be expected to affect the more superficial layers first, which would be closest to the epidural sites of 5FU application. This should result in PTNs, located in layer V, being encountered at shallower depths after 5FU treatment. Depths of PTNs were measured relative to the point at which neuronal activity as first detected after transdural penetration. In M24, PTNs were recorded over depths varying from 0.8 to 6.3 mm; the mean depth was 3.4 ± 1.6 mm (see Fig. 3.3). In the 5FU treated monkey (M36), PTNs were again recorded between 0.8 and 6.3 mm, but the mean depth (2.3 ± 0.6 mm) was significantly shallower ($P < 0.001$). In addition, in M36, there were some small but significant decreases in the mean depth of recorded PTNs from the first half to the second half of the recording period (Fig. 3.3): from 2.2 ± 0.6 mm to 2.0 ± 0.4 mm in chamber 1 ($P < 0.01$) and from 2.7 ± 0.7 mm to 2.4 ± 0.7 mm in chamber 2, ($P < 0.02$). These differences may reflect 5FU-induced changes in the recorded cortical tissue, although other factors must be taken into account, including the location of penetrations (anterior bank of central sulcus vs. precentral convexity of gyrus) and differences in the type of electrode used and amount of dimpling (discussed later).

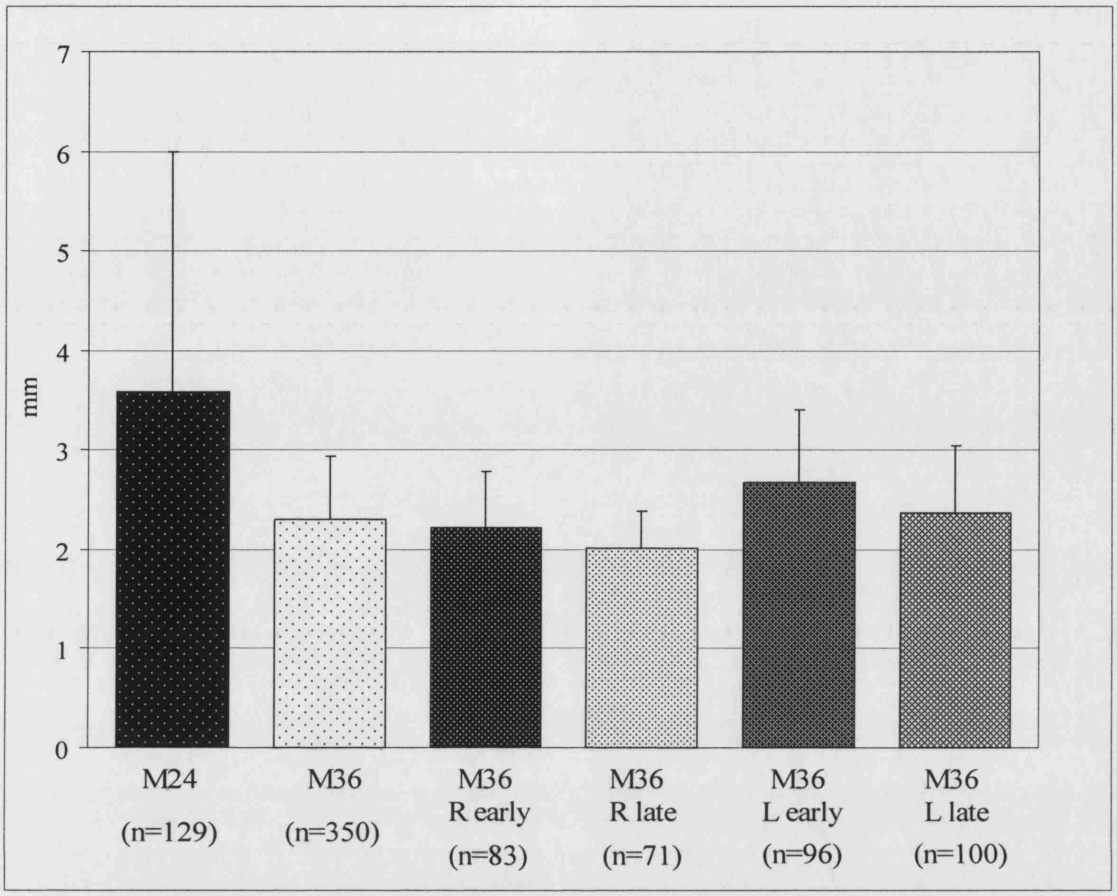

Figure 3.3 Mean depth (± SD) at which PTNs were recorded.

3.3.2.3 rICMS Thresholds

Movements evoked by rICMS in M1 depend upon complex trans-synaptic activation of PTNs and require the integrity of both superficial and deep cortical layers (Asanuma & Sakata, 1967; Stoney, Jr. et al., 1968; Jankowska et al., 1975; Lemon et al., 1987). Thresholds for these effects might be expected to be very sensitive to any damage to the cortical neuropil by 5FU. However, there was no significant difference in the mean rICMS threshold for hand and finger movements in the two monkeys: in M24 the mean threshold was identical in both chambers at 12.9μA (SDs 6.3 and 6.5, n= 32 and 28 sites, chamber 1 and 2, respectively). This is shown in Fig. 3.4. In M36 the mean thresholds for each chamber were 15.7 ± 4.9 μA (n= 115 sites) and 13.0 ± 5.1 μA (n= 162 sites).

There was no significant difference overall between the threshold in M24 compared to that in M36 (Students T-test, P= 0.15). In M36, the average threshold for rICMS effects showed a small but insignificant decrease from the first to the second half of the recording period. For chamber 1 it decreased from 13.3 ± 4.8 μA (n=64) to12.9 ± 5.4 μA (n=98), and for chamber 2 it fell from 16.9 ± 4.6 μA (n=47) to14.8 ± 4.9 μA (n=68). Thus these data suggest that 5FU had no demonstrable effect on the mean rICMS threshold.

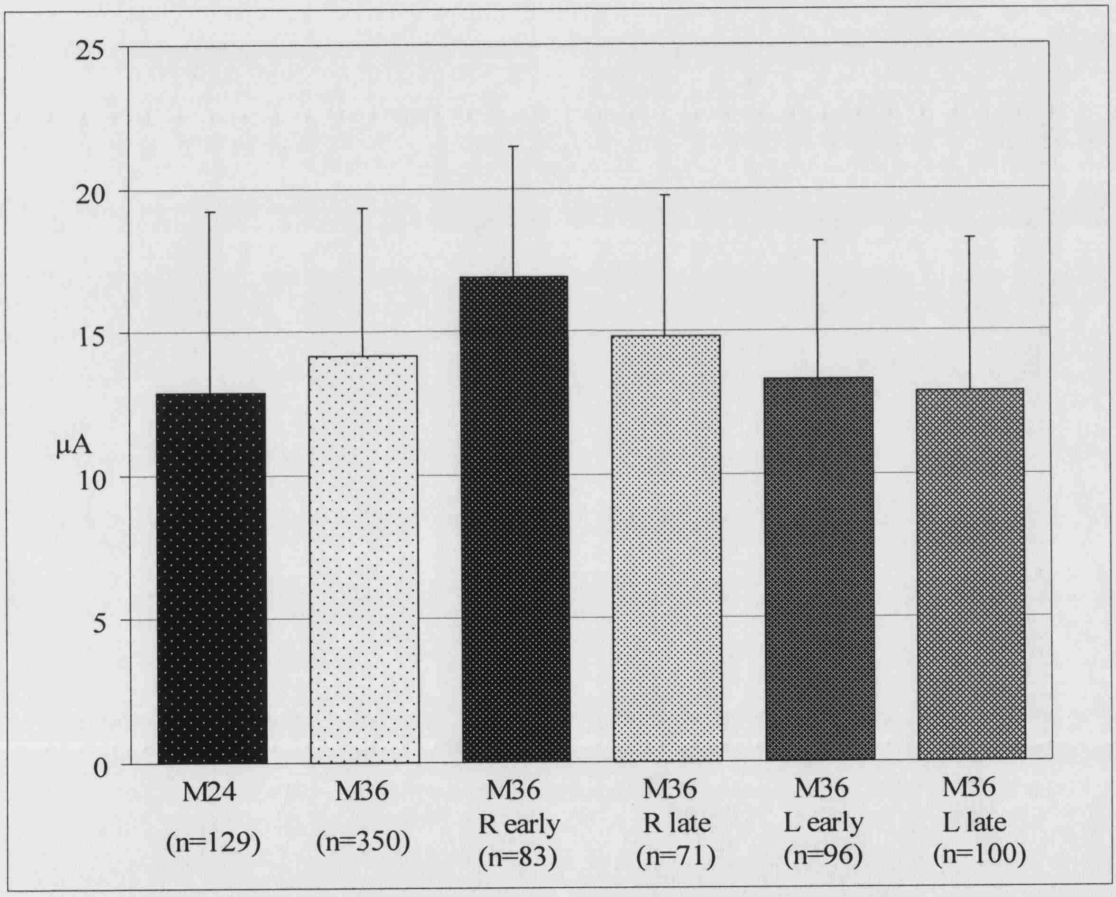

Figure 3.4 Mean thresholds for evoking hand and finger movement by rICMS

3.3.3 Histology of Cortex Underlying 5FU-Treated Dura Mater

To confirm that no abnormalities of the cortex were present, a histological analysis of the cortical tissue underlying the 5FU treated dura was undertaken. In M36 the analysis was carried out on blocks of primary motor cortex (M1) from the left and right hemispheres. This cortical tissue was accessed through chambers in which the dura had been treated approximately three times per week for 32 and 13 weeks, respectively. As can be seen from Figure 3.5A, the histological appearance of the M1 cortex was normal. The major distinguishing features of M1 are clear to see, including the thickened cortex and presence of large pyramidal (Betz) cells in the deep part of lamina V. Note that the superficial layers also have a normal appearance. In the left M1, a small (100 nL) injection of the tracer biotenylated dextra amine (BDA, 10% in saline) was made in the anterior bank of the central sulcus three days prior to sacrifice of the monkey. Figure 3.5B shows a section through M1 taken a few mm away from the injection site and showing several retrogradely labelled pyramidal neurones. This established that normal axonal transport was present in these neurones. Cortical tissue from two other 5FU-treated monkeys was also examined, and appeared normal.

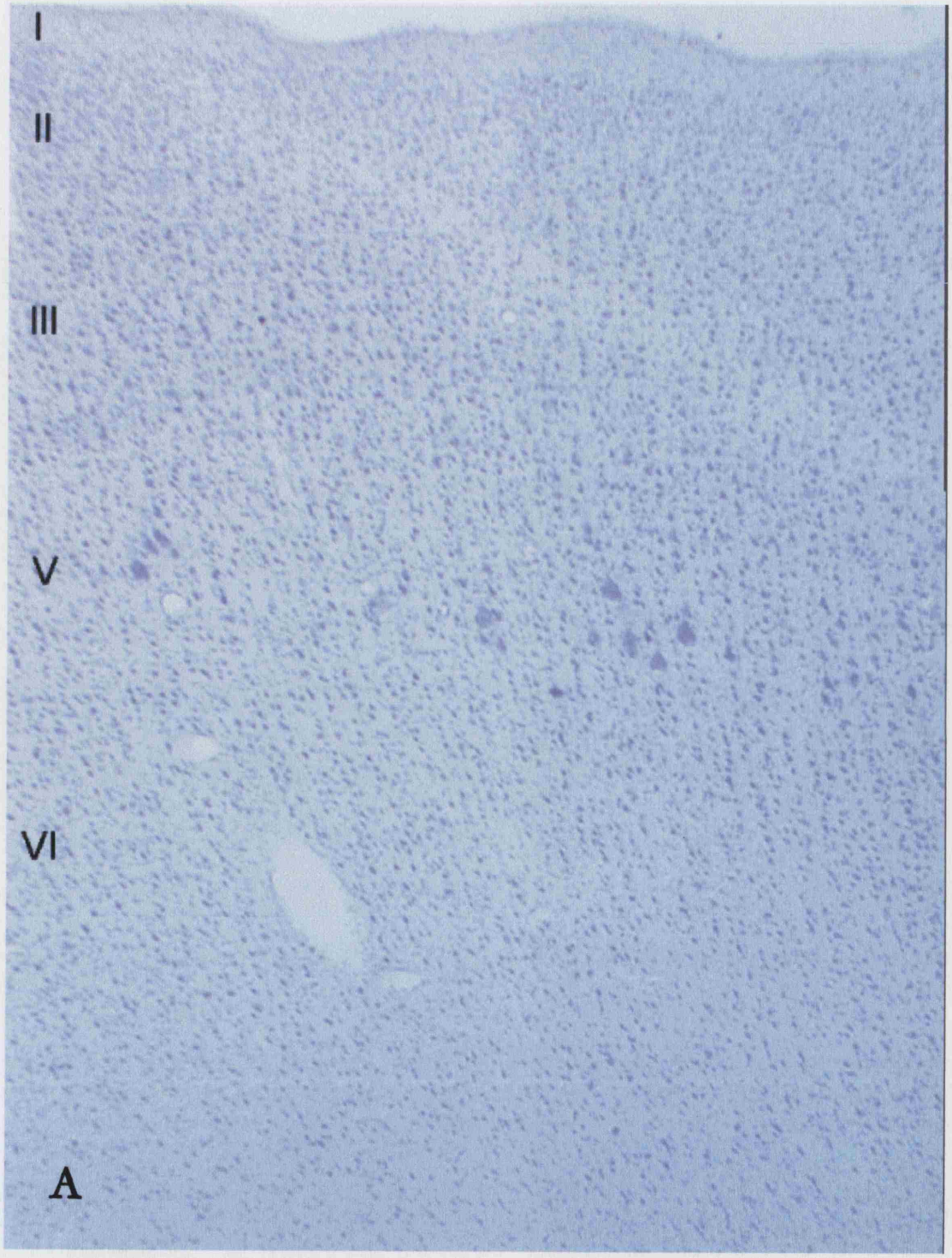
I
II
III
V
VI
A

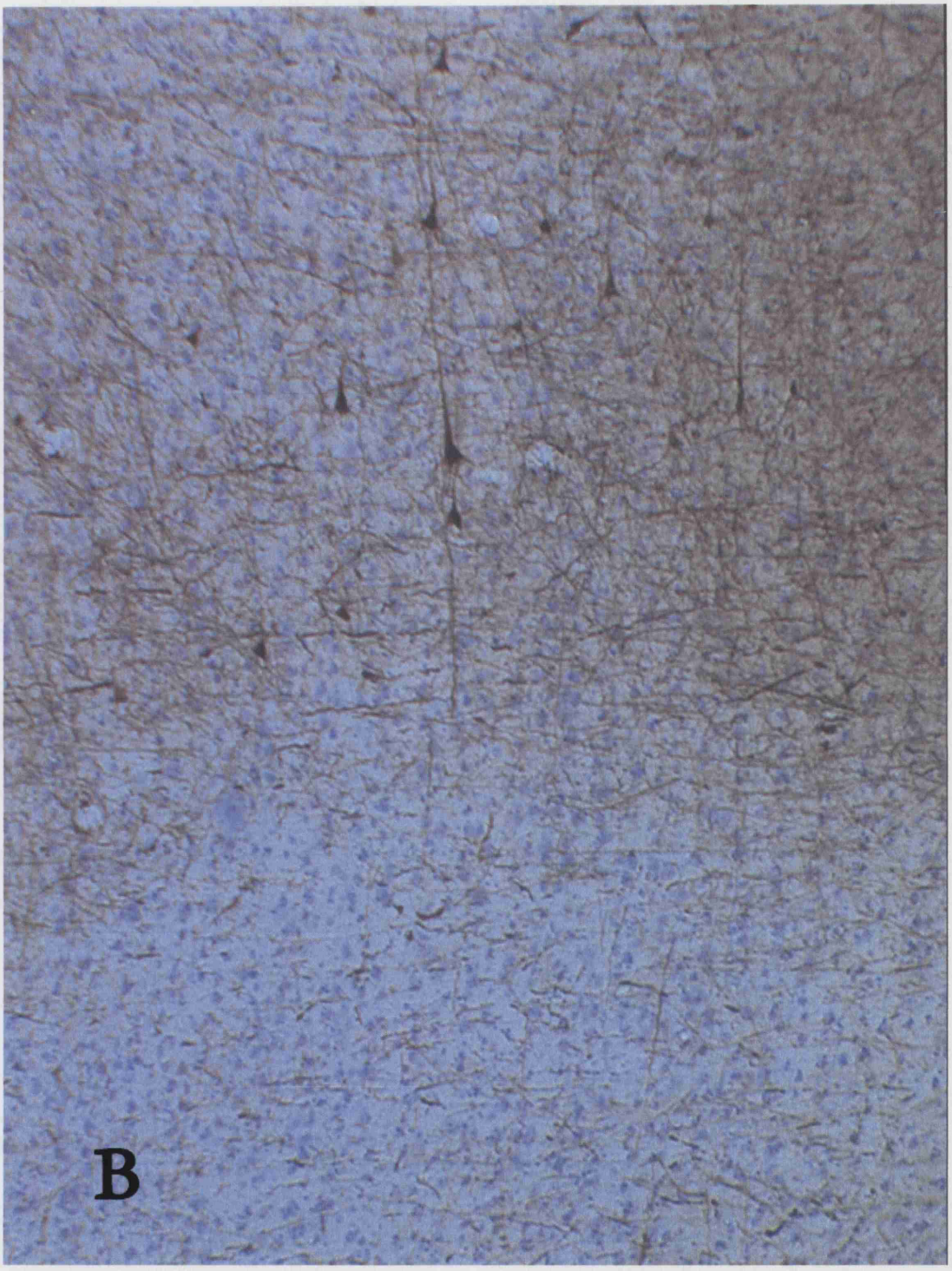

Figure 3.5 Post-mortem histology (M36). A. Nissl stained transverse section through the convexity of the left precentral gyrus showing lamination of cells in primary motor cortex, with laminae I-VI labelled. **B.** High power image of the convexity of the right primary motor cortex showing BDA labelling resulting from an injection of BDA a few mm away within the anterior bank of the ipsilateral central sulcus.

3.3.4 Effects on Recorded Data Yield from Monkeys Treated With 5FU

The use of 5FU improved the efficiency of recording sessions, and increased the total yield of data from each chamber. Prior to the use of 5FU, recording periods had to be interrupted approximately every two weeks to perform a surgical strip or removal of excess tough connective tissue in the chamber. This was carried out under general anaesthetic or deep sedation. This meant a smaller number of sessions over a given period, compared with that which is possible with 5FU treatment. With 5FU treatment, it is possible to continue recording within a given chamber for much longer periods before such an operation became necessary. For example, in M36, major dura 'strips' under sedation were carried out roughly once every six weeks, a period three times longer than the average without 5FU use. These operations were generally rather straightforward, largely because the suppression by 5FU of tissue growth and vascularisation within the chamber substantially reduced the amount of bleeding.

3.3.5 Electrode Usage and Breakage When Using 5FU

There are two main causes of electrode breakage when using the Thomas microdrive – the major one is attempting to penetrate tissue that is too tough or thick, and the other is operator error during loading and unloading of electrodes from the drive. It would have been ideal to compare the experience of using the Thomas multiple electrode recording system in chambers with and without treatment with 5FU. This might have yielded a better comparison than with data obtained using conventional single electrode methods, as reported above. However, such a comparison was not possible because within two weeks of exposing the dura at the start of new recording period, it becomes virtually impenetrable to the fragile Thomas electrodes. Indeed, it has been found that unless the dura was stripped every two weeks or so under anaesthetic, recording became

impossible and many or most electrodes were damaged; based on a small sample of recordings, it was only possible to use each electrode on average for less than two recording sessions before it broke or failed. This is in contrast to recording in M36, when each electrode lasted an average of 8.5 sessions (± 4.6, range 1-22 sessions).

3.4 Discussion

The benefits of treating the dura in recording chambers when microelectrodes are to be used appear to be fourfold. The first and major advantage is that because 5FU suppresses fibroblast growth in the chambers, dural penetration with the microelectrodes is easier. There is therefore less damage to the cortex (due to excessive downward pressure or dimpling when attempting to penetrate tough dura) and to the electrodes (which frequently break during such attempts). Secondly, with 5FU treatment, it is possible to carry on successful recording sessions for longer periods than for untreated dura, with fewer interruptions for surgical removal of connective tissue build up. The reduction in the number of procedures under anaesthesia represents a considerable improvement in animal well-being, and leads to improved task performance, and also greater recording time. Thirdly, because 5FU affects tissue regrowth and vascularisation, these operations to 'strip' or 'scrape' the dura are relatively easy and avascular. Finally, the antimitotic properties of 5FU appear to help in controlling bacterial infections within the recording chamber.

The advantages of 5FU treatment are reflected in the excellent yield of high-quality data recorded simultaneously from single neurons in different cortical motor areas (see Baker *et al.*, 1999a; Baker *et al.*, 2001; Baker *et al.*, 2003; Baker & Lemon, 2000). Because 5FU is a powerful anti-mitotic agent, it is important to be sure that it has no deleterious

side-effects either on the cortex or on the monkey's general health. The use of 5FU for the reduction of dural scarring came about as a result of its use in suppressing scars following operations on the sclera for glaucoma and other ophthalmological disorders (Smith *et al.*, 1992; Asaria *et al.*, 2001). This treatment, which is now very widely used in ophthalmology clinics, has not resulted in any reported retinal damage or deficit, which might be expected if 5FU had toxic actions on neurons. Moreover, there is a wealth of literature on its use in cancer treatment, which involves the administration of systemic doses without any CNS side-effects. No signs of unwanted side-effects in either the cortex or the monkey's general health and well-being have been observed since 5FU use began.

No obvious deleterious changes in either the electrophysiology or histology of the cortex underlying dura treated regularly for long periods with 5FU have been shown. For example, the studies of identified PTNs, the antidromic threshold and recorded depths of these neurons was very similar in M1 cortex beneath 5FU-treated dura and in a control experiment in which PTNs were recorded with conventional techniques and without 5FU treatment in the chamber. In addition, no obvious changes were seen in the properties of the neurons recorded in the early phase of 5FU treatment (in the first weeks after the chamber had been implanted) compared with those sampled during later periods of recording towards the end of the chamber. There was a high yield of properly identified PTNs in 5FU-treated chambers and close similarity of thresholds for rICMS evoking hand and digit movements in monkeys with and without 5FU treatment. Since the production of such movements depends upon the activation of complex local circuits leading to repetitive discharge of corticospinal neurons, it is assumed that any damage

caused by 5FU should reflect an increased threshold for rICMS effects. This was not the case (Figure 3.4).

There were some small changes in the mean depth at which PTNs were recorded, being significantly deeper in the control cortex (monkey M24) than in the 5FU treated monkey (M36, see Fig. 3.3). This might have implied damage of superficial layers in the treated monkey, such that PTNs were encountered at shallower depths than in the control. However, no loss of superficial layers after 5FU was observed (see Fig. 3.5A, B). The difference in PTN depths could result from other factors: for example, the proportion of tracks made in the convexity of the precentral gyrus, where the deepest PTNs are encountered at depths up to ~3 mm, compared to those made in the anterior bank of the central sulcus, where PTNs can be encountered up ~6 mm. Further, it is possible that the larger conventional microelectrodes used in the control monkey may actually have caused more damage to the relatively superficial layer V PTNs, and deeper penetrations were required to find other PTNs.

3.6 Conclusions

This evidence suggests that use of 5FU as an anti-mitotic agent to control the growth of tough extradural connective tissue is a safe and useful method with several advantages. It refines the method of single neuron recording from awake, behaving monkeys, and reduces the number and severity of procedures. It can improve the amount and quality of data collected from a given area, and reduces both the time taken and cost of electrodes. No evidence was found that treatment along the lines described here damages or otherwise changes the properties of the underlying cortical tissue. 5FU is now part of the standard laboratory protocol. Several other labs around the world are also now using it.

It may also be of use in other situations where there is dural scarring after surgical intervention or injury.

Chapter 4. Analysis of LFPs in the Motor Cortex

4.1 Introduction.

There are many ways to study the function of the brain. Although studies on single cells provide considerable information about what an area does, they do not provide the whole picture. Neurons do not act independently, but by their many connections. There is considerable divergence and convergence of cortical connectivity such that each neuron receives a large number (~60000) of relatively weak inputs from numerous pre-synaptic cells and conveys output to a correspondingly large number of targets (~12000) (Abeles, 1991). Another approach to the understanding of brain function therefore comes from the study of neurons at the assembly level, either in a highly localised way (e.g. within a single cortical area), or on a larger scale (e.g. in a network of areas). For the motor system, the synchronous, activity of many neurons and the activity of more localised neuronal assemblies have been studied using the electro-encephalogram, (EEG), (Halliday *et al.*, 1998) and magneto-encephalogram (MEG), (Conway *et al.*, 1995). These approaches detect the synchronised activity of many neurons to provide a large, non-invasively measurable signal which can be recorded at the scalp. This has many advantages, in particular its non-invasive nature which allows it to be used on human subjects and patients. However, MEG and EEG do not have a very high spatial resolution (typical spacing approximately 20-25 mm for standard EEG, Halliday *et al.*, 1998, and 5 mm for MEG, Lounasmaa et al., 1996). MEG and EEG surface recordings can therefore be complemented by the invasive, intra-cortical recording of local field potentials (LFPs).

Local field potentials are a reflection of the summated spiking activity of neurons local to the electrode, and both inhibitory and excitatory post-synaptic potentials in the dendrites contributes to the potential. Using closely spaced microelectrodes inserted through the dura to record these LFPs allows a much more localised signal to be recorded from the area of interest, and the spatial resolution is much higher than for MEG and EEG. Whichever method is used, these more global signals provide a valuable insight into the functioning of the brain. Oscillatory activity in these assembly recordings was noted in the early work of Berger in 1929 (reviewed by Gloor, 1969). Oscillations occur when neuronal activity becomes highly synchronised, and may be related to information processing within the area. Activities in separate areas can become synchronised and phase-locked, leading to coherence. This may provide a way in which activity patterns in spatially separate regions of the cortex can become temporally coordinated. This was highlighted by Gray & Singer (1989), when they showed that stimulus-specific synchronous oscillations could result from such an intracortical mechanism.

Oscillations are widespread, having been observed and studied throughout the brain. They have been studied in the visual cortex (Eckhorn *et al.*, 1993; Bekisz & Wrobel, 1993; Kayser & Konig, 2004), the motor cortex (Murthy & Fetz, 1992; Baker *et al.*, 1999a; Conway *et al.*, 1995), the cerebellum (Courtemanche *et al.*, 2002; Pellerin & Lamarre, 1997), the hippocampus (Buzsaki, 2002) and many other parts of the brain. The frequencies at which these oscillations are found vary considerably, from the fast gamma to the slower alpha and theta rhythms.

In the visual cortex, LFPs have been found to be stimulus-locked in specific frequency bands to such features of the stimulus as orientation, spatial and temporal frequency

(Gray & Singer, 1989; Kayser & Konig, 2004). This property of the LFPs has been described as 'tuning' to these features, and suggests that the oscillatory power of the LFPs at particular frequencies was related to the processing of visual and sensory stimuli. In the auditory cortex, tuning curves of LFPs to auditory stimuli of different frequencies have been established (Galvan *et al.*, 2001), suggesting that here also, LFPs show tuning. LFPs recorded from the lateral intraparietal area are spatially tuned in the gamma frequency band to the direction of a saccade (Pesaran *et al.*, 2002), but the tuning of motor cortical LFPs to task parameters has not been studied extensively. Mehring and colleagues (2003) studied LFPs in the motor cortex during a centre-out reaching task, and found a directional tuning to be present for both the contra- and ipsilateral hand. They also found that on a single trial basis, multiple LFPs could be decoded to predict the movement target with the same degree of accuracy as multiple single units recorded on the same electrodes. Parameters such as hand used, direction of movement and hand speed could be decoded from the multiple LFP signals, demonstrating that motor cortical LFPs can be tuned to task parameters in the same way as visual and auditory LFPs. However, tuning to other relevent motor task parameters has not been established.

Oscillations can be studied from a specific area in isolation. However, the relationship between two oscillatory signals may also be studied using coherence analysis. This is a mathematical measure of the linear dependence of two signals in the frequency domain (described by Challis & Kitney, 1991) and therefore identifies the degree to which two signals contain a common oscillatory frequency from a common source. Two coherent signals therefore signify a common frequency of phase-locked oscillations, and the

relative phases of the signals and the delay between them indicates which signal precedes the other and by how much.

4.1.1 Oscillatory Activity in the Motor Cortex

In the motor cortex of both humans and monkeys, the most prevalent activity is in the beta range of 15-30 Hz (Hari & Salenius, 1999; Baker *et al.*, 1997; Conway *et al.*, 1995; Sanes & Donoghue, 1993; Donoghue *et al.*, 1998; Murthy & Fetz, 1992; Murthy & Fetz, 1996b). These beta oscillations are related to a variety of motor tasks and behaviours. Generally, cortical beta oscillations are found to be suppressed during movement, and to have a rebound increase during the following period, often a static posture or at rest. These phenomena are often described as event related desynchronisation (ERD) and synchronisation (ERS) respectively. For example, Sanes & Donoghue (1993), used a wrist flexion/extension task in macaque monkeys. They reported pronounced beta oscillations during the static, pre-movement phase; these were suppressed during movement, and reappeared after the monkey had successfully moved to the final position. Other studies have focused on a precision grip task, involving the use of the index finger and thumb to squeeze two levers into a position window and requiring a steady force to be generated. The grip requires activity in a relatively small number of distal muscles to achieve successful performance (Maier & Hepp-Reymond, 1995). In the first of a series of studies beginning in 1997, Baker et al. showed that during such a precision grip task, LFP oscillations recorded in the primary motor cortex of the macaque were particularly prevalent during the period of steady grip, when the hand posture was maintained and a steady force required to hold the levers in a position window. In human subjects, Salmelin & Hari (1994), found that during self-paced thumb movements, cortical 20 Hz oscillations recorded with MEG were suppressed during

movement and increased afterwards once movement was completed. The common factor for the appearance of cortical oscillations appears to be a static posture either before or after movement; they are absent during a goal directed movement.

4.1.2 Possible Roles for Oscillatory Activity

Post-movement ERS has been interpreted in several ways. One possibility was put forward by Pfurtscheller *et al.* (1996), who suggested that as the beta oscillations were suppressed during movement but returned after, they could be interpreted as an 'idling rhythm' of the inactive cortex. Another is that they represent an efficient output for the production of a stable set of motor commands such as are required for either a steady posture such as grasp, or at rest (Baker *et al.*, 1999a), that is to say when the cortex is not merely 'idling' but is involved in tasks where muscles are active and therefore a cortical drive may be present.

Kilner *et al.* (1999), used a precision grip task in human subjects, and found beta oscillations in MEG recordings from the motor cortex contralateral to the hand and in EMG recordings made in the active hand and arm muscles. MEG and EMG were recorded simultaneously, and the oscillatory activity was shown to be coherent in the beta range, showing a functional relationship. This study also reported a lack of oscillatory activity during movement of the digits, but clear coherence during steady grasp. This coherence between cortex and muscles suggests that the oscillatory drive from the motor cortex is relayed to the muscles. The phase lags between cortex and muscle can be consistent with conduction via the corticospinal pathway (Mima et al., 2000; Gross et al., 2000), although other studies have found this not to be the case (Salenius *et al.*, 1997b). Coherence has been found to be generally stronger with more distal muscles, such as the intrinsic hand muscles (Kilner *et al.*, 2000). The more distal

muscles also have more direct cortico-motoneuronal connections, possibly suggesting a link between direct CM connections and higher coherence.

Cortical oscillations and their coherence with muscle have also been correlated with other task parameters. The compliance of a grasped object relates directly to the amount of beta coherence between cortex and muscle (Kilner *et al.*, 2000), while there was no obvious relationship to either digit displacement or to grip force. Beta frequency ERD and post movement ERS were related to force levels in a finger extension task against a variable load (Stancak, Jr. *et al.*, 1997). Thus the physical parameters of objects in a grasping task such as shape, size or compliance may therefore be expected to have an effect on beta oscillations and their power in the motor cortex.

Cerebellar oscillations have also been reported during motor tasks (Courtemanche *et al.*, 2002) and coherence between motor cortex and the cerebellum has also been reported during a precision grip task (Jackson, 2002), suggesting a possible cerebro-cerebellar oscillatory drive. The basal ganglia also show modulation of beta oscillations during motor tasks in macaques (Courtemanche *et al.*, 2003).

There is therefore much evidence to suggest motor cortical oscillations may have a role in the maintenance of a stable grip, or resting posture, both directly through their drive to the muscles, possibly via corticospinal pathways, and also via cerebro-cerebellar and cortico-cortical pathways.

There are other interpretations for the role of cortical oscillations. Murthy and Fetz (1996a) have reported 25-35 Hz oscillations in the primate motor cortex, and observed that they are present during movement. They were present most frequently during free, unconstrained movements when reaching for objects outside of the visual field, but less often while the monkey was at rest. They concluded that oscillations may not be related

to the movement *per se*, but represent a neural correlate of the attentional demands made by performing a complex movement. Kristeva-Feige *et al.* (2002) investigated the effect of the level of attention on the beta coherence between EEG and EMG in human subjects performing a controlled force production task. They found that when attention was focused on the motor task being performed, synchronization between cortex and muscle was highest, with coherence being non-significant when subjects divided their attention between the motor task and a mental arithmetic task. They also found that the frequency of oscillations increased as a higher level of precision in the task was required. This alternative view of the role of oscillations is not incompatible with the results described previously – attention is required for the accurate execution of the precision grip or the flexion/extension of the wrist to a target. Recordings from other parts of the brain also imply a role of oscillatory activity in attention, such as in the visual system (Bekisz & Wrobel, 1993, Wrobel *et al.*, 1994) and the basal ganglia (Brown & Marsden, 1998). However, the 1994 study by Salmelin and Hari noted earlier also found that the suppression of oscillations during movement and their post-movement rebound were also observed when the thumb movement was elicited by median nerve stimulation, albeit at a slightly reduced level, as did Pfurtscheller *et al.*, (2002). Salenius *et al.*, (1997b) not only found beta oscillations during movement generated by median nerve stimulation, but, in contrast to Murthy and Fetz (1996b), also found 20Hz oscillations were abolished during active exploration of objects and a reduction in power for even passive tactile stimulation of the fingertips. As neither the electrical nor passive tactile stimulation required attention from the subject, this would argue against the oscillations being solely related to attentional factors, but of course does not rule out their being contributory.

4.1.3 Origin of Local Field Potential Oscillations

These EEG and MEG studies are based on scalp recordings above motor cortex. Some investigators have attempted to locate the sources of beta oscillations in the cortex. Using MEG, the primary motor area is usually identified as the source of beta synchronization (Conway *et al.*, 1995; Salenius *et al.*, 1997a, Kilner *et al.*, 2000). MEG recordings are only sensitive to tangential current components of active neuronal populations (Williamson & Kaufman, 1981) as would be the case for activity in the exposed convexity of the human precentral gyrus. However, other potential sources have been found when other techniques of source reconstruction and localisation have been used, such as those which also measure radial currents. Feige *et al.* (2000) found that the generators were not only located in M1, but also in premotor areas, which have more radial current components.

4.1.4 LFPs in Motor and Premotor Cortex

When studied specifically through LFPs in primates, the premotor cortex appears to have similar properties to M1, also showing beta frequency oscillations (Sanes & Donoghue, 1993), and showing the same relation to task performance as the M1 recordings. These authors also found coherence between LFPs recorded simultaneously in M1 and premotor areas which was not correlated to the distance between electrodes, suggesting functional linkages between the areas especially during motor tasks. Murthy and Fetz (1996) found that the closer together two simultaneously recorded LFPs were, the higher the probability of significant coherence but that there was no significant phase shift with increasing horizontal separation within precentral motor cortex.

Single cell studies have found representations of physical properties of objects within F5 (Murata *et al.*, 1997). This study revealed that two main types of neuron were found

within F5; motor neurons which discharged in association with grasping movements, most of which were selective for a particular type of grip, regardless of object, and visuomotor neurons which not only discharged during grasp, but also in response to the presentation of graspable objects. Most of these showed selectivity for one or a few objects. The onset of activity in the visuomotor neurons was temporally locked to the visual presentation of the object, indicating a role in the motoric representation of the object.

The oscillatory features of single units in premotor cortex were studied by Lebedev & Wise (2000). Some units showed directional selectivity of the beta oscillations during the instructed delay period of an arm movement task, indicating the possibility of oscillations reflecting aspects of an intended action. Ventral premotor cortical LFPs have not been extensively studied, but might therefore also be expected reflect object and grasping related properties during a reach to grasp task; these may occur not only during steady grasp, but possibly during an instructed delay period. This potential role for premotor cortex oscillations is poorly understood.

Simultaneous recordings of primary and premotor areas could define whether beta oscillations in these motor areas have similar or contrasting roles during performance of a visuomotor task. It seems likely that the local field potentials of F5, in particular the beta power, may contain object-related as well as more general task-related activity. The role of oscillations, in particular their beta power, during preparation and execution of grasp of different objects has not been elucidated, nor during the motor preparation for the grasp. It was therefore decided to study the simultaneously recorded LFPs from M1 and F5 during a reach to grasp task, involving several differently shaped objects. This task also involved a period of object observation before movement was cued, allowing

us to study whether there is object-related oscillatory activity in this period of motor preparation. The objective of the study was a greater understanding of the role of beta oscillations in M1 and F5 and their interrelationship in a task which is representative of everyday visuomotor actions.

4.2 Methods

4.2.1 Subjects

The data presented here were recorded from two purpose-bred adult female *Macaca mulatta* monkeys (M37 and M39, weights 5.1 kg and 6.0 kg respectively). Before commencing training on the task, monkeys were taught to voluntarily move from their home cage to a smaller training cage and accept fruit from the experimenters. The complexity of the task was gradually increased from reaching for fruit to touching objects and equipment to receive a reward, before starting to use the full task apparatus. At various stages, the monkeys were taught to accept increasing degrees of restraint including a metal neck collar, and later, head fixation. Whenever a new restraint was introduced, 1 – 2 mg/kg diazepam (APS Ltd.) was administered orally for the first few sessions to minimise stress to the animal. All procedures were carried out in accordance with the UK Animals (Scientific Procedures) Act 1986.

4.2.2 Behavioural Task

The apparatus used was similar to one used by Murata *et al.* in 1996. It consisted of a box divided into a lower and upper half by a semi-silvered mirror, shown in Fig 4.1A.

A

B

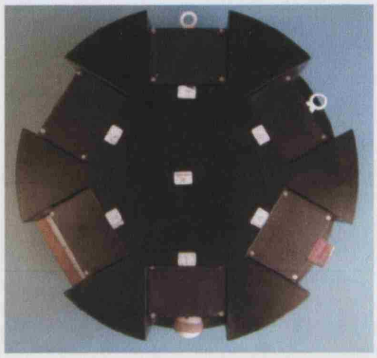

C

Figure 4.1 Black box apparatus A. Front View of Apparatus. **B.** Top view of carousel. **C.** Detail of two sectors.

The lower part contained a carousel, sub-divided into 6 sectors, shown from above after removal of the carousel from the box in B. Two sectors are shown in detail in C. Each sector contained a module, which consisted of a graspable object mounted on a low-friction horizontal shuttle with a weak spring to provide resistance. A Hall Effect sensor allowed measurement of the displacement of the object from its starting position at rest. A red-green light emitting diode (LED) was positioned in the upper part of the apparatus such that it reflected in the semi-silvered mirror and was superimposed onto the object. A computer controlled motor allowed the carousel to rotate to present different objects in a pseudorandom order. The box was positioned in front of the monkey and the objects

presented for grasping one at a time. The monkey also had two 'home pads' attached to the cage at approximately waist level, one for each hand. These were small boxes containing switches which could be closed by the application of gentle downwards pressure from the monkey's hands. The task sequence was as follows:

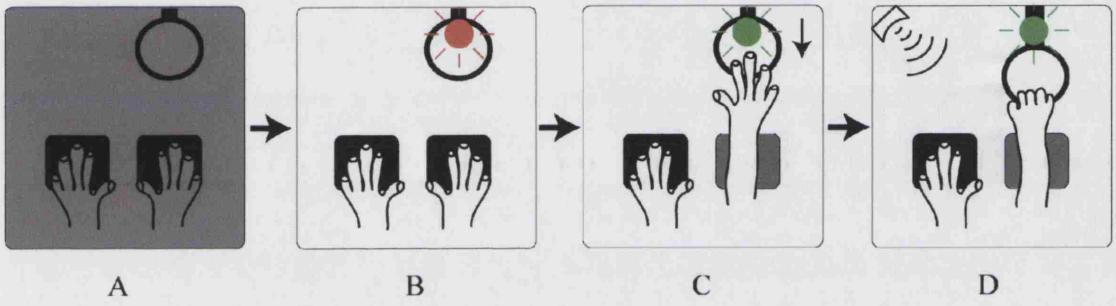

Figure 4.2 Task sequence. A. Carousel Rotation and Intertrial Interval. **B.** Object Fixation. **C.** Reach and Grasp. **D.** Hold.

The monkey was sitting quietly in darkness during the intertrial interval (usually 1 to 2.5 sec, variable, Fig. 4.2, A). When both home pads were depressed simultaneously, a light illuminated the lower part of the box, showing the monkey the object to be grasped, and a red LED was lit over the object (Fig. 4.2, B). After a variable delay period (1±0.5 sec), the LED changed from red to green to indicate a 'GO' signal. The monkey was then required to use the trained hand to reach for, grasp and pull the object into a position window between 4 and 14 mm from the starting point for a period of 1 second (Fig. 4.2, C). This displacement required a gentle force of 0.9N (4 mm) to 2.4N (14 mm), the spring behaving in a near linear manner. An auditory cue of a continuous tone was given

as feedback to the monkey when the correct position was reached (Fig 4.2, D). When 1 sec of correct holding had occurred the tone was terminated, the monkey released the object, and was then able to take a food reward from the experimenter with the other hand. The light was then extinguished, and the carousel rotated so as to present a new object for the subsequent trial.

Throughout the trial, the non-grasping hand was required to remain on its home pad. M39 maintained pressure using the hand, and remained still until the 'GO' signal. M37 however, tended to depress the home pad using the hand initially, but then slid the hand forward in anticipation of the grasp, using the forearm to depress the home pad.

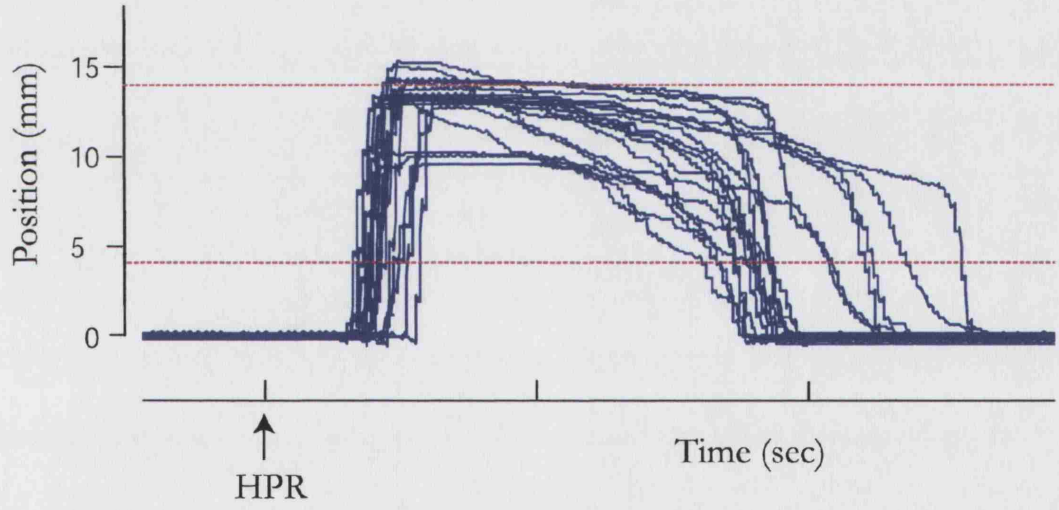

Figure 4.3 Overlay of object displacement traces for 20 trials. The position window for successful completion of a trial is shown between the red, dotted lines. Data taken from a recording made in M39.

Figure 4.3 shows the variability of object displacement traces, aligned to the release of the home pad. It can be seen that displacement onset varies only slightly from trial to trial, whereas the cessation of grasp is much more variable, but was always a minimum

of 1 sec after reaching the position window. The monkeys sometimes chose to hold the object for longer than was required, usually until the food reward was forthcoming.

The monkeys were trained to use a specific grasp for each object presented. This was monitored with 2 video cameras on sample sessions to verify that the required grasps were indeed being used. More than one carousel of objects was available, and a different selection of objects was used in each monkey for each hand and hemisphere of recordings. In the carousel used for the recordings in the right hemisphere of M39, two objects were represented twice, the only difference being a small piece of red tape on one of each pair. This cued the monkey to perform a different style of grasp for the same object, allowing us to see the effect of using a different grip type for the same object. The objects and grasps used are depicted in Figure 4.4.

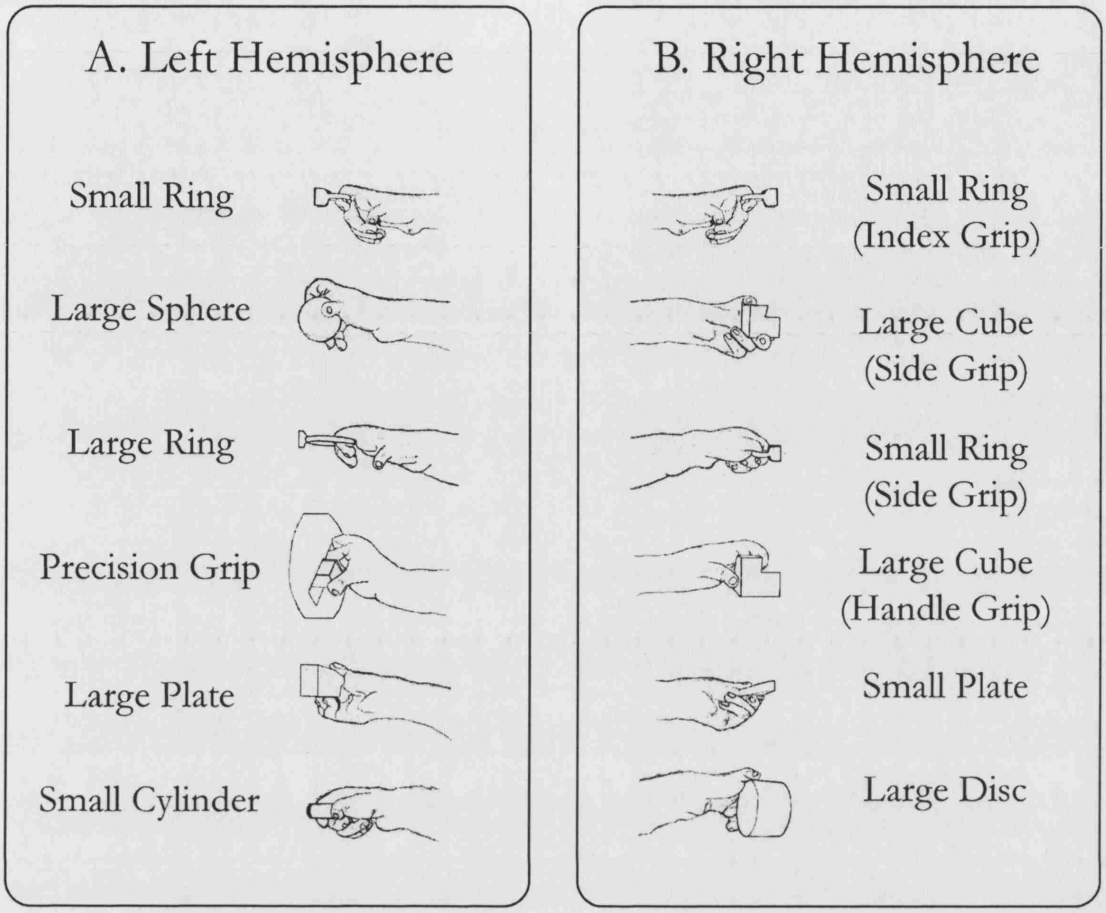

Figure 4.4 Objects and grasps. A. Used in Left Hemisphere (right hand) of M39, and **B.** Right Hemisphere (left hand).

Complete training took around 8 months in M37 and 10 months in M39. Each monkey typically performed a total of 50-100 grasping movements per object during a standard recording session.

4.2.3 Surgery.

All procedures were carried out in accordance with UK Home Office Regulations, set out in the Scientific Procedures (Animals) Act. 24 hours prior to invasive procedures, animals received glucocorticoid premedication (25 mg/kg i.m., Solu-Medrone, Pharmacia & Upjohn Ltd.) to prevent cerebral oedema. All surgeries were performed

under deep general anaesthesia, induced with 10mg.kg^{-1} ketamine i.m. (Ketaset, Fort Dodge Ltd.) administered concurrently with atropine sulphate (20 μg/kg i.m., Atrocare, Animalcare Ltd.). Surgical anaesthesia was maintained with 1.5-2.5% isofluorane in 50:50 O_2:N_2O. Full aseptic procedures and a full regime of post operative analgesia and antibiotic treatment were used. To prevent dehydration, 0.9% sodium chloride solution was administered intravenously to the animal (10-12 drops/min). Heart and respiration rate, body temperature, exhaled pCO_2 and SpO_2 were monitored throughout all surgeries to monitor the animal's condition.

Minor procedures such as removal of stitches and clearing of the dura mater were performed under sedation with ketamine and medetomidine (Dormitor, Pfizer Ltd.). 15 mg/kg i.m. Ketamine:Dormitor (mixed 80:1 by weight) was reversed with atipamezole hydrochloride (4 mg/kg i.m., Antisedan, Pfizer Ltd.).

4.2.3.1 MRI and Headpiece Implantation

Full details of this procedure have already been described in chapter 2. The procedures were followed for both M37 and M39. Briefly, the monkey was scanned in the MRI. Subsequently, a plastic model of the skull was made from the edited scan and a reconstruction of the surface anatomy of the brain performed to provide stereotaxic coordinates of landmarks such as the central sulcus etc. At a first surgery, a custom designed stainless steel circular headpiece was securely attached to the monkey's skull. The headpiece was custom fitted using the plastic mould produced from the MRI scan. The implant technique is fully described elsewhere (Baker *et al.*, 1999b). Once in place, the headpiece was used for the restraint of the monkeys head during recording sessions, to allow stable recordings from the cortex.

4.2.3.2 Chambers

In subsequent surgeries, a small custom-designed recording chamber was placed over craniotomies above M1 and F5 cortical areas. The positioning of this chamber was guided by the measurements obtained during the MRI scan (as previously described in Chapter 2) to allow optimal access to both areas at suitable angles. The chamber allowed access to the cortex for repeated recordings over an extended period of time. Full details of the care of the chamber and the procedures for recording sessions are detailed in Baker *et al.*, 1999b, and have been described previously here (see Chapter 3).

4.2.3.3 Care of the Dura Mater and Implants

Once exposed by craniotomy, the dura mater quickly becomes covered by scar tissue, and penetration with electrodes becomes difficult, as described fully in chapter 3. Briefly, after each recording session, this tissue was stripped with a corneal hook after the area had first been covered with local anaesthetic cream (lignocaine/prilocaine; EMLA, Astra Pharmaceuticals Ltd.). Following this, it was treated with an antimitotic solution (25 mg/ml 5-fluorouracil, Sigma Chemicals Ltd.) for 5 min before thorough rinsing with a large volume of sterile saline. Topical antibiotic (0.3% Gentamicin; Genticin, Roche Products Ltd.) was added to each chamber before it was filled with sterile saline and sealed with an airtight lid.

To prevent infection, exposed implants and skin edges were cleaned when necessary with 3% hydrogen peroxide and coated with neomycin powder (Cicatrin, Wellcome). Any incidence of infection was treated with topical application of enroflaxin (Baytril 2.5%, Bayer), and Duphamox LA, (subcutaneous injection, 0.1ml kg^{-1}, Fort Dodge).

4.2.4 Experimental Procedures

4.2.4.1 Cortical Recording

All M1 and F5 data were recorded using two Eckhorn multiple-electrode drives (Thomas Recording Ltd., Marburg, Germany). One was a 16-channel model, the other a 7-channel. The complete system has been described in detail (Baker *et al.*, 1999b). The 16 channel drive, shown in Figure 4.5, allows a 4x4 grid of glass-insulated platinum electrodes (impedance 1-3 MΩ, interelectrode spacing 300 μm) to be lowered independently into the cortex to search for cells and to record the LFP. The 7-channel drive works in a similar manner, allowing up to 7 electrodes to be used in a concentric array. When used together, a maximum of 16 channels could be used, up to 9 in the 16 channel drive, (usually used in M1) and all 7 channels in the 7-channel drive (usually used in F5). A detailed schematic of the drive being used in the chamber was shown in Figure 3.1.

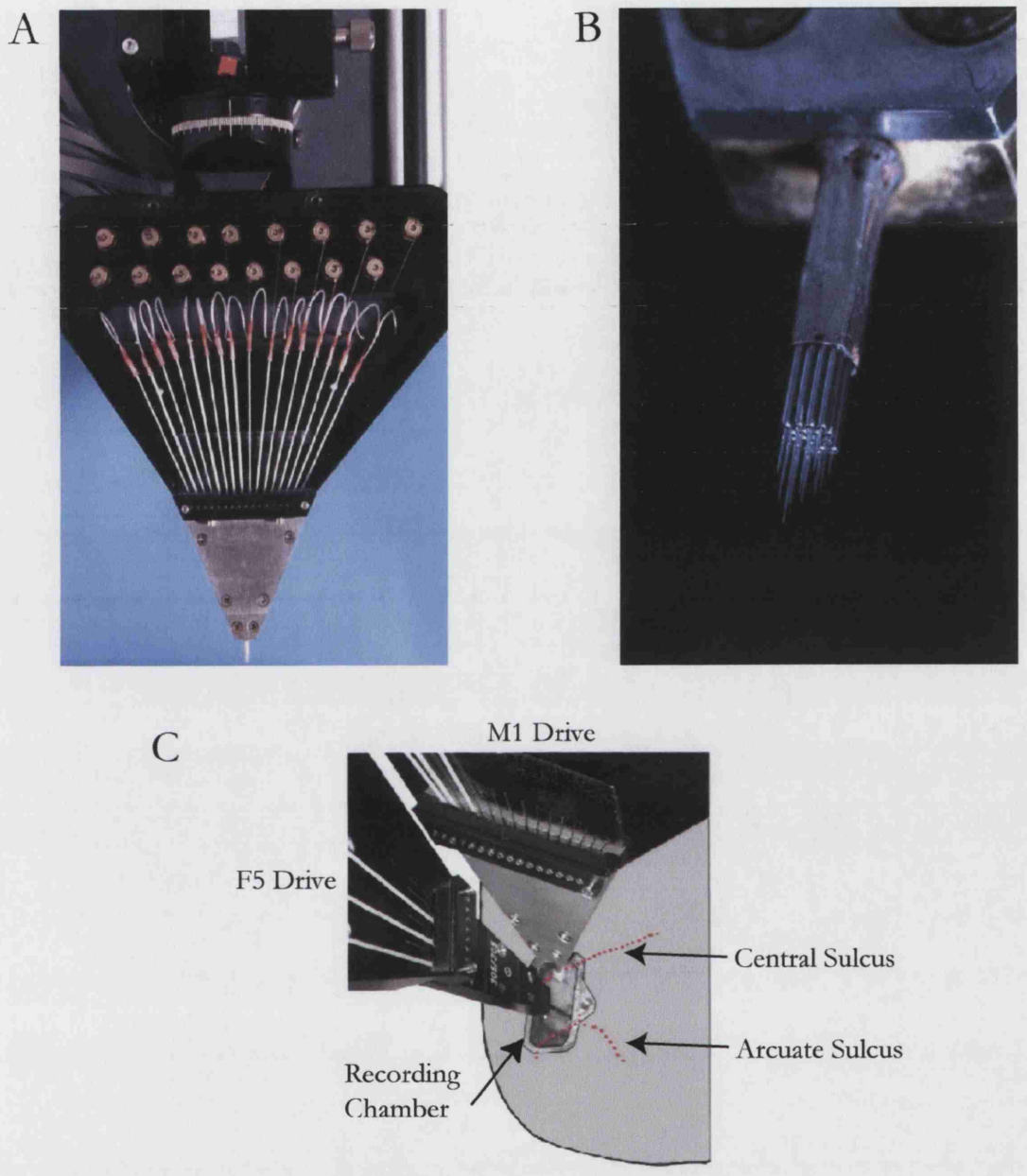

Figure 4.5 Eckhorn multi-electrode system. A. 16-channel drive, showing arrangement of electrodes and motors. **B.** Close-up of drive head showing 4x4 electrode array (electrode separation 300μm). **C.** Illustration of the two drives being used simultaneously in one recording chamber, with 3 electrodes in each area.

In order to ascertain the exact penetration location of the electrodes, the position of the guide tube tips of each drive was referenced to three triangulation points on the lid of the

chamber, the stereotaxic locations of which had been measured during surgery. This allowed the positions of the penetration sites to be calculated in stereotaxic co-ordinates. Once a site had been chosen for each drive, they were recorded to create a chamber map of recording sites. The location of recordings in M1 was verified by the use of ICMS, which elicited mostly hand and arm movements.

The locations of the drives for each recording session are shown in figure 4.6. Measurements of the sulci and the fundi were taken post-mortem.

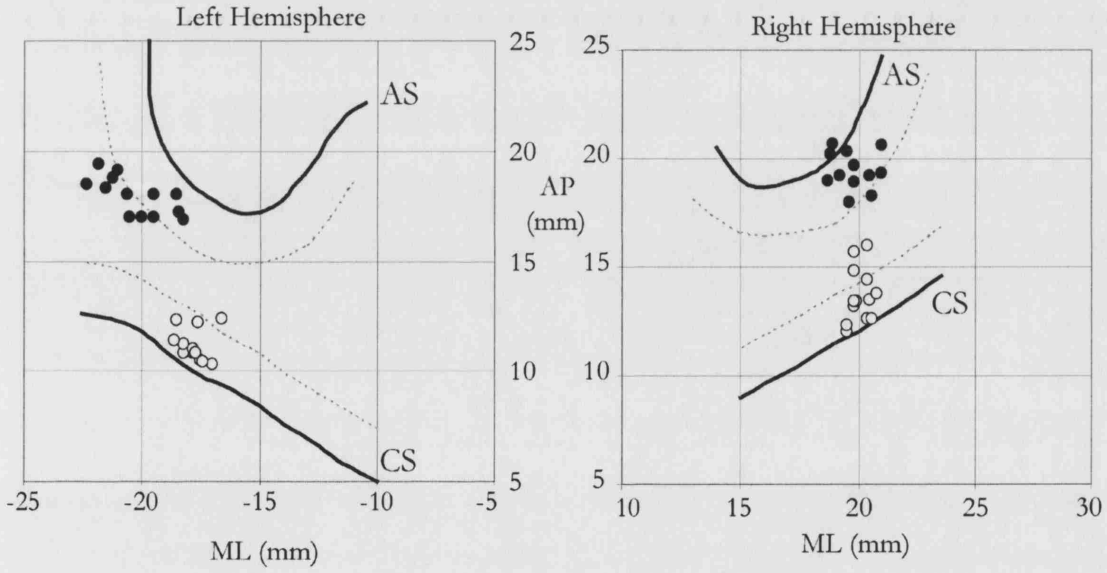

Figure 4.6 Chamber maps to show location of LFP recordings in M39. Solid lines represent the arcuate (AS) and central sulci (CS), dotted lines the caudal bank of the AS and rostral bank of the CS. Open circles show the locations of the M1 recording sessions, solid circles, F5.

For each drive in turn, the guide tubes were positioned close to the dura mater and the electrodes were driven through one at a time. To allow the tissue to recover from

mechanical depression, electrodes were left for approximately 10 minutes before being advanced further into the cortex.

A single operator can reliably monitor at most 3 electrodes, so a network of computers was used to allow up to four people to simultaneously control electrodes. In these experiments, between 2 and 5 electrodes were used in each area in a typical session.

The signal from each recording electrode was pre-amplified then filtered for LFP (10-250 Hz) and spike activity (1-10 kHz).

4.2.4.2 Data Capture

The following signals were recorded during each experiment:

- Analogue LFP data.
- Analogue object displacement signals, obtained from the task computer via a digital to analog (D2A) card (PCL-818L, Advantech).
- Digital events (onset of object illumination, release of home pad, entry and exit of object in the position window, object grasped and other trial parameters)

Data were recorded directly to computer hard disk via two analog to digital (A2D) cards (PCI-6071E, National Instruments). The sampling rate for LFP and object displacement was 500 Hz.

4.3 Data Processing

4.3.1 Trial Acceptance

Analysis was performed only on data recorded during successful trials. A successful trial was completed when the monkey held the home pads down until the LED changed from red to green, and then released only the home pad for the correct, working hand. The

object was required to be displaced into the position window within 1 second, and held entirely within that window for the full duration of 1 sec. A custom written program removed all trials where these criteria were not met. Typically, over 90% of trials were defined as successful.

4.3.2 Raw Data

For the analysis of LFPs in M39, 30 recording sessions were chosen, and 144 LFPs fully analysed. These sessions were selected from the entire set of recordings as they contained multiple simultaneous recordings with at least one clean, task-related LFP from each area.

On initial inspection of the raw data for task related activity, it is apparent that there are two main epochs of interest with regards to oscillations. These were during the period of object observation/preparation for movement, and after the reach to grasp movement when the monkey is holding the object steadily in the position window. This can be clearly seen in figure 4.7, where typical raw data is shown with the object displacement trace.

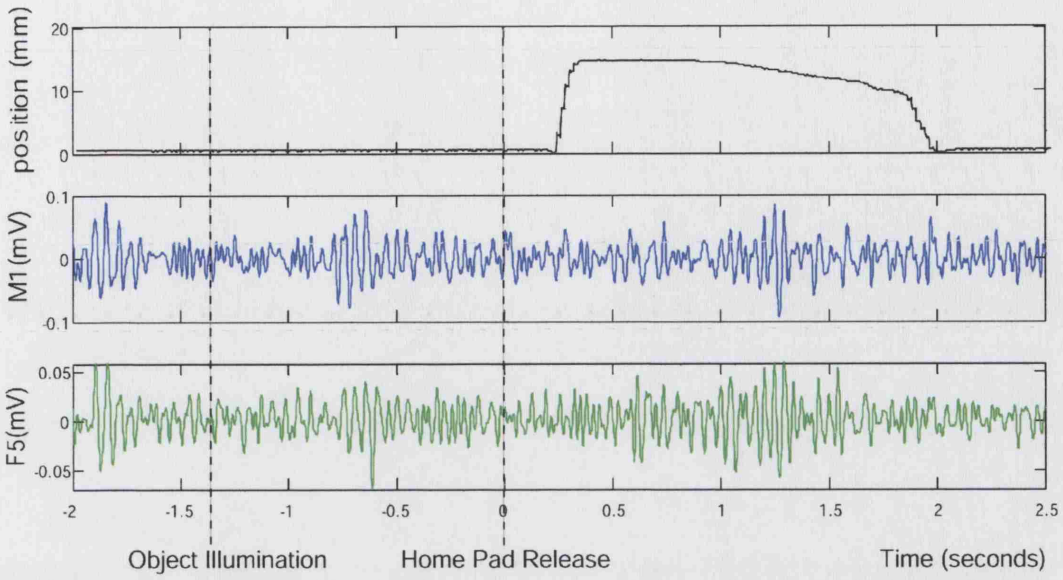

Figure 4.7 Object displacement trace and LFP raw data. Sections are taken from continuous recording. The top trace shows the displacement of the object. The lower two traces are the corresponding M1 and F5 LFP signals.

4.3.3 Spectral Analysis

4.3.3.1 Data recorded from M39.

A power spectrogram was compiled for a typical session to establish the frequency, and the onset and cessation times of oscillations over many trials. The spectrogram is a time-frequency plot of LFP power, and was generated using spectral analysis of 4 sec sections of data centred on the home pad release (HPR) trigger (2 sec before and 2 sec after HPR).

Power spectra were calculated as follows using standard spectral analysis. The calculation utilises the Fast Fourier Transform (FFT, MatLab, MathWorks) algorithm on sections of data aligned to each time marker (e.g. HPR) of length L sample points. The

Fourier coefficient $F_n(f)$ for the n^{th} marker (n = 1,2,..,N) is a complex number representing the amplitude $a_n(f)$ and phase $\phi_n(f)$ of the component at frequency f:

$$F_n(f) = \frac{L}{2} a_n(f) e^{i\phi_n(f)} \qquad (4.1)$$

To compute the power spectrum P(f), the squared magnitude of each coefficient was averaged across trials according to standard spectral analysis:

$$P(f) = \frac{1}{NL} \sum_{n=1}^{N} |F_n(f)|^2 \qquad (4.2)$$

The spectrogram is then calculated by creating power spectra for a window of length 256 data points, i.e. 0.51 sec starting 2 sec before the reference time marker. The time dimension is then obtained by sliding this window through the data in 16 sample point steps, each overlapping with the 15/16ths of the previous window, to produce a matrix of power spectra and time. The frequency resolution was 1.95Hz (the sampling rate divided by length of the FFT window).

This false-colour spectrogram gives a graphical representation of the amount of power at different frequencies during the different phases of the task.

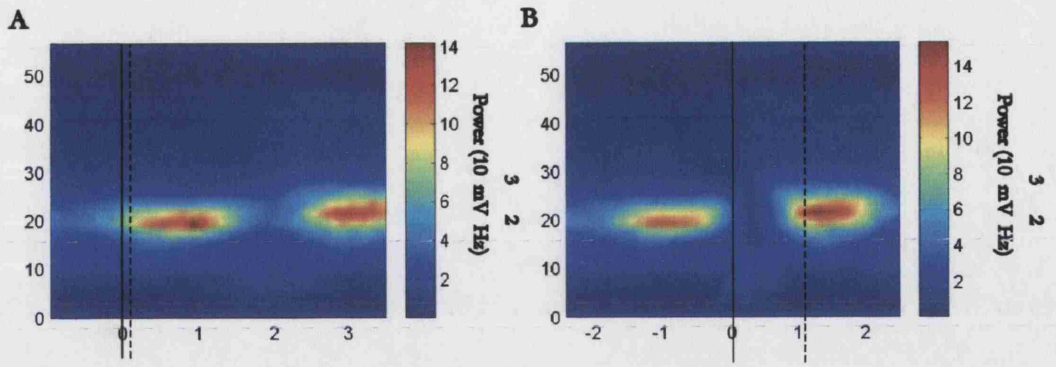

Figure 4.8 Power spectrograms from data recorded in M39 A. Centred on object illumination (time t=0). **B.** Centred on HPR (time t=0). Dotted lines represent onset of periods of 'object observation' and 'object grasp'.

Figure 4.8 shows a typical spectrogram from a single session in M39, consisting of a total of 308 successful trials. Firstly, it can clearly be seen that the largest amplitude and most task-related power was in the beta frequency range, in this case at 20Hz. The periods of highest power occur during the object observation and object grasp phases of the task. A spectrogram centred on object illumination markers (Fig 4.8A) shows maximal beta power approximately 0.1 sec after illumination, defined for subsequent analyses as 'object observation'. As the delay period before the 'GO' signal to move was variable, (1 ± 0.5 sec), the cessation of beta power is not clearly defined in this plot, but was always absent before movement. This can be seen on the HPR centred spectrogram (Fig. 4.8B) where power was greatly reduced approximately 0.1 sec before HPR. The onset of the object grasp phase of beta power can be seen to reach its maximum at approximately 1.1 sec after HPR. This was after stable object grasp had been achieved. The beta power continues until 1.8 sec after HPR, approximately when the monkey releases the object, having held it for 1 sec. This period from HPR + 1.1 sec when the object is being held stably with a constant grasp was defined as 'object grasp'. These two epochs were subsequently used for all further analyses. During movement, oscillations were rarely seen in the raw data and were absent when trials were averaged,

indicating a lack of beta power during the reaching movement, the active grasp and the early displacement of the object (taking on average 400-500 ms).

To calculate power for each epoch, 256 point (0.51 sec) sections of data beginning 0.1 sec after object illumination, and 1.1 sec after home pad release of each trial, respectively the object observation period and the object grasp period were analysed. The average value of the spectrum between 18–30 Hz was calculated as a measure of beta power. These spectra were then calculated for all the successful trials for each object.

LFPs were sometimes contaminated by noise. This occurred occasionally when, for example, the electrode had been advanced by an experimenter slightly during the trial, usually in order to maintain clean neuronal recordings, which were obtained simultaneously to the LFP data for another project. This electrode movement often causes electro-mechanical vibrations of the electrodes and could contaminate the LFP signals. This was a relatively rare occurrence, as experimenters were requested to refrain from moving electrodes during trials, but occasionally this was unavoidable. Other sources of noise were movements by the monkey (such as chewing, the occasional sneeze, or fidgeting). Outliers were removed by discarding the 5% of trials with the highest and lowest total beta power to exclude trials where artefacts may be present.

For each LFP, the average power recorded during the observation or grasp for each object was calculated by taking the average for all trials using each object. Since the absolute magnitude of an LFP signal can depend on a number of factors, particularly the impedance of the recording electrode, these values were normalised to allow averaging across different electrodes and sessions. This was done by dividing by the average power during each epoch for all objects for that electrode in that session. The frequency

corresponding to maximum power in the 18–30 Hz range was found for each electrode in each epoch averaged over all trials.

4.3.3.2 Data recorded from M37.

Data from M37 proved more difficult to analyse. During recordings, there were problems due to a loose headpiece – this caused stability problems with the neuronal recordings being made, leading to frequent movements of the electrodes being neccesary to maintain clean recordings, as well as microphonics. This led to significant noise in the majority of LFP recordings made. Analysis of the electromyogram (EMG) recordings in M37 showed that the hand was preshaped for object grasp before HPR (see comments by Brochier *et al.*, 2004). This was not the case in M39. The preshaping makes analysis of the observation epoch unreliable, as the monkey is not only observing the object, but actually already initiating the grasp. However, clean LFPs were recorded in some sessions. An example is shown in Figure 4.9. This is a spectrogram of the LFP power, aligned to HPR, as in Fig. 4.8B.

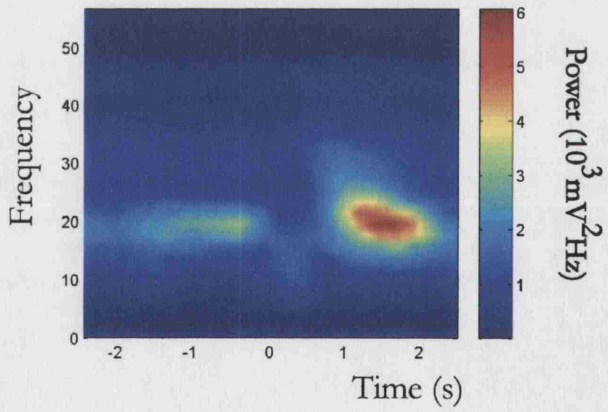

Figure 4.9 Power spectrogram from data recorded in M37. Time=0 represents HPR.

In these recordings where the signal to noise level was acceptable and the number of trials remaining after those containing movement artefact were removed, the same pattern of task relationship as in M39 was seen, and the frequency at which power is highest was again in the beta range, at approximately 20 Hz, as in M39. The ratio of the power present in the observation epoch compared to the grasp epoch was somewhat lower than that seen in M39, probably because of the anticipatory movement of the hand.

Insufficient data sets of good quality were obtained from M37 for a full analysis to be performed.

4.3.4 Coherence Analysis

In order to assess the relationships between pairs of simultaneously recorded LFPs, coherence analysis was used. This can assess the phase coupling between the oscillations both within and across areas (Rosenberg *et al.*, 1989; Baker *et al.*, 1997). Coherence represents the linear correlation between two signals calculated in the frequency domain from the cross spectrum, $X_{12}(f)$:

$$X_{12}(f) = \frac{1}{NL}\sum_{n=1}^{N} F_{1,n}(f)F_{2,n}^{*}(f) \qquad (4.3)$$

where $F_{i,n}(f)$ is the Fourier component for the n^{th} section of data (n = 1,2,..,N) from signal i, length L sample points long. The coherence, $C_{12}(f)$ equals the squared cross-spectrum, normalised by the power spectra for each signal, $P_1(f)$ and $P_2(f)$ (Equ. 4.2):

$$C_{12}(f) = \frac{X_{12}(f)X_{12}^{*}(f)}{P_1(f)P_2(f)} \qquad (4.4)$$

Coherence values for each frequency measure the phase-coupling between signals, from 0 (no coupling) to 1 (perfect coupling). The significance of coherence values obtained during individual sessions was assessed from the expected statistical distribution of coherence in the absence of coupling which has a 95% upper limit given by Rosenberg et al., (1989):

$$C_{P=0.05} = 1 - 0.05^{1/N-1} \qquad (4.5)$$

A time frequency plot of coherence, equivalent to the spectrogram was calculated to assess the frequencies and task relationship of any coherence present. This was done

using a 128 point window sliding through the data in 40 sampling point steps. A typical result is shown in Figure 4.10

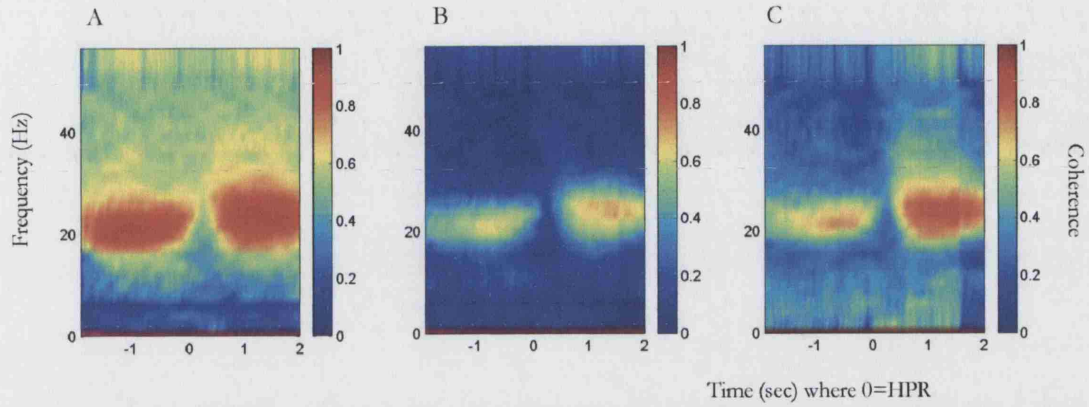

Figure 4.10 Coherence spectrogram. A. M1-M1 B. M1-F5 C. F5-F5. All centred on HPR.

Figure 4.10 shows that coherence between LFPs, both within areas and across areas was task related and is restricted to the periods of object observation and of stable object grasp. It was also predominant in the beta frequencies, in this case at 20-25Hz, the same frequency as the peak power during this session. No other frequency shows strong coherence. It may be seen that the M1-M1 pairing (Fig. 4.8A) and the F5-F5 pair (Fig. 4.8C) show considerably higher coherence, and at a broader range of frequencies than the across areas pairing (B). Coherence is also absent during the reach to grasp movement.

For subsequent analyses, coherence was calculated for a 256 sampling point window during the same object observation and grasp epochs used for the power spectral analysis.

According to standard linear systems theory, one way to characterise the relationship between two coupled oscillators is with a phase shift and a time delay. These were

calculated from a linear regession line fitted to a plot of the cross-spectrum phase. The phase values at the frequency corresponding to peak coherence and the three adjacent points on either side were used for fitting. The circular mean value of this range determined the phase shift, and the time delay was given by the slope of the regression line divided by 360°. These values indicate whether one signal consistently 'lead' the other and to what extent.

Data from M39 was used for full coherence analysis. Insufficient good quality simultaneously recorded LFPs were obtained in M37 to perform coherence analysis in any meaningful way.

These analyses of frequency, power, object related power and the coherence measures form the basis for all subsequent analyses to investigate the similarities, differences, and relationships between the LFPs in M1 and F5.

Chapter 5. Analysis of the Properties of M1 and F5 Beta Oscillation Power

5.1 Introduction

The normalised beta power present in a given local field potential for different objects in the two epochs (object observation and object grasp) can be used to examine the relationship of the LFP to the task being performed. For each motor area in each epoch, the relative amounts of beta power of each recorded LFP for different objects and their significance can be used firstly to assess if there is any 'tuning' present, i.e., if the amount of power varies across different objects. Secondly it can be used to establish the 'preferred' object for the LFP (defined as the object for which the total beta power was maximal), and thirdly, to assess the similarity of any tuning between different LFPs. Lastly, the frequency at which the beta power is maximal can also be calculated in each epoch for each object. This chapter will attempt to answer these questions, and therefore to establish qualitatively and quantitatively the behaviour of the LFPs in relation to a reach-to-grasp task. This will further understanding of the functional significance of the LFPs in the two areas. The use of simultaneous multi-electrode recording techniques from the two areas also provides a valuable contribution to the question of just how 'local' a local field potential is, by allowing us to compare the LFPs recorded simultaneously on different electrodes, in some cases only 300μm apart, and in some cases in separate motor areas up to 15 mm apart.

5.2 Independence of Signals

5.2.1 Introduction

When multiple electrodes are used in the Thomas microdrive, the minimum horizontal separation of two electrodes is 300μm, the maximum 900μm. It is not clear whether LFPs recorded at this separation would be expected to be independent of each other, or merely redundant recordings of the same signal. In order to establish whether simultaneously recorded LFPs with these separations should be treated individually or as redundant, a comparison was made.

5.2.2 Methods

For each LFP, the normalised beta power present in all trials of each object was determined and an average for each object in each area and epoch was produced (i.e. each LFP was treated independently). These values were compared with two different measures. The first was a weighted average; each recording session contributed one value towards the weighted average for each object and this value was the average for all electrodes in that session; in this way, recording sessions with many electrodes did not bias the overall average, and contributed as equally to the final average as a session where only 1 or 2 electrodes were used. This effectively treats the LFPs as partially redundant, since all LFPs within a session contribute equally. The second measure was a cortical area average. For each session, the raw LFP data from each electrode was averaged to produce a single LFP for each area (M1 and F5) and the beta power was calculated from this averaged signal. This also treats the signals as redundant, but could bias the resultant averaged LFPs towards those LFPs with a larger raw data signal, e.g. lower impedence electrodes, or the best located to record a large LFP. By comparing the

area averages for each object produced in these three ways, some assessment of the independence or redundancy of the signals could be made. This analysis was performed for data recorded in the left hemisphere of M39, during the object grasp epoch.

5.2.3 Results

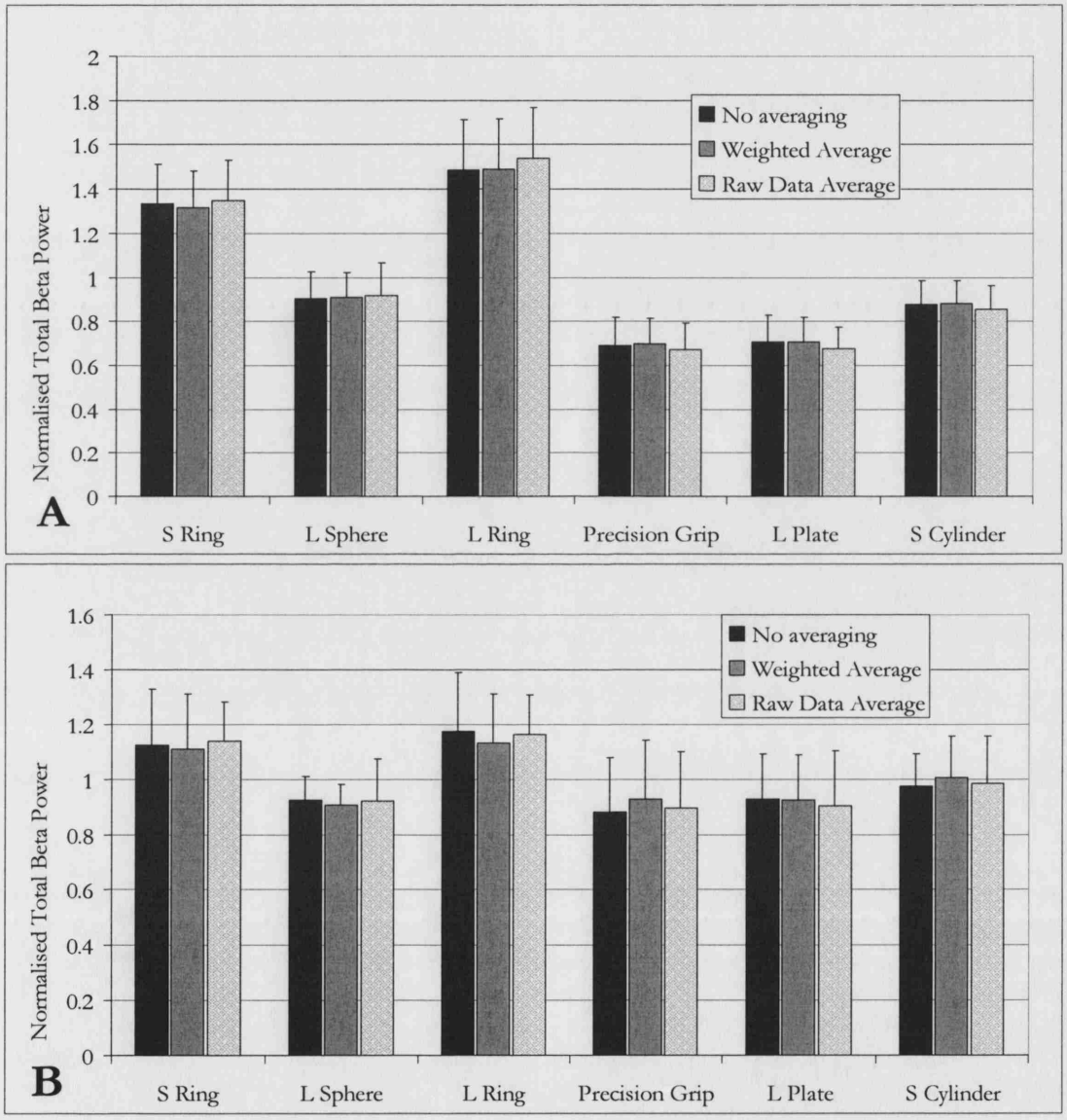

Figure 5.1 Comparison between beta powers calculated during object grasp with 3 different types of averaging in A. M1 and B. F5. Error bars show standard deviations.

The averaged raw data slightly enhanced the amount of tuning, perhaps because of the over emphasis of larger signal LFPs (which biased the average), and the weighted average slightly reduced the amount of tuning (perhaps by reducing the bias), but overall, when compared (multiple Students T-Tests, $P>0.1$) there were no significant differences in the results in either cortical area, whether LFPs were assessed individually, by a weighted average, or by averaging the raw data. If the LFPs were redundant, it might be expected that the non-averaged data would be significantly different to the averaged, as individual sessions with larger numbers of electrodes would bias the averaged towards the preferred objects in those sessions. This was not the case.

5.2.4 Conclusions

Whichever way the data is averaged, no significant effect on the normalised total beta power was found. Although this result does not prove that all LFPs recorded are independent, it does show that it is not unreasonable to treat each LFP channel individually for further analysis. In this way, any potential bias caused by over- or de-emphasising large signals was removed, and the data pool was maximised, making statistical analysis more robust. For all subsequent analyses, LFPs will therefore be treated individually.

5.3 Maximal Frequency of Beta Power

5.3.1 Introduction

In the above analysis, the total beta power between 18-35 Hz has been used as a measure of the oscillations. This does not take into account the frequency at which the maximal power occurs. It is of interest to see whether this peak frequency of the beta power is consistent for all objects and epochs for each LFP.

5.3.2 Methods

For each LFP, the frequency at which the maximal beta power occurred for each object in each epoch was calculated. An average for all trials was also made.

5.3.3 Results

5.3.3.1 Left Hemisphere.

The results for the left hemisphere of M39 are shown in Fig. 5.2.

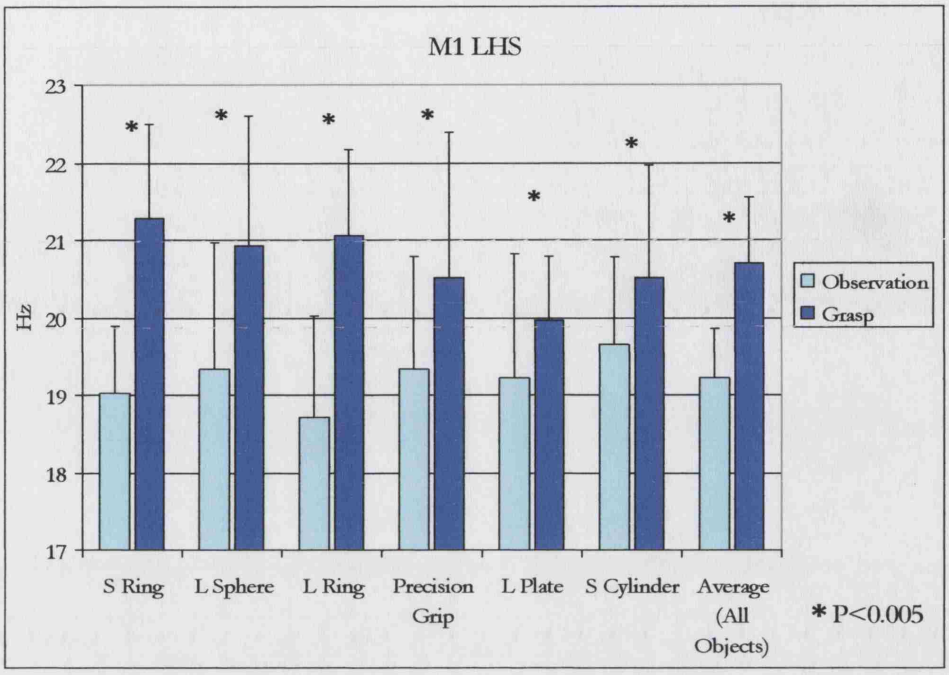

Figure 5.2 Peak object-related beta frequencies for M1 (left hemisphere). Error bars show the standard deviation.

There was a significant increase in peak beta frequency from the observation epoch to the grasp epoch for all objects (T-Test, $P<0.005$). The average change was from 19.2 Hz to 20.7 Hz.

The results for F5 are shown below in Fig. 5.3.

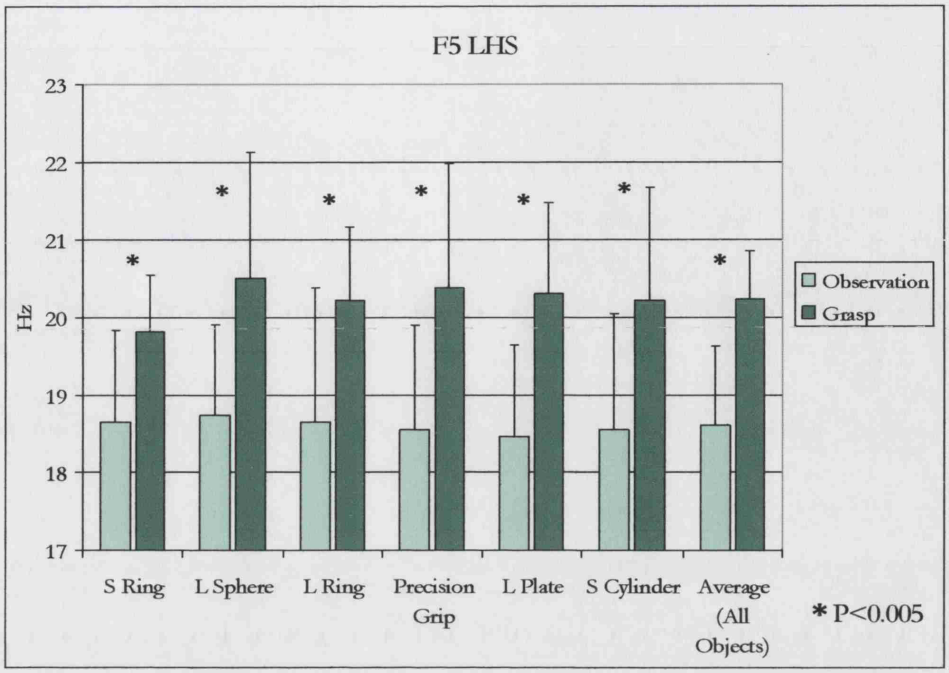

Figure 5.3 Peak object-related beta frequencies for F5 (left hemisphere). Error bars show the standard deviation.

Again, there was a significant increase in peak beta frequency from observation to grasp for all objects, a change in the average from 18.6 Hz to 20.4 Hz.

5.3.3.2 Right Hemisphere

The results for M1 are shown in Fig. 5.4. As with the left hemisphere, there was a significant change in frequency from the observation to the grasp epoch for all objects. The change in the averaged data was from 18.6 Hz to 19.7 Hz.

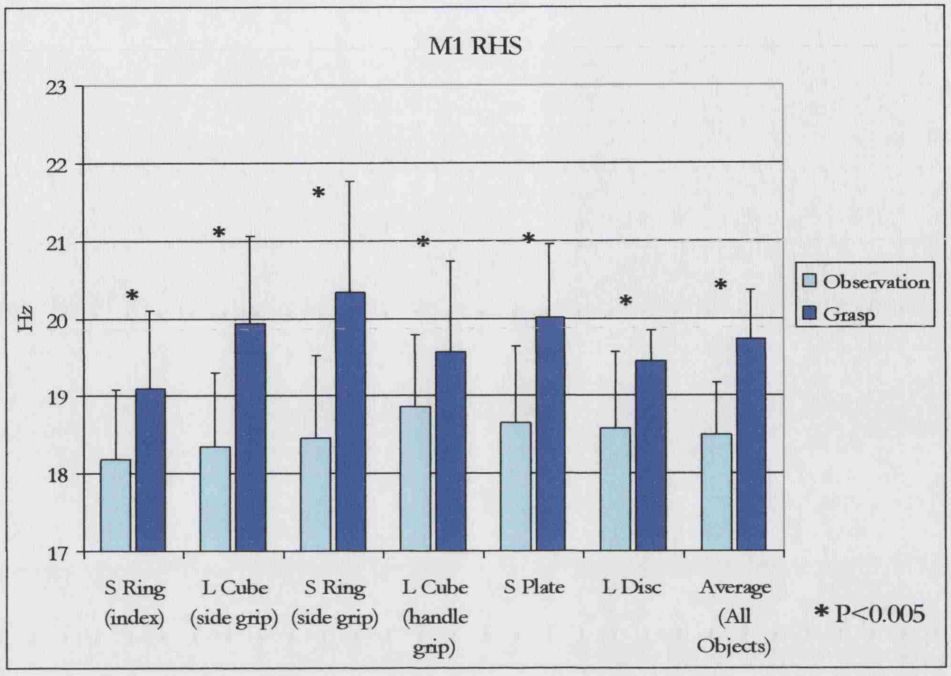

Figure 5.4 Peak object-related beta frequencies for M1 (right hemisphere). Error bars show the standard deviation.

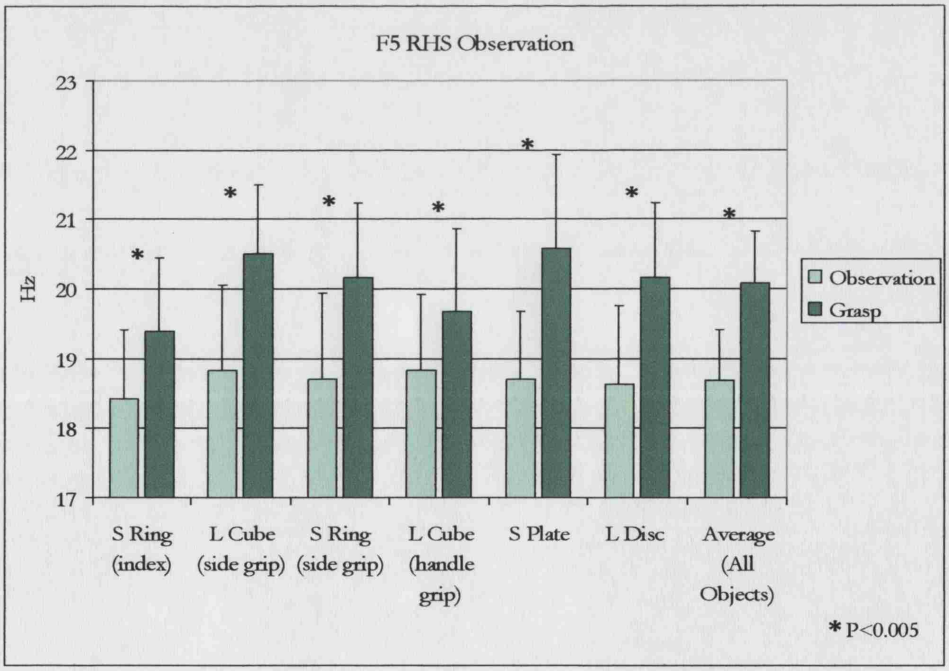

Figure 5.5 Peak object-related beta frequencies for F5 (right hemisphere). Error bars show the standard deviation.

Fig. 5.5 shows the results for F5. As with all other datasets, there was a significant difference in the frequency of the beta oscillactions between observation and grasp for all objects (average change 18.7 Hz to 20.1 Hz).

5.3.4 Conclusions

In both cortical areas in both hemispheres there was a small but significant increase in the frequency of the beta oscillations from the object observation epoch to the steady object grasp. This was true for all objects. On average, a change of 1-2 Hz was found. Generally, the variation in peak beta frequency for different objects was much less pronounced than the difference between epochs. The steady grasp appeared to evoke a higher peak frequency of beta oscillatory power than the observation of objects in preparation for movement. This type of change in oscillatory frequency within an area has not been described before, and is of interest in understanding the nature of cortical oscillations. This will be discussed fully later in this thesis.

5.4 Degree of Tuning in Each Area

5.4.1 Introduction

The amount of total beta power for each object may vary, such that a given LFP channel may have significantly more beta power when the monkey is observing or grasping one or more objects. In this way, the LFP could be said to show object tuning, or selectivity. In order to assess the amount of tuning present in the two areas during the two epochs, the degree of tuning of each LFP was calculated. This allows comparisons between the areas both within an epoch and across the two epochs, object observation and grasp.

5.4.2 Methods

The degree of tuning was calculated using a method described by Murata *et al.* (2000). This analysis allows the classification of an LFP's tuning during a given epoch. The normalised levels of total beta power on a trial-by-trial basis were calculated as previously described and trials with the same object are grouped. This is shown in Figure 5.6. This example from the grasp epoch of a single session shows the averaged power spectra for each of 6 objects, and demonstrates the variability of the beta power for different objects.

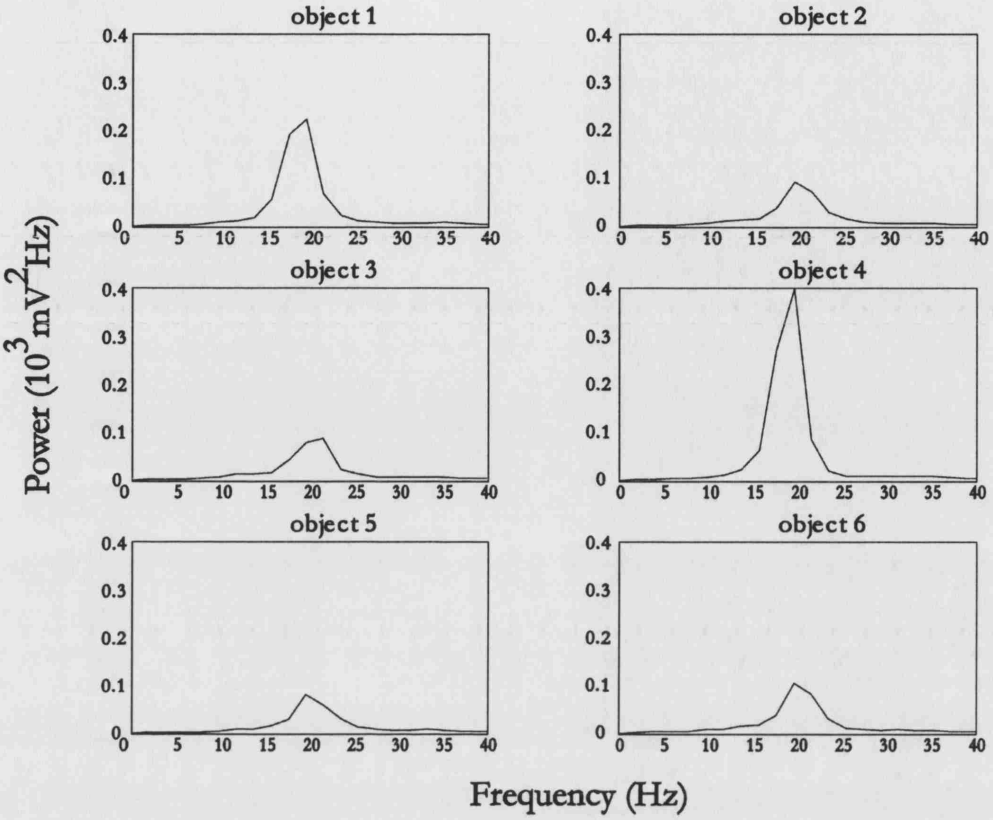

Figure 5.6 Object-related variance of power spectra. A typical set of results, recorded from M1 during the grasp epoch. Data was averaged over all trials of that object (n=52 to 55).

The Student-Newman-Keuls procedure, (2-tails, $P<0.05$) was used to test for object-related differences in the total beta power. This effectively 'groups' the objects, such that any objects whose beta powers were statistically similar (e.g. objects 2, 3, 5 and 6 in Fig. 5.6) are in the same group. The LFPs were classified as follows: if there were no significant difference between the objects, i.e. all 6 fell into one single group, the LFP was classified as untuned; when the objects fell into more than one group where a significant difference between groups was present, the LFP was classified as tuned. A further classification separated the tuned LFPs into highly and moderately tuned. An LFP was defined as highly tuned when the total beta power for a single object was

significantly higher than that for all the others, and as moderately tuned when the power for the 'preferred' object was not significantly higher than that for at least one other object. This classification was performed for each area and each epoch in order to test for significant differences in the amount of tuning present.

5.4.3 Results

The results are shown in table 5.1 and graphically in Figure 5.7.

Tuning % (n)	Observation		Grasp	
	M1	F5	M1	F5
Highly Tuned	3.8 (3)	0 (0)	58.2 (46)	23.9 (11)
Moderately Tuned	10.1 (8)	21.7 (10)	41.8 (33)	60.9 (28)
Any Tuning	13.9 (11)	21.7 (10)	100 (79)	84.8 (39)
Untuned	86.1 (68)	78.3 (36)	0 (0)	15.2 (7)

Table 5.1 Amounts of tuning in M1 and F5 during object observation and object grasp.

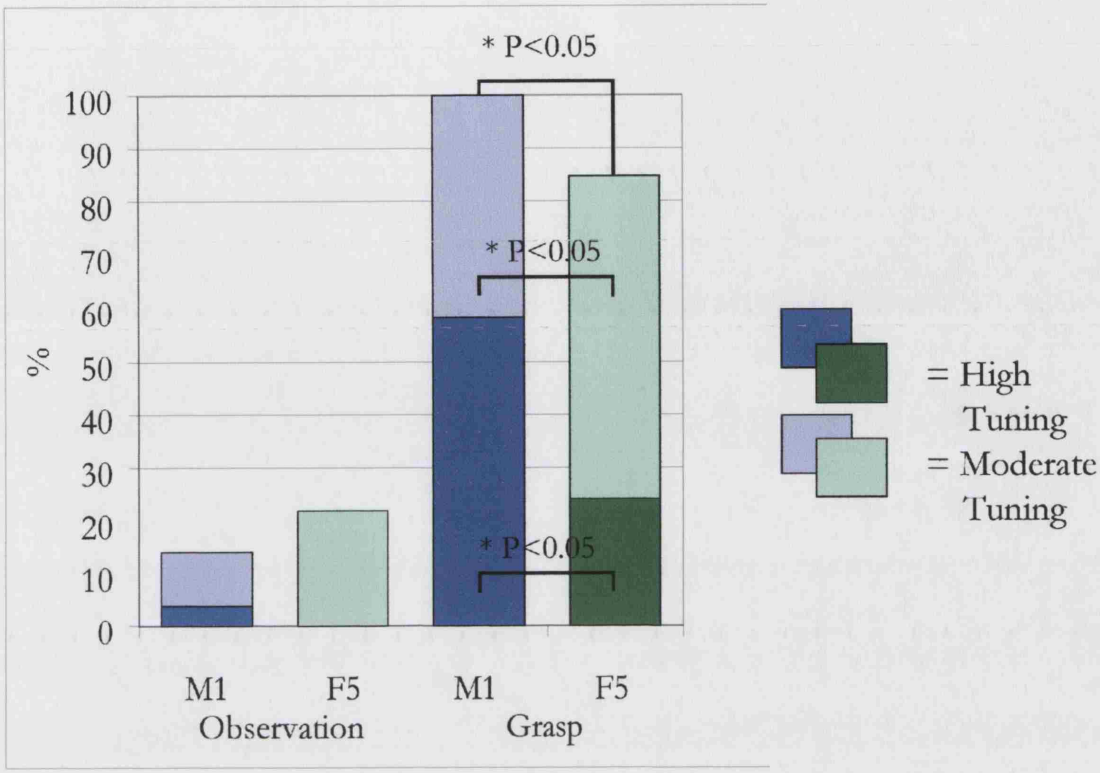

Figure 5.7 Chart to show amounts of tuning in M1 and F5 during object observation and grasp.

There were considerably more LFP sites that were object selective during object grasp than during object observation for both M1 and F5. During grasp, and also overall, M1 had significantly more highly tuned sites than F5, whereas F5 had significantly more moderate tuning during grasp and overall. During grasp, significantly more sites were tuned in M1 than F5, and during object observation, F5 showed more tuned sites, although this did not reach statistical significance.

5.4.4 Conclusions

The proportion of LFPs that showed significant object-related activity varied with the task epoch and the motor area from which recordings are made. M1 LFPs showed object-related tuning predominantly during grasp, with a majority of LFPs showing high tuning, indicating specificity for one object above all others. The proportion of highly

tuned LFPs was significantly higher than for F5, where tuning tended to be moderate. F5 had more LFPs that showed tuning during object observation than M1.

The finding that the degree of tuning in the two epochs varied between areas suggests that LFPs recorded in F5 are not merely a weaker, diluted version of the M1 signal, but are genuine, task-related phenomena, and that LFPs in the two motor areas may play different roles during the two task epochs. F5 is known to contain neurons which are active during object observation (Murata *et al.*, 1997) as well as during object grasp, designated as visuomotor neurons. Their study used a very similar task to that used here. It found that 24/49 of recorded task-related neurons in F5 showed some response to the presentation of a graspable object, and of these, 16 were selective for a specific object during grasp, 32.7% of the total (selectivity and tuning being an identical measure). Tuning during observation is not stated. This finding is not dissimilar to the proportion of LFPs that were found to be tuned in F5 (21.7%) during object observation.

During active grasp, Murata *et al.* (1997) found that 68% of purely 'motor' neurons in F5 were selective (i.e. tuned) for one or more objects, and 67% of all F5 neurons were object selective. This is slightly fewer than the number of grasp-tuned F5 LFPs (84.8%). Murata and colleagues used a higher significance level ($P<0.001$) to define selectivity than was used to ascertain tuning in the present study ($P<0.05$), which may explain the slight differences and higher proportion of tuning found in LFPs. However, it is also possible that a higher proportion of LFPs than neurons genuinely carry object grasp related information.

M1 is known to be highly active during reach and grasp of objects. The objects were chosen to elicit varied hand and therefore arm postures, requiring differential and characteristic activation of muscle synergies (Brochier *et al.*, 2004). M1 is the major

source of descending corticospinal projections influencing hand and arm musculature (Porter & Lemon, 1993; Dum & Strick, 1991; Maier *et al.*, 2002) and might therefore be expected to have such a high degree of object-related activity during the grasp epoch. It is well established that motor cortical oscillations are prevalent during a pre-movement delay period in the macacque (Donoghue *et al.*, 1998) and are related to task engagement. Although beta oscillations were clearly present during observation, only a small number (13.9%) of M1 LFPs showed a significant tuning of these oscillations to the object, compared to 100% demonstrating tuning during grasp. The ratio of LFPs in M1 which showed observation tuning to grasp tuning was 1:7.2 whereas for F5 it was 1:3.9, suggesting that relatively, the tuning of M1 was less concerned with the observation of objects than F5, but that these roles were reversed during active grasp.

5.5 Patterns of Tuning I – Preferred Objects

5.5.1 Introduction

The assessment of the degree of tuning in M1 and F5 did not take into account the specific object for which the LFP was tuned. It was of interest to see whether one particular object was 'preferred' throughout each area, or indeed across areas, and whether it was the same for both epochs of the task. The expression 'preferred' will be used throughout this section as a convienient terminology to refer to the object for which the total beta power was maximal, as is common in single unit literature.

5.5.2 Methods

Data was collected and analysed from M39. Only LFPs categorised as tuned in the previous analysis were considered. LFPs which were statistically untuned were disregarded as their preferred objects might be expected (and were generally found) to be randomly distributed. The preferred object for each LFP in each epoch was designated as the object with the highest beta power. As the set of objects used during recordings from each hemisphere was different, the two hemispheres were considered separately.

5.5.3 Results.

5.5.3.1 Left Hemisphere, M39.

The results for the left hemisphere of M39 are shown below. The numbers of LFPs in M1 for which a given object was the most preferred, during object observation and during object grasp are depicted in Figure 5.8.

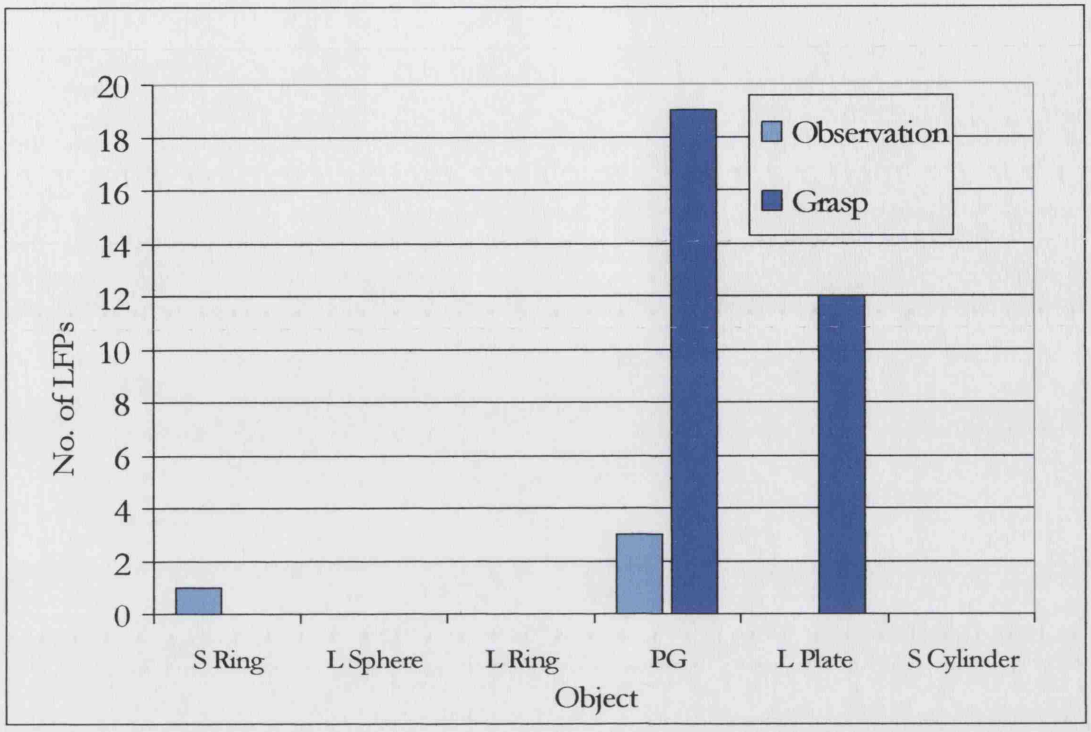

Figure 5.8 Chart to show preferred objects of tuned LFPs in M1 (left hemisphere) during object observation and object grasp.

During object observation, only 2 objects were ever preferred, and one of those was only preferred once (although the sample size was small). The two preferred objects were the small ring and the precision grip (PG). During object grasp, the PG remained the most preferred object. However, the large plate was also well represented, despite never being the preferred object during observation. During both epochs, M1 showed only a narrow range of preferred objects. Figure 5.9 shows the same analysis for F5 LFPs.

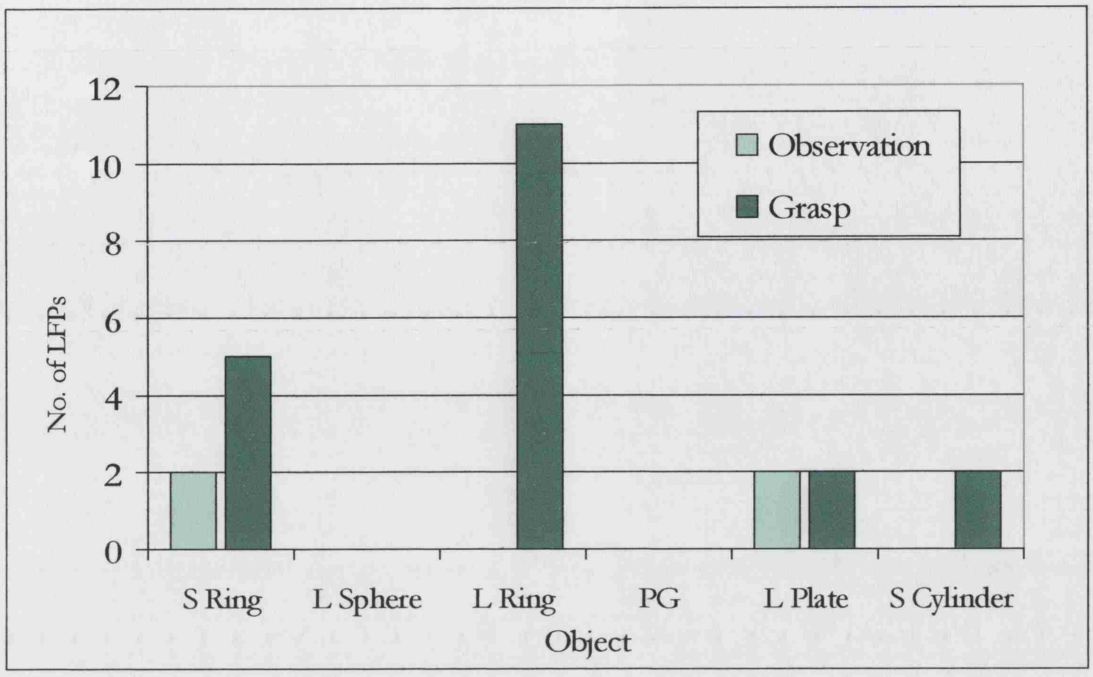

Figure 5.9 Chart to show preferred objects of tuned LFPs in F5 (left hemisphere) during object observation and object grasp.

During object observation, the preferences of the tuned LFPs were for the small ring and the large plate, although there were only a very small number of tuned LFPs. During object grasp, the range was broader, where 4/6 objects were preferred, twice as many as were preferred by M1. F5 appears therefore to show a broader range of preferred objects overall, perhaps indicating representation of more variety of object-related characteristics than M1. The PG, which was most strongly favoured in M1, was not the preferred object of any tuned LFP in F5, and the two rings which were the preferred objects in F5 were not favoured by M1 LFPs, indicating a difference in preferred objects for the two areas. These data further reinforce the conclusion that M1 and F5 LFPs are genuinely different, with different properties and task relationships.

5.5.3.2 Right Hemisphere, M39.

For the recordings made in the left hemisphere of M39, all 6 objects were different to one another in grasp type and appearance. This was not the case for the right hemisphere. Here, amongst the 6 objects were two that were repeated twice, but grasped in different ways. They were visually identical (apart from a small piece of red tape) but elicited different grasps (the red tape indicated when a 'side' grip should be used). This is depicted graphically in Figure 4.4. The distribution for tuned LFPs in M1 is shown in Figure 5.10.

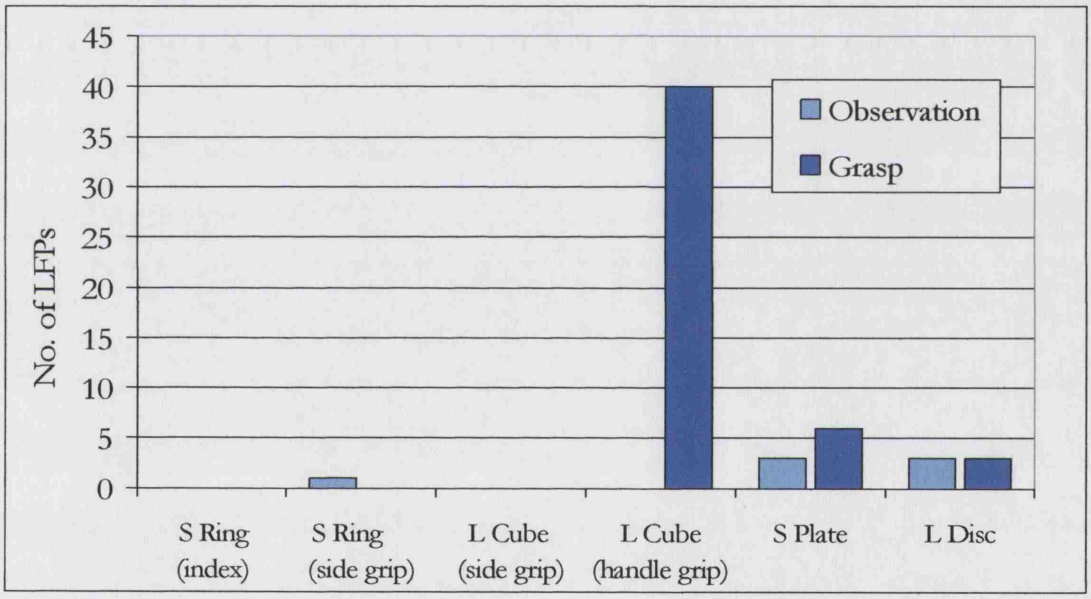

Figure 5.10 Chart to show preferred objects of tuned LFPs in M1 (right hemisphere) during object observation and object grasp.

During observation, 3/6 objects were the preferred object for at least one LFP. The same was true for object grasp, although in this epoch, one object, the large cube was the preferred object for the vast majority of LFPs and only a small number of LFPs showed maximal beta power for the other two objects, again suggesting a narrow range for M1 LFPs.

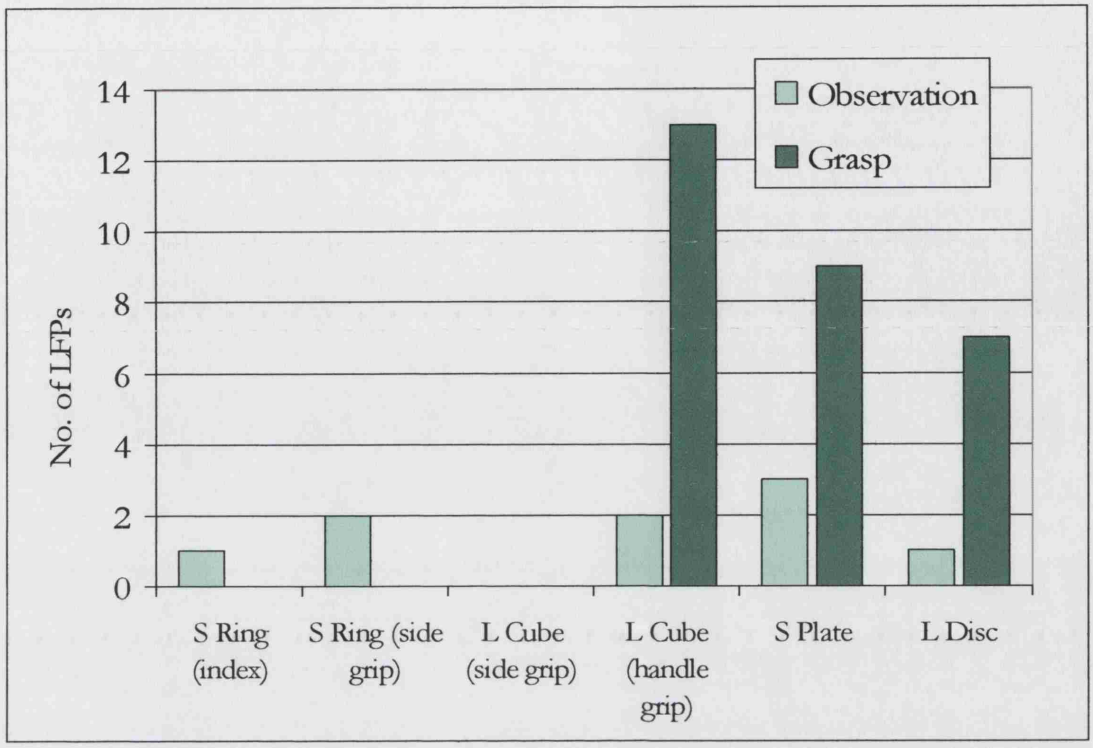

Figure 5.11 Chart to show preferred objects of tuned LFPs in F5 (right hemisphere).

In F5 (Fig. 5.11), during observation 5/6 objects were preferred at least once and no single object dominated the preferences. During object grasp, 3/6 objects were the most preferred for multiple LFPs – no single object dominated.

5.5.4 Conclusions

Although the sets of objects tested in each hemisphere were different, a similar overall pattern of tuning was observed. M1 LFPs generally 'preferred' only a small number of the objects during both epochs. As well as the tuning being mostly highly selective for objects (i.e. tuning for only one object) it appeared that the only one or a small number of objects were ever preferred. This may indicate that the beta power of the oscillations in M1 was maximally evoked by a narrow range of object and grasp characteristics, and

that the response of M1 to the different objects was quite homegenous. In contrast, F5 showed different properties. As well as showing more moderate tuning, that is, where maximal beta power was evoked by more than one object, the maximal beta power may occur for a broader range of objects, and hence a wider range of object charateristics – it was more heterogenous.

The tuning in M1 and F5 was therefore different not only in quantity but in quality – tuning in F5 was not only more moderate, but also broader in terms of object characteristics.

5.6 Patterns of Tuning II – Ordering of Objects

5.6.1 Introduction

The preferred object of a given LFP is only one aspect of its tuning. Beta oscillations were present during the grasp and observation of all objects to varying degrees. It is of interest to examine the order in which objects were ranked by total beta power, and the statistical degree of difference between objects. It was therefore possible to see if the order and groups could be related to the physical characteristics of the objects and the grasps used to perform the task. These orders and groupings are of particular interest where objects have been repeated but grasped differently, i.e. where they share visual properties such as size and shape, but elicit different grasps.

Different types of grasps and manipulative hand actions can be classified in many ways. Manipulative hand movements (Elliott & Connolly, 1984) can be reduced to three basic classes; simple synergies, reciprocal synergies and sequential patterns. A simple reach-to-grasp action usually involves a simple synergy, such as the convergent flexion of the fingers and thumb. Napier (1956) determined two main types of grasp – the power grip and the precision grip, based primarily on the number of fingers used to contact the object. This is a useful idea, but does not classify the wide range of hand postures and grip types that may use the same number of fingers, given that the hand has almost unlimited degrees of freedom. Later authors have suggested many other systems of classification. A schema of 'virtual fingers' (VFs) was proposed (Arbib *et al.*, 1985) that allowed the hand to be described in terms of 'grasping units', such that in a grasp of an object such as a small cube by the opposition of the index finger and thumb, each is acting as a VF, the thumb being VF1 and the finger VF2. For a larger cube, the grasp

would essentially be the same but with more fingers acting together as VF2. In this way, grasps that are essentially similar but involve differing numbers of digits can be classified. Iberall and colleagues (1986) used the concept of opposition to describe three motor directions in hand space coordinates through which force could be applied, given that prehension usually requires at least two forces to be applied to the object in opposition to each other. The idea of opposition space allow grasps to be described as pad opposition (forces parallel to the palm, fingers closing towards the palm, as in the grasp of a small ball, or a finger to thumb precision grip), palm opposition (forces perpendicular to the palm, such as the grasp of a cylinder with the fingers wrapping the cylinder into the palm) and side opposition (forces transverse to the palm, such as the grasp of a key between thumb and finger, often used for a thin, flat object). Some grasps utilise combinations of the above oppositions to provide a complex variety of stable grasps and grip postures that can nevertheless be categorised, such as when a narrow cylinder is grasped such that the index finger is in opposition to the thumb (side opposition) whilst the ulnar fingers are in a palm opposition, wrapped around the cylinder. Combined with the virtual finger approach, this allows grasps to be classified in a meaningful sense. A relatively small number of grasps are actually used from the number of possible hand configurations, and static grasp postures can be described using a small number of postural synergies (Santello *et al.*, 1998; Santello and Soechting, 1998), although much of the shaping involved in a reach-to-grasp action is a result of a base posture which is subsequently refined through finger and thumb movements to achieve the grasp required (Mason *et al*, 2001). Monkeys are known to use similar strategies to humans when reaching and grasping (Roy *et al.*, 2000; Roy *et al.* 2002), although despite these common postural synergies, in the macaque, unique muscular activation patterns are generated for many different objects (Brochier *et al.*, 2004).

The objects grasped in two different ways in this study allow us to investigate whether the two areas respond to different objects and grasps in the same way. Two objects were grasped in different ways, i.e. ways that utilise different opposition spaces and virtual fingers. A similar grasp (a side opposition with the fingers and thumb) was also used for two different objects to see whether grasp or object influenced the rank ordering by total beta power.

5.6.2 Methods

For each area and epoch, the average values of object-related beta power were averaged across all LFPs. The objects were ordered from the most to the least average total beta power. The values for each object were compared statistically (Students T-test, 2 tails, $P<0.05$) to determine which LFPs showed object-related beta power that was significantly different across objects. By pairwise examination of objects it was possible to establish not only an order of preference but also groupings of objects that could or could not be distinguished from each other purely on the basis of their beta power.

5.6.3 Results

5.6.3.1 Left Hemisphere

Figure 5.12 shows the ordering and grouping of the objects grasped during recording of LFPs in the left hemisphere of M39.

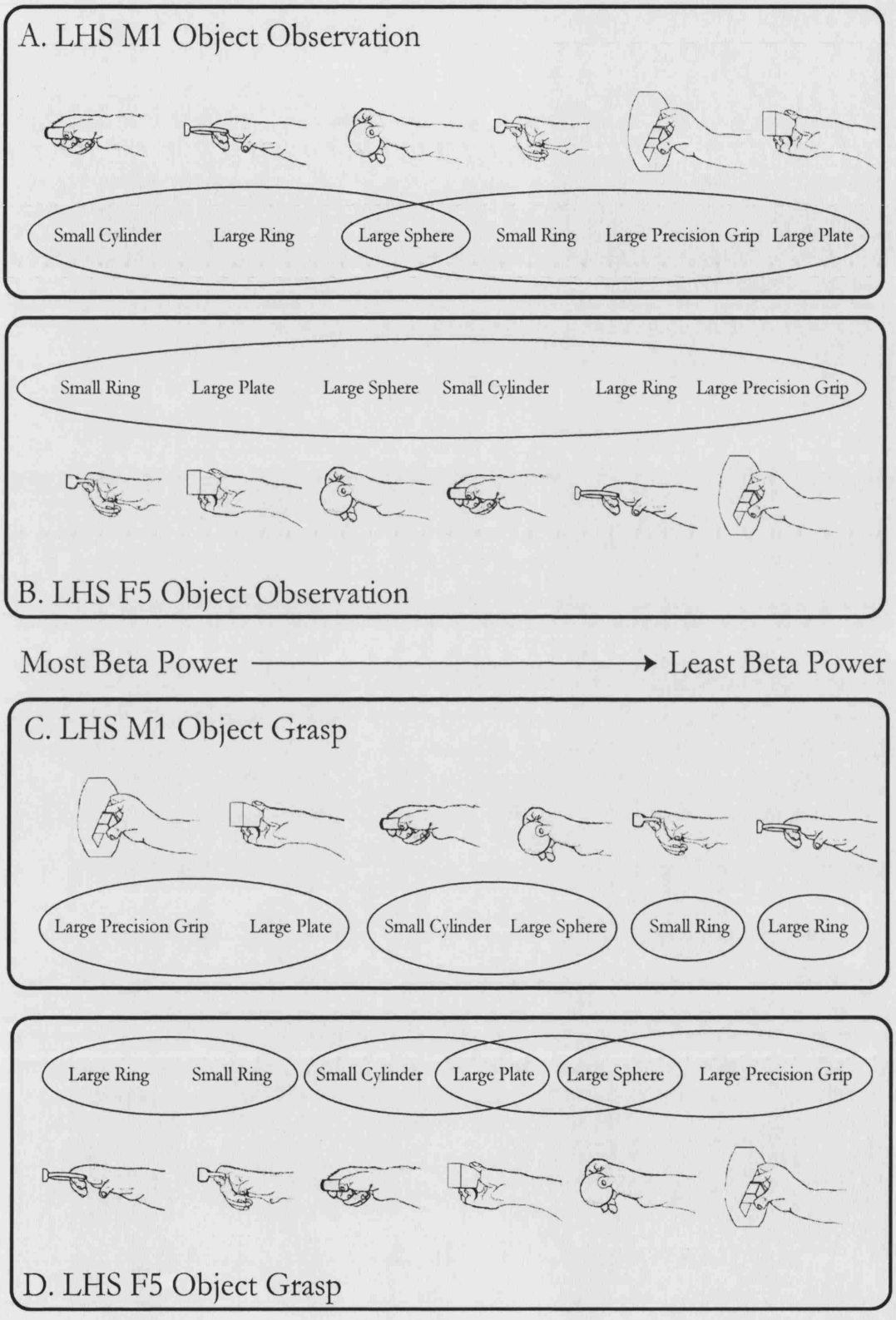

Figure 5.12 Object order and groupings for M39, LHS. Ovals group objects for which the beta powers were statistically indistinguishable, outline drawings depict the grasp used.

As would be expected from the degree of tuning results presented in section 5.4, the tuning was much less distinct during object observation than object grasp in both areas.

In M1 observation (Fig. 5.12A), there were two groups of objects, with the large sphere appearing in both, i.e its beta power could not be distinguished from any other object. The objects with similar visual characteristics, such as the large and small ring, appeared in different groups, but broadly, there was little generalised tuning across the area. Interestingly, the large precision grip was in the group with the least beta power, despite being the most frequently preferred object by the tuned LFPs. Of course, only a small percentage of M1 LFPs were tuned, so their effect may have been diluted.

In F5 observation (Fig. 5.12B), all objects were grouped together, i.e. when averaged, no particular pattern of tuning was revealed. This is not surprising given the result from the previous section which showed no single object dominating the tuning, even though the amount of tuning was larger than in M1.

A different pattern emerges for the object grasp epoch. In M1 (Fig. 5.12C), 4 groups were present, and none overlapped. There was therefore clear tuning across the area, even over multiple recording sessions. The small and large rings elicited the least beta power, and the precision grip and large plate the most - all of the LFPs (all of which were statistically tuned) showed a preference for one of these two objects.

In F5 (Fig. 5.12D), there were also four groups, although three of these overlapped, demonstrating again the broader tuning of F5. The two objects which elicited the most beta power were also the most visually similar – the large and small ring. Again, these were the two objects 'preferred' by the majority of tuned LFPs, and the next two highest were the small cylinder and large plate, which also were preferred by several LFPs.

There was a clear difference in the order between the two areas. During grasp, the object with the most beta power in M1 was the large precision grip – this had the least beta power in F5. Conversely, the large ring had the least power in M1 and the most in F5. Comparing across epochs revealed another difference. The ordering in F5 was similar in both epochs, with the small ring moving from having the second highest amount of beta power during observation to the most during grasp; the precision grip had the least beta power in both epochs. In M1 the order was almost reversed – the large plate and precision grip changed from having the lowest beta power to the highest, and the large ring from second highest to last. This suggests that F5 retained its general pattern of tuning throughout the task, whereas M1 was different in the two epochs.

5.6.3.2 Right Hemisphere

Figure 5.13 shows the results for the right hemisphere.

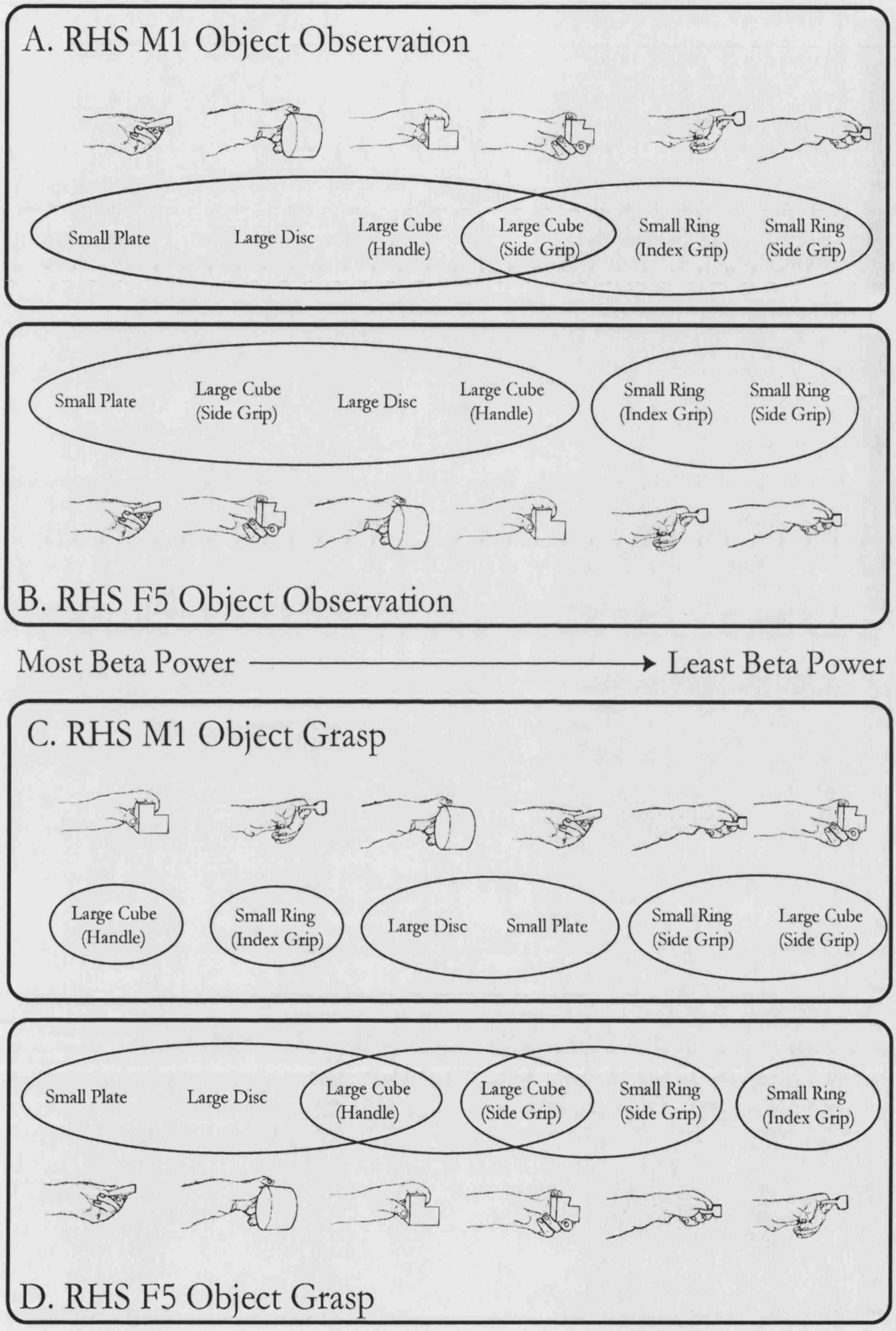

Figure 5.13 Object order and groupings for M39, RHS. Ovals group objects for which the beta powers were statistically indistinguishable, outline drawings depict the grasp used.

Here, we can see the effect of grasping the same object in two different ways, and also the effect of using a very similar grasp on two visually different objects; in both side grips (for the small ring and the large cube), a side opposition grasp is used which contrasts with the handle grip of the large cube (a pad opposition grip) and the index grip of the small ring (whre there is no opposition).

In M1 during object observation (Fig. 5.13A), there were two groupings of objects, with the small plate and large disc eliciting the highest beta power. These two objects were those which were preferred by the majority of tuned LFPs. The beta power for the two large cubes which were to be grasped differently were indistinguishable, as were the beta powers for the two small rings, even though tape on the objects indicated which grasp would subsequently be used, perhaps indicating a grouping according to visual (or physical) characteristics rather than the upcoming grasp – however, the beta powers elicited by the objects which would subsequently be grasped with similar grips, the large cube and small ring gripped from the side were also indistinguishable.

In F5 (Fig. 5.13B) during object observation, there were only two groupings. The object with the most power was the small plate; the beta power was indistinguishable from that elicited by the large cube (whichever way it would be grasped later in the trial) or the large disc, which together accounted for 2/3 of the tuned LFPs preferences. This suggests a genuinely broad representation of objects in F5. Objects again appear to be grouped by visual/physical appearance. However, in contrast to M1, the upcoming grasp appeared to affect the groupings less, as the two side grips were in separate groups.

During object grasp, as with the left hemisphere, the results were different. In M1 (Fig. 5.13C), there were four non-overlapping groupings. The large cube uniquely has the most beta power, and was also the object which the vast majority of tuned LFPs 'prefer'.

The two objects with the least beta power were the two rings. The two similar grasps produced indistinguishable amounts of beta power, whereas the identical objects grasped differently were clearly separable in both cases. This indicates that, as might be expected, the physical aspects of the grasp were more important in evoking beta power in M1 during grasp, and not the visual properties of the object.

Fig. 5.13D shows the results for F5. Here, the three objects which evoked the most beta power were indistinguishable – they were also the three most preferred objects among tuned LFPs. The two different grasps of the large cube were indistinguishable in F5 - the opposite of M1. The two different grasps of the small ring had the least beta power in F5, although they were separable. The two similar grips of the large cube and the small ring also grouped together uniquely. This appears very different to M1 – the visual properties of the object seem to be still strongly represented in the amount of beta power as well as the physical aspects of the grasp, even during active grasp.

The conservation of tuning from one epoch to the next was less clear than for the left hemisphere and was perhaps confounded by the repetition of objects. In M1, the small ring (side grip) and the large cube (side grip) remain in the grouping of objects which evoked the lowest power from observation to grasp, and the large disc and small plate remain adjacent. However, the small plate which evoked the most power during object observation was in the middle grouping during grasp, and the small ring (index grip) moved from the lowest power group to the second highest group. No clear pattern emerged; although some features of the order were certainly conserved, most others were not. In F5, it was clearer that the ordering of the objects was retained thoughout the task. The grouping which elicited the highest power in observation contained the small plate, large cube (both grasps) and the large disc – during grasp, the small plate

remained at the highest power end of the group with the most power, with the large disc and large cube (handle grip) in the same grouping. The two grasps of the large cube remained indistinguishable, and the two grasps of the small ring stayed as the two objects which elicited the least power.

5.6.4 Conclusions

The object-related properties of the beta power in the LFPs recorded in two motor areas, M1 and F5, were not the same. During observation, the beta power of the F5 LFPs for each object would seem to be grouped by visual similarity, regardless of the upcoming grasp. In M1, similar grasps are closer in the order, but the visual properties still have an influence on the tuning order and groupings. During grasp, M1 ordering changes from that of observation and becomes strongly related to grasp type, regardless of object. The more similar the grasps, with respect to the arm and hand orientation, and also the involvement of the thumb, the closer they appear in the order. In F5, the ordering was more conserved throughout the trials. The visual properties of the objects as well as the grasp seem to influence the total beta power, even during grasp. A more systematic selection of objects and grasps would allow this to be confirmed in a future experiment. It has already been established that neurons in F5 can reflect purely motor or visuomotor properties in their activity, and the results described here are entirely consistent with these previous findings.

5.7 Comparision of Tuning Within and Between Areas.

5.7.1 Introduction

Two measures of the tuning of the LFP have already been presented, covering the pattern of objects which are the most preferred, i.e. have the highest beta power, and the generalised order of tuning, which assesses which objects are more or less preferred and which can be distinguished from each other on the basis of their beta power. These are population measures. However, on an individual basis, any two LFPs recorded simultaneously may have very similar or very different patterns of tuning. One way to assess this is by calculating a comparative measure, the Euclidean distance.

5.7.2 Methods

The Euclidean Distance (ED) between two vectors is a mathematical representation of the total similarity of their dimensions. In this case, the ED of a pair of LFPs is calculated from the normalised beta powers for each object in two simultaneously recorded LFPs. These normalised values are represented as two 6-dimensional vectors, where the normalised power for each object is one dimension. This can be represented as follows:

if the vectors for LFPa and LFPb are given by

$$a = (x_1, x_2, \ldots, x_n)\ b = (y_1, y_2, \ldots, y_n)$$

,

where x and y represent the normalised power for each object, number of objects, n=6, then their Euclidean distance, d(a,b), is given by

$$d(a,b) = \sqrt{(x_1 - y_1)^2 + (x_2 - y_2)^2 + \cdots + (x_n - y_n)^2}.$$

If the relative amounts of total beta power for each object are the same for two LFPs, i.e. x_1 is approximately equal to y_1, x_2 to y_2, etc., the ED between the two LFPs will be small - identical tuning patterns would result in an ED of 0. Conversely, the more dissimilar the tuning of LFPs, the greater the value of the ED. ED calculated in this way from the object-related beta powers therefore represents a measure of tuning similarity, and provide a way of comparing the intra and inter-area tuning similarity. If tuning was relatively homogenous throughout an area, the EDs would be lower than if tuning was varied, and if inter-area tuning was more varied than intra-area tuning, there would be a higher average ED for inter-area pairings than for the intra-area pairings.

This measure does not, however, reflect the strength of tuning, only the similarity, hence a low ED value could be obtained by comparing two highly tuned LFPs with very similar tuning, or two untuned LFPs.

EDs were calculated for all pairs of simultaneously recorded LFPs from both hemispheres, both within and across areas, during both epochs.

5.7.2 Results

5.7.2.1 Observation Epoch

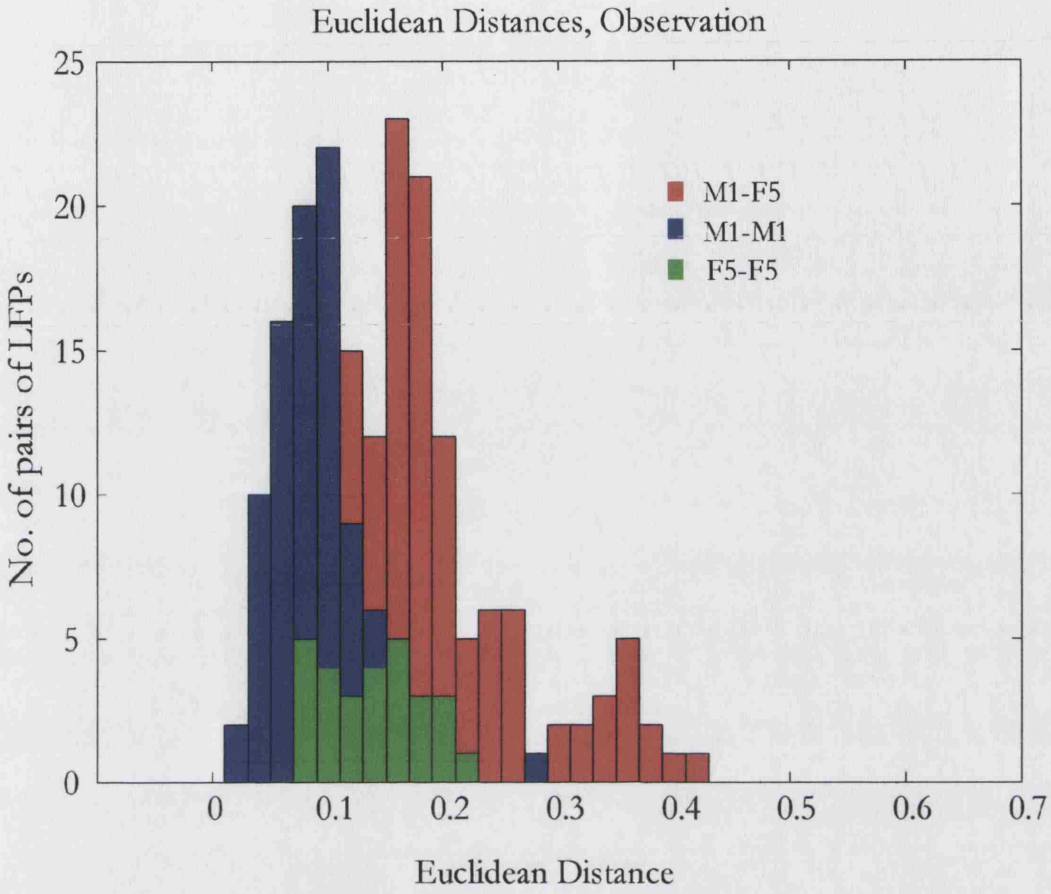

Figure 5.14 Euclidean distances – observation.

Figure 5.14 shows the results for all pairs of simultaneously recorded LFPs in M39, both hemispheres. The category with the lowest and most similar EDs was the M1-M1 pairings, average ED 0.09, s.d. 0.03. The majority of M1 LFPs were found to show no statistical tuning during observation, so the ED between two untuned LFPs will be small, as well as the distance between two highly but similarly tuned LFPs. F5-F5 pairs showed slightly more variability in their tuning, average E.D., 0.14, s.d. 0.04. The across-area pairings showed the most variability, average, 0.19, s.d. 0.08. The range of values was narrowest for M1 pairs and broadest for pairs recorded in two different areas. Some M1-F5 pairs showed much more similarity in their tuning than others, whereas within areas, the ranges were narrower.

The results for the grasp epoch are shown below in Fig. 5.15.

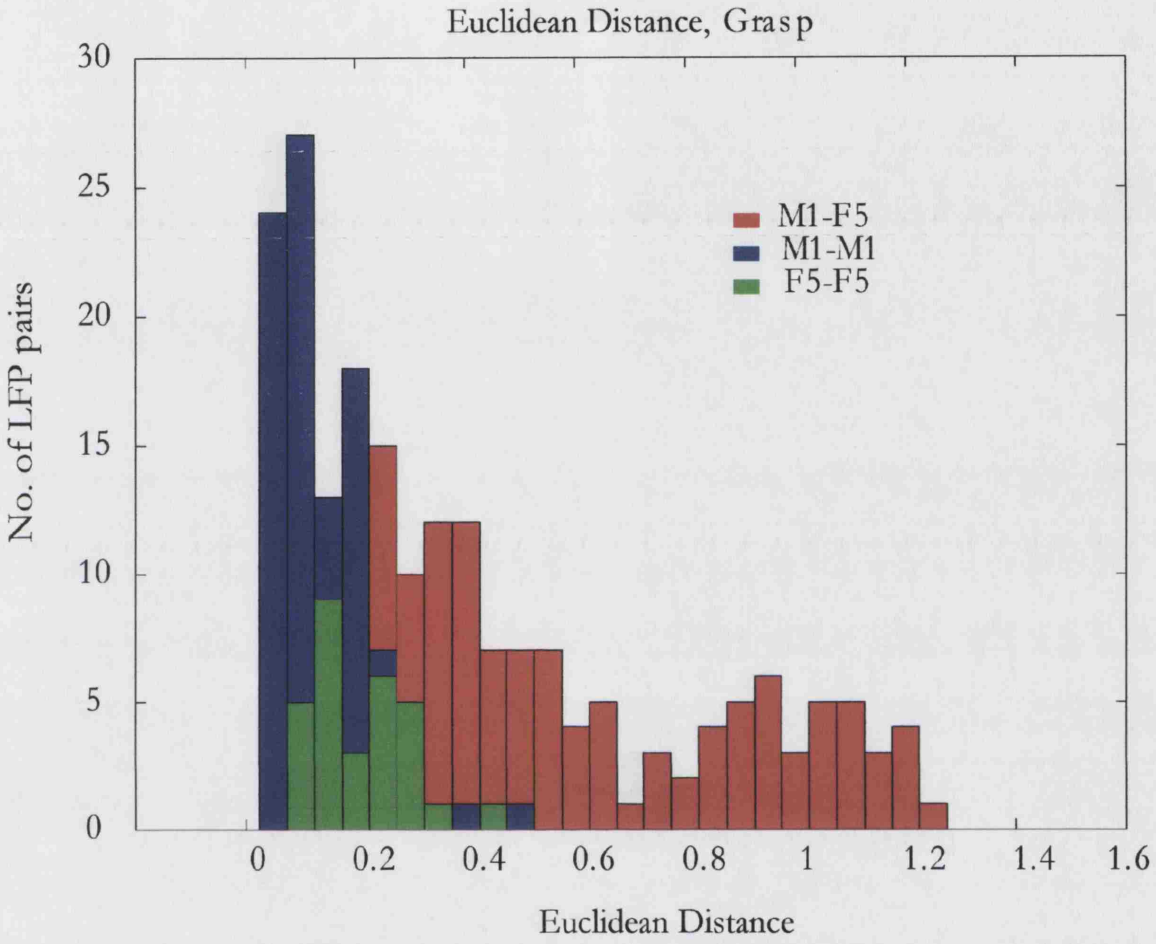

Figure 5.15 Euclidean distance – grasp

The average for M1-M1 pairs during grasp was 0.15, s.d. 0.09, again, the lowest value, indicating that M1 LFPs were more similar to each other in their tuning than either F5-F5 pairings or the across-area M1-F5 pairs. The average ED was higher than for the observation epoch, indicating that there was more variability in tuning during grasp than observation. F5-F5 pairs had an average ED of 0.21, s.d. 0.09, again indicating more variation in tuning during grasp than observation. The highest EDs were again found across areas, with an average of 0.54, s.d. 0.32. The range of ED values for the M1-F5 pairings during grasp was broad, indicating that during object grasp, M1 and F5 LFPs

are often showing quite different strengths of beta oscillations for the same objects. The distribution was possibly bi-modal, perhaps as a result of the presence of tuned and untuned LFPs in the data set. A pairing of two untuned LFPs will result in a low ED, as will a pairing of two tuned and similar LFPs, whereas if one is tuned and the other much less so, the ED will be large, indicating a genuine difference in the tuning.

5.7.3 Conclusions.

The relatively narrow range of EDs between simultaneously recorded M1 LFPs supports the hypothesis that M1 LFPs are more homogenous than the F5 pairs, which show a broader range of EDs. This was true for both epochs. The across-area pairings showed more variability, with some pairs showing a high degree of similarity, and others a large degree of difference. The results also support the idea that the LFPs recorded simultaneously are not redundant – if they were, very low EDs would be found for all pairs with similar ranges for the M1-M1 and F5-F5 pairings, as the physical distances between pairs of simultaneously recorded LFPs were approximately equal in the two areas. This was not the case – M1 pairs had smaller average values than F5 pairs during both epochs.

These data show that on an individual level as well as at a population level, M1 LFPs showed more homogeneity in the relation of the beta oscillations to the task than F5 LFPs.

5.8 Summary

The total beta power of the oscillations seen in the LFPs of both M1 and F5 has been shown to be related to a reach-to-grasp task in several ways. The amount of power

varied with the epoch of the task, being most prevalent during steady object grasp, and also during object observation. The oscillations were abolished during movement. The peak frequency of the beta power was also task dependent, and increased by 1-2 Hz from the observation to the grasp epoch.

The amount of power in the LFPs was different for different objects, showing that LFPs can be 'tuned' for particular objects during both epochs. M1 and F5 showed different amounts of tuning in the two epochs, and the type of tuning was different. M1 LFPs showed more homogeneity in their tuning, with respect to the object which evoked the most beta power, and also the general order of tuning for all objects. Their tuning was predominantly during the steady grasp of the objects. F5 LFPs exhibited a broader degree of tuning for a more varied set of objects, indicating a wider object representation. More F5 than M1 LFPs showed tuning during the observation epoch, and fewer during the grasp epoch.

The LFP signals in the two areas behave differently with repect to the task, and must therefore be distinct from each other, and not merely the same signal recorded twice at two different locations. It has also been shown that the signals are not totally redundant, even when recorded at closely spaced locations, although they are clearly not totally independent either, but somewhere in between.

These results show that 'tuning' of LFPs in the motor cortex can be demonstrated, and further the understanding of how M1 and F5 LFPs vary with aspects of a reach-to-grasp task.

Chapter 6. Coherence between M1 and F5

6.1 Introduction

Chapter 4 demonstrated that oscillations in the premotor and motor cortex LFPs are not only task related, but coherent at the same beta frequencies as the task related power. This indicates that the signals were phase-locked to a common oscillatory frequency from a common source. In this chapter, the coherence in the beta frequency band (calculated as described in Chapter 4, section 4.3.4) during the object observation and the object grasp epochs of the task has been used to examine further the relationship between M1 and F5 during the performance of the reach-to-grasp task. The relationship of the coherence between a pair of LFPs and the degree of similarity of tuning of that pair, represented by the Euclidean distance, will also be examined during both object observation and grasp. The association between the coherence and the object being grasped will also be examined. The coherence between two LFPs assesses the phase coupling between the oscillations both within and across areas (Rosenberg *et al.*, 1989; Baker *et al.*, 1997) and can be further characterised with a phase shift and a time delay. These indicate whether one signal consistently 'leads' the other and to what extent, and can be used to examine the relationship between the beta oscillations in M1 and F5 during the two epochs of task performance.

6.2 Coherence Values

6.2.1 Methods

Coherence was calculated as described in Chapter 4 for all possible pairs of simultaneously recorded LFPs in both hemispheres of M39 during both epochs. The

coherence for a pairing was defined as the peak coherence in the 18-35 Hz beta range, calculated for all trials in a session. The coherence values obtained for the three different possible categories of pairings, M1-M1, F5-F5 and M1-F5 were compared for each epoch.

6.2.2 Results

Across all sessions, the frequency of peak coherence was significantly higher during the observation epoch than during the grasp epoch, and the coherence was significantly higher during the grasp epoch than the observation epoch (left hemisphere, frequency, 22.1 Hz to 23.5 Hz, $p<0.00001$, coherence 0.40 to 0.51, $p<0.00001$; right hemisphere, frequency, 21.1 Hz to 21.4 Hz, $p<0.01$, coherence, 0.55 to 0.77, $p<0.00001$, all comparisons, T-test, 2 tails).

The coherence values grouped by the pairings are show below in Figure 6.1.

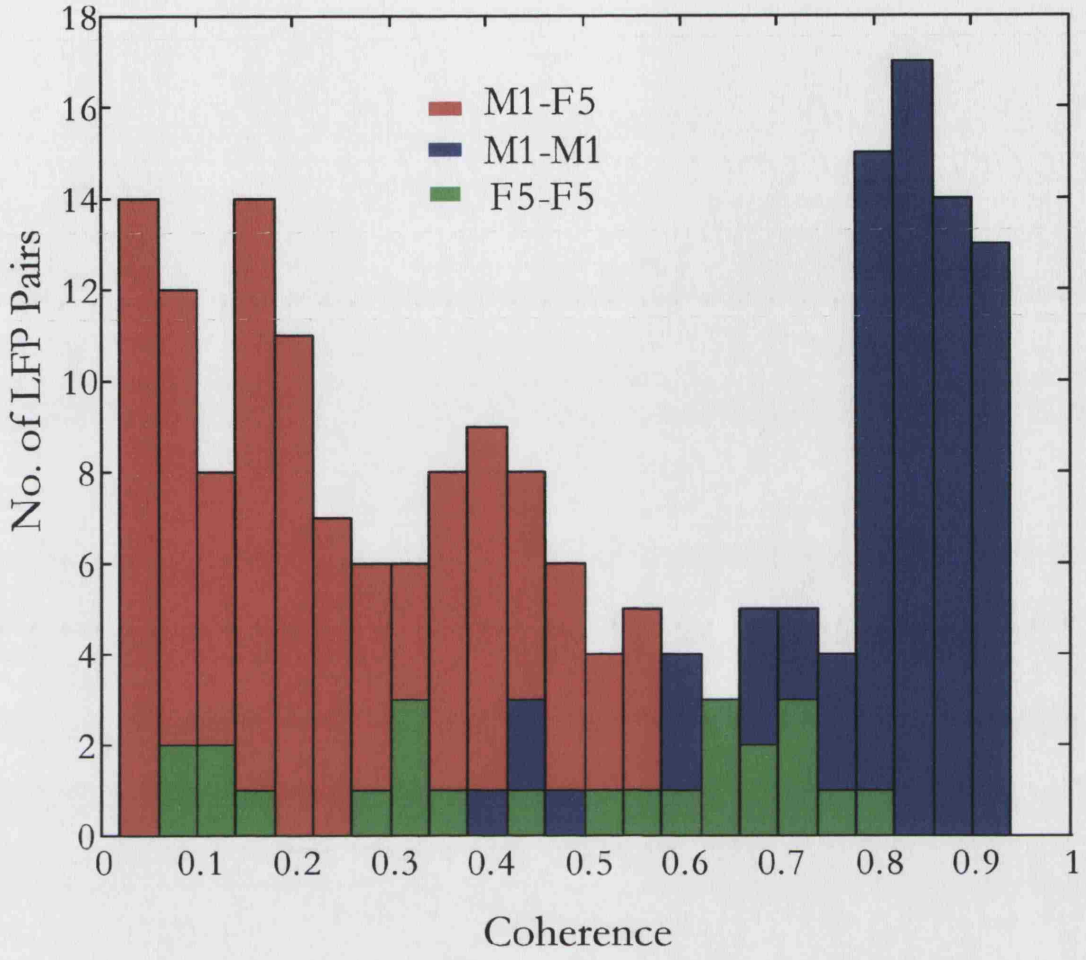

Figure 6.1 Histogram of coherence values during object observation.

As would be expected, the intra-area (M1-M1 and F5-F5) coherences were generally higher than the inter-area (M1-F5) coherence (mean values, M1-M1, 0.78, s.d. 0.13; F5-F5, 0.47, s.d. 0.24; M1-F5, 0.26, s.d. 0.16). M1-M1 pairings of LFPs had the highest coherence.

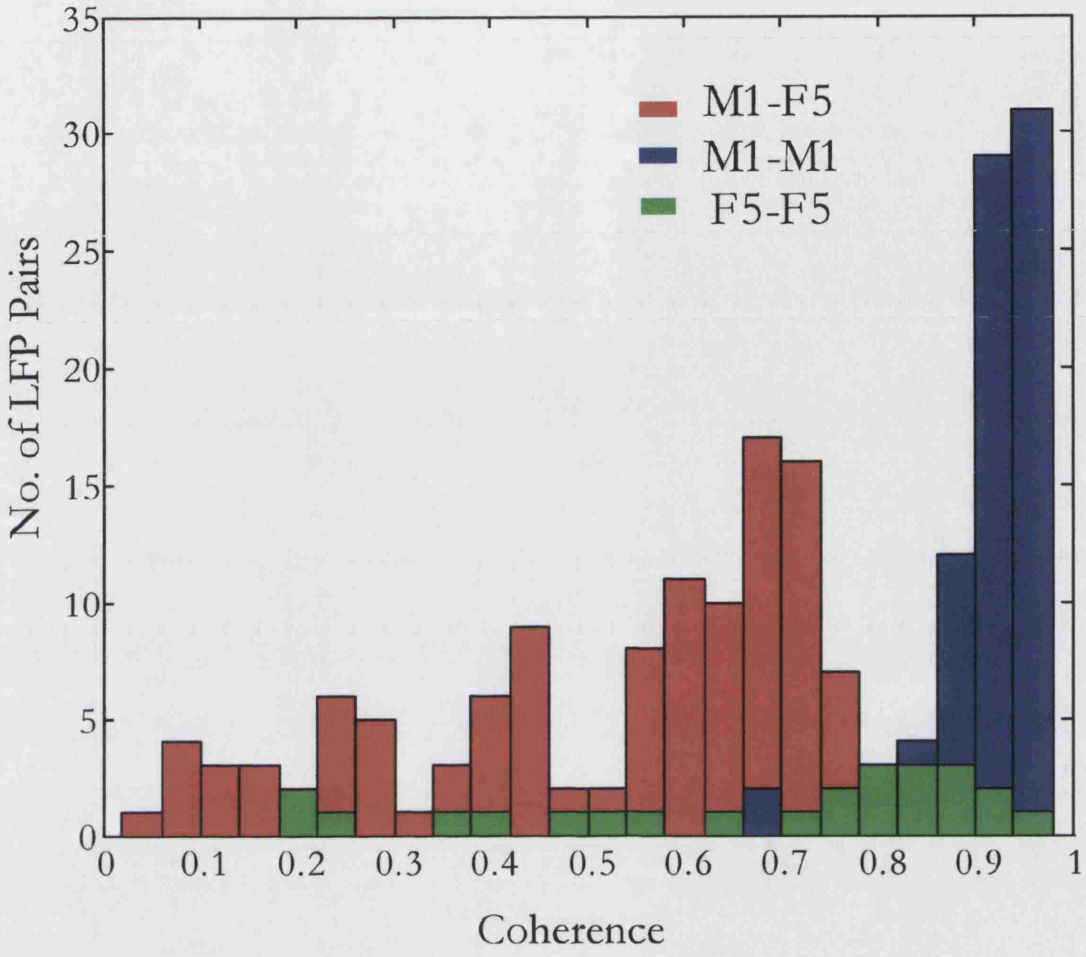

Figure 6.2 Histogram of coherence values during object grasp.

During object grasp, the same pattern was present (averages, M1-M1, 0.90 s.d. 0.09; F5-F5, 0.67 s.d. 0.24; M1-F5, 0.52 s.d. 0.21). The mean level of coherence for each group increased from the observation epoch to the grasp epoch; M1-M1 increased by the smallest amount, 15%, F5-F5 by 43.2%, whereas the average M1-F5 coherence increased by 103.6%.

6.2.3 Conclusions

There was clear task related coherence, which was highest in the beta frequency range. The coherence between pairs of simultaneously recorded LFPs varied considerably

depending on the area in which each of the pair of electrodes were sited, and the stage of the task being performed.

Generally, during the observation epoch, coherence values for each of the three categories of pairings were lower than the corresponding values for the grasp epoch. The power of the beta oscillations was generally higher during active grasp, and this result shows that the coherence (which is independent of the amplitude of the power) was also higher. The M1-M1 pairings always had the highest levels of coherence, which in some cases were close to 1. These very high levels of coherence reflect a certain degree of signal redundancy due to the close spacing of the electrodes used to record the LFPs, leading to large volume conduction effects. However, as a much broader range of coherence values was observed in F5, and those LFPs were recorded at similar separation distances, the high coherences in M1 cannot be solely attributed to redundancy and volume conductance. This will be investigated in a later section. The inter-area pairings were separated by the largest inter-electrode spacings and generally showed lower coherence values. The values were significant in the beta frequency range, as were those for the intra-area recordings, although these interarea pairings often showed significant coherence at other frequencies.

It can be concluded that there was task-related coherence between nearly all pairs of simultaneously recorded LFPs, whether from M1, F5, or one from each.

6.3 Coherence and Tuning

6.3.1 Introduction

It is not yet established whether the coherence found was related to the task in terms of the object observed then grasped. In order to ascertain whether the coherence observed

was related to the object properties of the task, firstly, the coherence for each object in a sample session was calculated to establish whether there was any variation. Secondly, the values of coherence for each pairing of electrodes were compared with the similarity of their tuning, as represented by the Euclidean Distance (ED) between the tunings of the LFPs recorded on each of the pair. This analysis will assess whether the coherence between a pair of LFPs is related to the similarity of their responses to the different objects used in the task, i.e. whether those pairings with similar tuning patterns are more coherent than those with dissimilar patterns of object related tuning. If this were the case, this could imply a functional relationship between LFPs, especially those in different areas, providing a means by which information about specific objects and grasps could be encoded and transformed.

6.3.2 Methods

Coherence was calculated as described in Chapter 4 for a single session, with the trials subdivided by object grasped, and the maximum coherence value in the beta range was calculated. Secondly, the coherence was calculated for all objects for all pairs of simultaneously recorded LFPs in both hemispheres of M39 during both epochs. The Euclidean Distance for each pair (as calculated for Chapter 5, section 5.6) was used to determine the relationship between the amount of coherence between two LFPs and the degree of similarity of their tuning.

6.3.2 Results

The object-related coherence for an inter-area pairing of LFPs recorded in the right hemisphere of M39 during both object observation and object grasp is shown in Fig. 6.3. In this example, there was clear, significant beta coherence for all objects in both epochs. However, the peak value of the coherence varied from object to object; during

observation, the lowest value was for the small ring (0.14, blue line in Fig 6.3A) and the highest for the large disc (0.33, yellow in 6.3A); during grasp it varied from from 0.51 for the small ring grasped with an index grip (blue line in Fig. 6.3B) to 0.67 for the large cube grasped with a handle grip (cyan line in Fig. 6.3B).

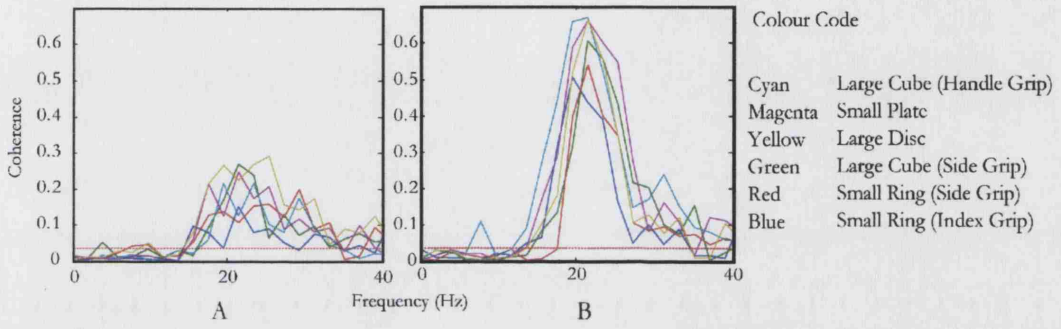

Figure 6.3 Object-related coherence for a typical M1-F5 pair of LFPs. Coherence calculated during **A.** the observation epoch and **B.** the grasp epoch. Red dotted lines represent significance.

The peaks were generally less defined during object observation than during grasp. This establishes that coherence varied with parameters of the task, in this case, the object being grasped as well as the epoch. Coherence did not always vary with the object in this manner. By inspection, 13/30 sessions showed no clear pattern of object-related variance. Object-related coherence also depended on the pairing – inter-area pairings were more likely to show object effects than intra-area pairs.

The comparison between overall coherence levels for all objects between pairs of LFPs and tuning, as indicated by the ED is shown below in figure 6.4.

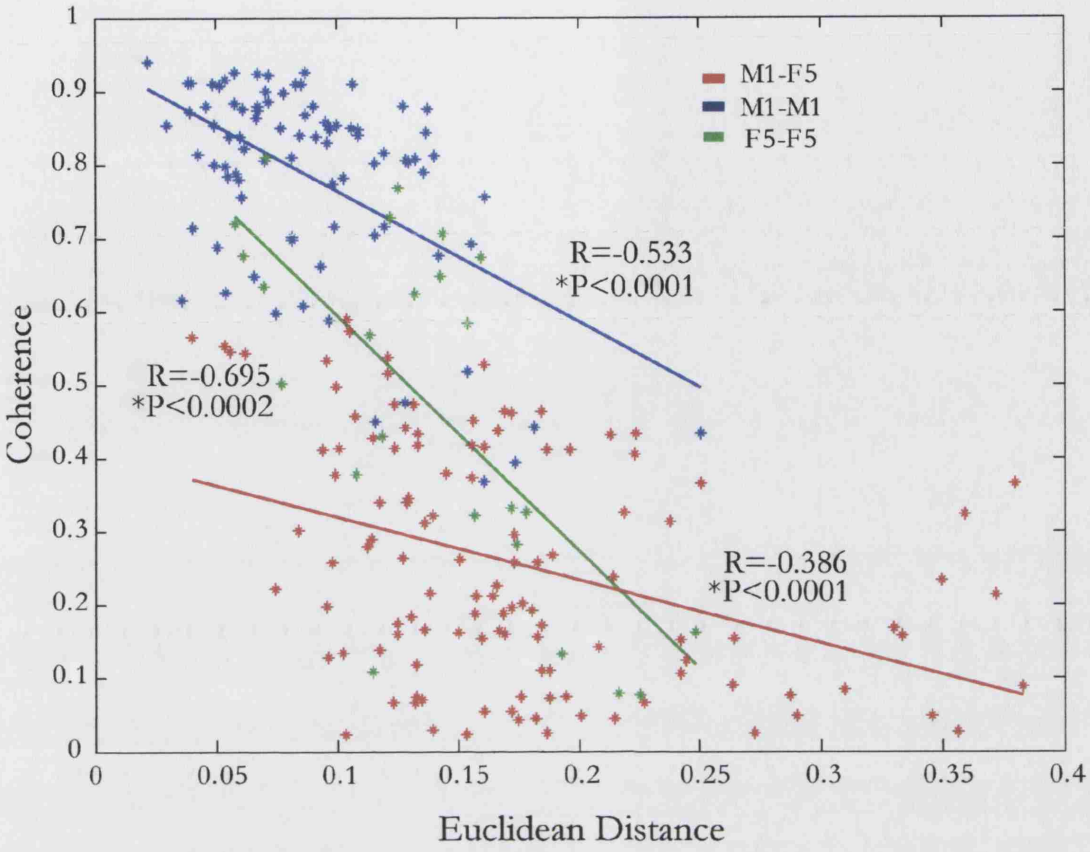

Figure 6.4 Coherence vs. Euclidean distance – observation. Each dot represents one pairing of LFPs recorded simultaneously, with the areas of each LFP indicated by the colour.

During observation, there was a significant negative correlation between coherence and ED for all three possible types of pairs – M1-M1 ($P<0.0001$), F5-F5 ($P<0.0002$) and M1-F5 ($P<0.0001$). In all cases, higher coherence was correlated to lower ED, that is to say, the more similar the tuning, the higher the coherence. The M1-M1 pairs produced the most highly clustered data points, reflecting their smaller range of EDs and their consistently high coherence levels. The results for the object grasp epoch are shown in Fig. 6.5. Again, there is a highly significant negative correlation between coherence and E.D.

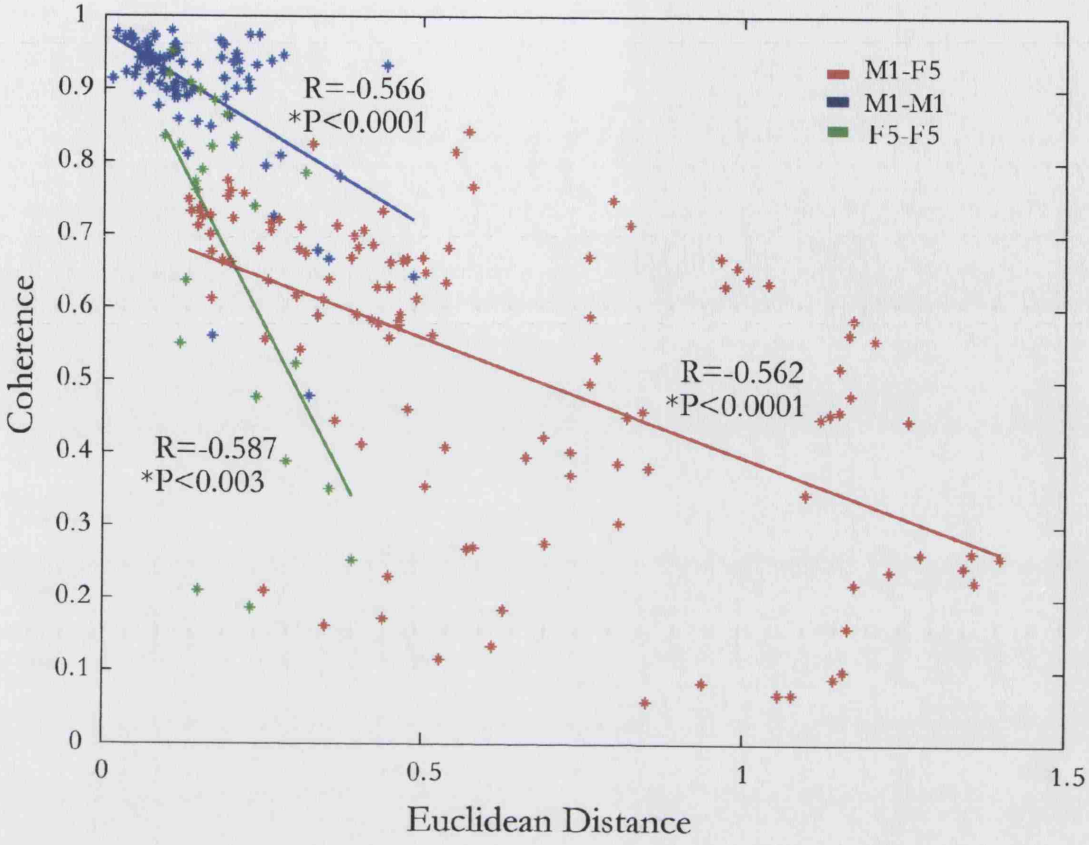

Figure 6.5 Coherence vs. Euclidean distance – grasp. Each dot represents one pairing of LFPs recorded simultaneously, with the areas of each LFP indicated by the colour.

The highest coherence levels, seen in M1-M1 pairings of LFPs were reliably associated with low EDs, indicating that the most coherent pairs of LFPs were also the most similarly tuned. This was also true for F5-F5 pairs. For the M1-F5 pairs, there was a large range of values for ED and coherence, more than twice the range that the inter-area pairings had, and the correlation was highly significant again.

6.3.3 Conclusions

Not only was the coherence found to be object-dependent on an indvidual level, i.e. between a single pairing of LFPs during a single session, but it was also highly dependent on the overall similarity of tuning of the pair of LFPs. This is partly due to the

fact that both ED and coherence are measures of the correlation between two LFPs, so the higher the correlation in one respect, the higher it might be expected to be in the other, given that it is the same pair of LFPs each time. However, it is likely that the increased coherence between LFPs with similar tuning might indicate that such sites are linked in a functional way with respect to task parameters, and have a role in 'binding' the two areas together for successful completion of the visually-guided grasp task.

6.4 Bipolar vs. Monopolar Recordings

6.4.1 Introduction

Very high (>0.9) levels of coherence were observed in some intra-area recordings and even the inter-area coherences were often rather high (>0.5). This could be a genuinely high coherence, but is more likely to reflect a large degree of volume conduction or have another alternative explanation. The LFP data analysed was recorded in a unipolar fashion (i.e. against a remote indifferent, which was grounded). These LFPs reflect the difference in signal voltage between the tip of the electrode and the remote ground (in this case usually the monkey's head). LFPs therefore represent the signal from the cortex surrounding the electrode tip, with the volume of the region depending on the impedence of the electrode. It has already been established that the LFP signals are not completely redundant when recorded at separations of approximately 300 – 900 μm (see Chapter 5.2). If a bipolar montage is used to record the LFP between the the tips of two electrodes, then a much more localised signal can be analysed to establish whether true coherence between the areas exist, and whether there is a genuinely different LFP signal in the two cortical areas.

6.4.2 Methods

Two sessions in which four clean LFP recordings were obtained, two in M1 and two in F5, were chosen from the data recorded in M39. These recording sessions were chosen as they contained two signals in each area which were well matched in amplitude of signal and signal to noise ratio. This was important to prevent one signal dominating the other and skewing the resultant signal. From the four simultaneous recordings, bipolar LFP signals for M1 and F5 were calculated by subtracting the signals recorded on the two original monopolar LFPs within each area to create a differential bipolar signal.

Firstly, power spectra for these bipolar LFPs were calculated and compared to the original recordings. Secondly, the coherence between the original LFPs and between the two bipolar LFPs was calculated. These were then compared.

Because of the requirement to have two well-matched simultaneous signals in each area, there were insufficient sessions where these conditions were met to perform a systematic analysis of the bipolar coherence levels. The two sessions shown here provide proof of principle.

6.4.3 Results

The power spectra are shown in figure 6.6.

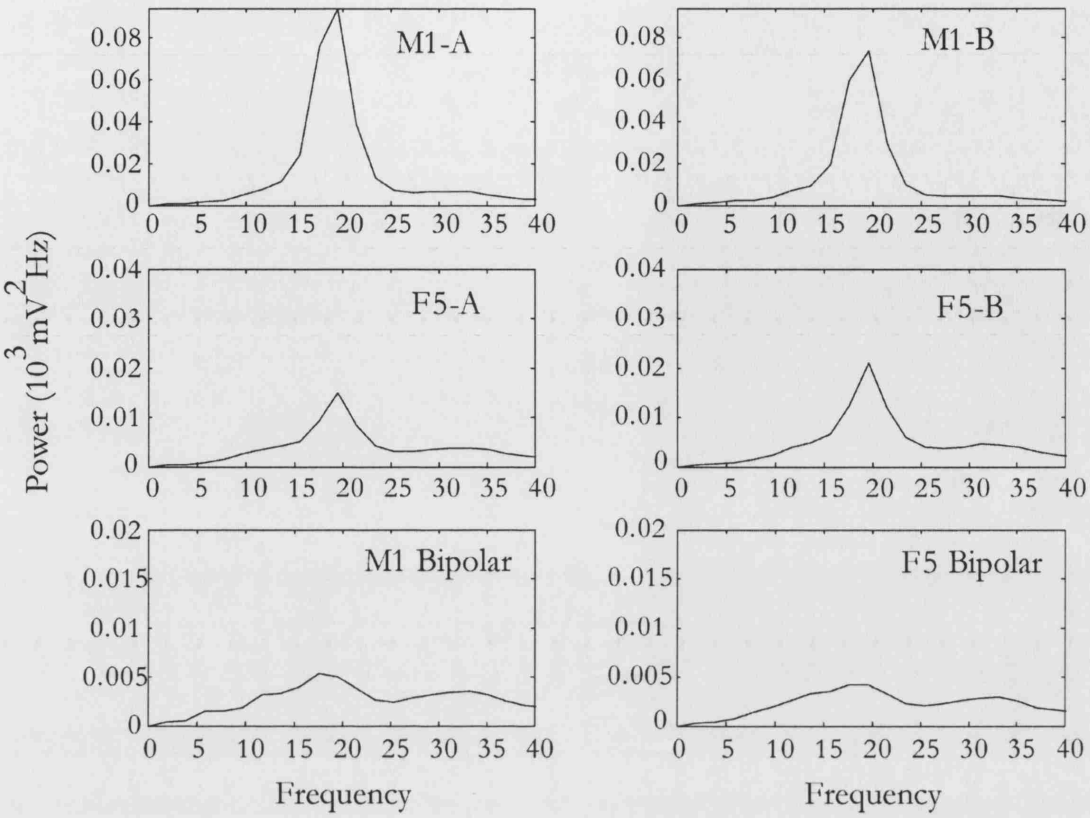

Figure 6.6 Power spectra of monopolar and bipolar LFPs. Power spectra calculated during the object grasp epoch.

The top two panels show the two original M1 LFP power spectra. Both showed clear beta power, with a peak value of 0.09 for M1-A and 0.07 for M1-B. The middle panels show the power spectra for the two original F5 LFPs. Again, there was clear beta power, although typically, this was smaller than that for M1 (peak values, 0.015 and 0.022). The bottom left panel shows the power spectrum of the bipolar M1. Here, the peak was much less pronounced, but is still present. The same is true for the bipolar F5 shown in the bottom right panel.

Figure 6.7 shows the coherence between the pairs of monopolar LFPs and the pair of bipolar recordings.

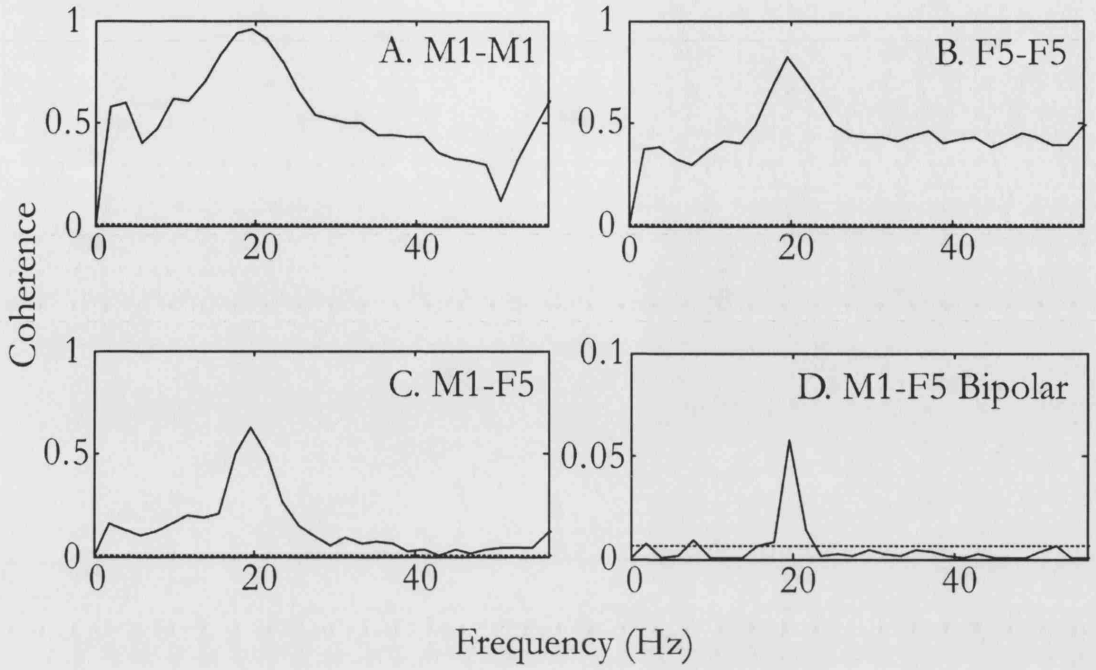

Figure 6.7 Coherence of monopolar and bipolar LFPs – case 1. Coherence calculated during the grasp epoch. Note the different coherence scale for D. Dotted line represents the significance level.

Fig. 6.7A shows the coherence between a pairing of monopolar LFPs recorded in M1. There was significant coherence at all frequencies, with the highest being at approximately 20 Hz. The same was true in the F5-F5 monopolar LFPs, shown in 6.7B. As might be expected, the inter-area (6.7C) coherence level was lower, but was still above the significance level ($P<0.05$). The coherence between the two bipolar recordings however shows that the only frequency at which coherence was truly significant was at ~20 Hz – other frequencies were non-significant. This implies that the statistically significant coherence seen at other frequencies in the single ended recordings was more likely to be due to volume conduction or other reasons than simple coherence. The value of the coherence was approximately 10 times smaller than the single ended inter-area recording (0.06 compared to 0.6), suggesting that some of the coherence observed in this

case was intrinsic and some due to volume conduction or other reasons which will be discussed further.

A second example is shown in 6.8.

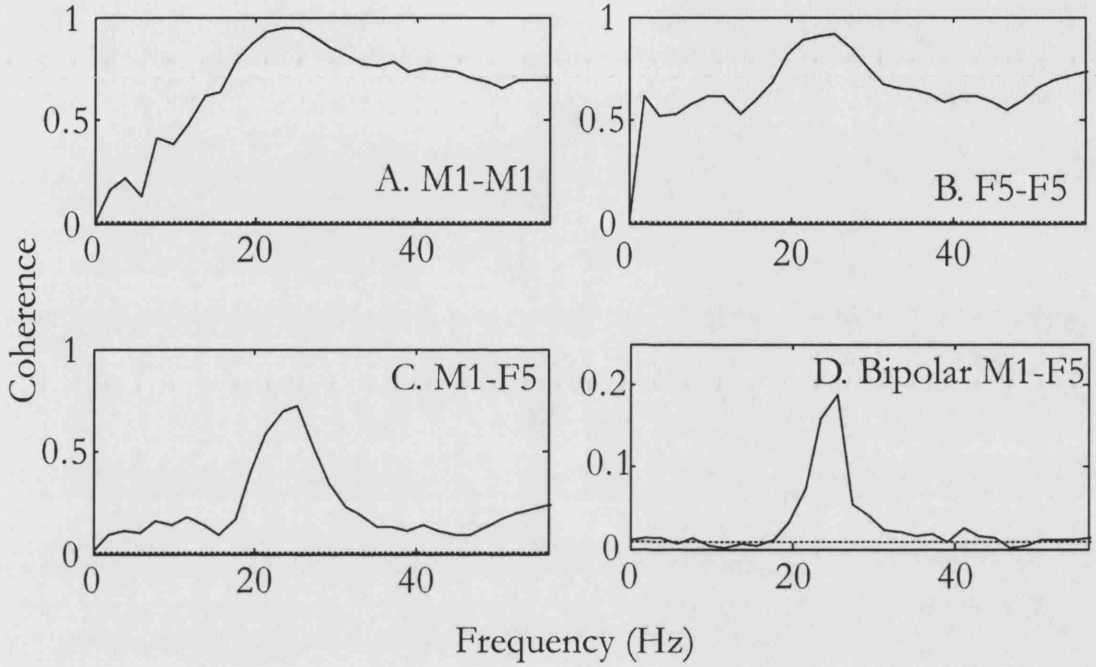

Figure 6.8 Coherence of monopolar and bipolar LFPs – case 2. Coherence calculated during the grasp epoch. Note the different coherence scale for D. Dotted line represents the significance level.

In this example from a second session in M39, coherences are shown between the monopolar and the bipolar LFPs. In this example, as with the first, coherence levels between the bipolar recordings are lower than for the monopolar recordings, 0.19 compared to 0.72. The bipolar LFP has approximately a quarter of the coherence of the monopolar, indicating that in this case, there was less volume conduction or other reasons for coherence in the monopolar recordings than in the first example. Again, significant coherence was only present in the beta range.

6.4.3 Conclusions

By making a local bipolar recording, it can be seen that the significant coherence observed between LFPs in M1 and F5 cannot be simply due to volume conduction across tissue. The recordings in the two areas were separated by between 9 and 13 mm; if a large signal from a remote source was being volume conducted to both areas, i.e. they were the same, this would cause LFPs recorded to be coherent, but the coherence would have been completely abolished in differential recordings. This was not the case.

The coherence remaining in the bipolar signals was small but still significant in the beta frequency range. Volume conduction is the most likely, but not the only other explanation for the additional coherence seen in the monopolar recordings; a larger volume of cortical tissue contributes to the monopolar LFP signal, so the chances of coherence are increased (in the same way that is easier to find coherence between two LFPs than the spike trains of two single neurons (Baker *et al.*, 2003)). Coherence will also be lower because the values of the bipolar LFP power spectra were lower, leading to a lower signal to noise ratio. These factors account in part for the reduced coherence in the bipolar recordings, as well as volume conduction. The power spectra of the bipolar recordings showed narrower peaks of beta power with respect to that at other frequencies, when compared to the monopolar recordings. This may also explain the reduced overall coherence value.

The coherence was only significant at the beta frequency of 20 Hz in the bipolar recordings; the significant coherence in the monopolar recodings at other frequencies is likely to be due to volume conduction, confirming the validity of concentrating on this beta range for all other coherence analyses. This result also provides strong evidence for the non-redundancy of the LFP signals recorded in M1 and F5.

6.5 Phase and Delay

6.5.1 Introduction

When two signals are coherent, the phase shift and the time delay of coherence are an indication of which of the two signals is leading the other, and by how much. M1 and F5 are strongly reciprocally connected, with a likely neuronal conduction time of 2-3 ms. It has been established that M1 and F5 LFPs are coherent, and the phase shift and delay measurements may give additional information for the interpretation of the coherence.

6.5.2 Methods

Delay and phase shift were calculated according to the methods described earlier in section 4.3.4. Briefly, these were calculated from a linear regession line fitted to a plot of the cross-spectrum phase. The phase values at the frequency corresponding to peak coherence and the three adjacent frequency points on either side were used for fitting. The circular mean value of this range determined the phase shift, and the time delay was given by the slope of the regression line divided by 360°. These were calculated for both the observation and grasp epoch for all pairings of LFPs, catergorised into M1-M1, F5-F5 and M1-F5 pairings. In the inter-area pairings, M1 LFPs were taken as the first signal, resulting in phase shift values which indicate by how much M1 leads F5 - a negative value would indicate F5 leading M1. For the intra-area pairs, the 'lead' signal is chosen arbitrarily.

6.5.3 Results

Figure 6.9 shows the results for the object observation epoch. Here, the phase shifts are represented on a polar plot, and the time delays as histograms.

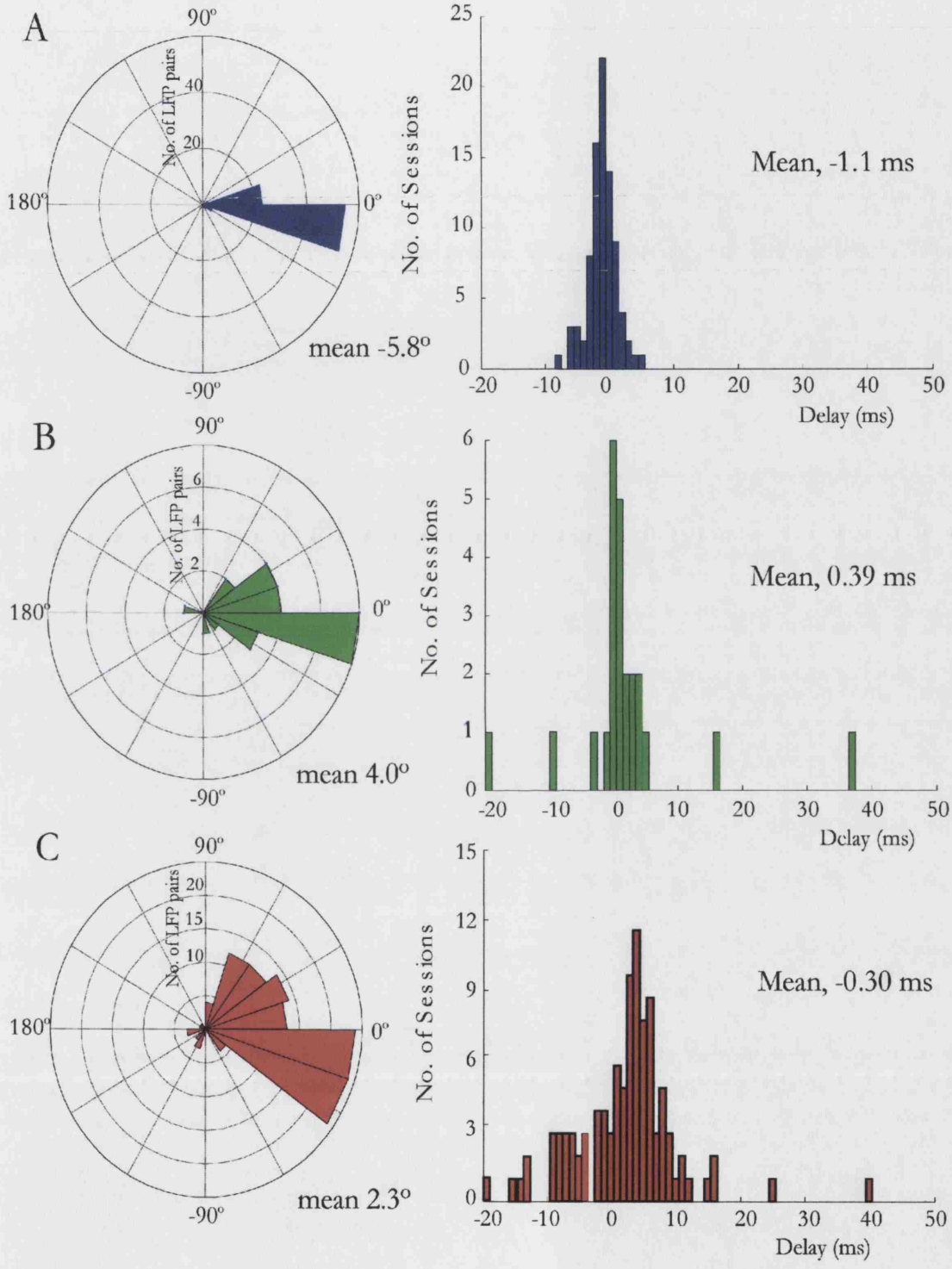

Figure 6.9 Phase shifts and time delays for the object observation epoch. A. M1-M1, **B.** F5-F5, and **C.** M1-F5.

The phase shifts for all pairs of LFPs were small. M1-M1 and F5-F5 pairings (Fig. 6.9A and B) showed a smaller distribution of values than the M1-F5 pairs. The intra-area recording phase shifts were tightly clustered around 0°, which is to be expected – within an area, and with an arbitrary choice of which LFP is leading, no significant phase shift is expected, and the sign of the values is arbitrary also. The time delays were consequently clustered around zero. F5-F5 pairings showed a slightly wider distribution of values than M1-M1 pairings, with one or two anti-phase LFP recordings.

The M1-F5 pairings (Fig. 6.9C) showed an average phase shift of 2.3°, i.e. M1 led F5. However, the distribution of values was wide, and in many cases, a negative value was obtained, indicating that F5 was leading M1. Several pairings produced values of - 180°, indiating signals which are anti-phase. During observation, there was no consistent phase relationship between the M1 and F5 LFPs. This can also be seen in the time delay values. These were distributed widely in comparison to the intra-area delay values, with a possibly bi-modal distribution. One group of values was negative, with a mean of approximately -3 to -4 ms, corresponding to those phase shifts which indicated that F5 was leading M1, and another group which were positive, with a peak at approximately 4 to 5 ms, indicating M1 leading F5. The time delay for these reciprocal leads was consistent with the conduction time between M1 and F5, and may suggest a bi-directional transfer of information during this phase of the task.

The results for the object grasp epoch are shown below in figure 6.10.

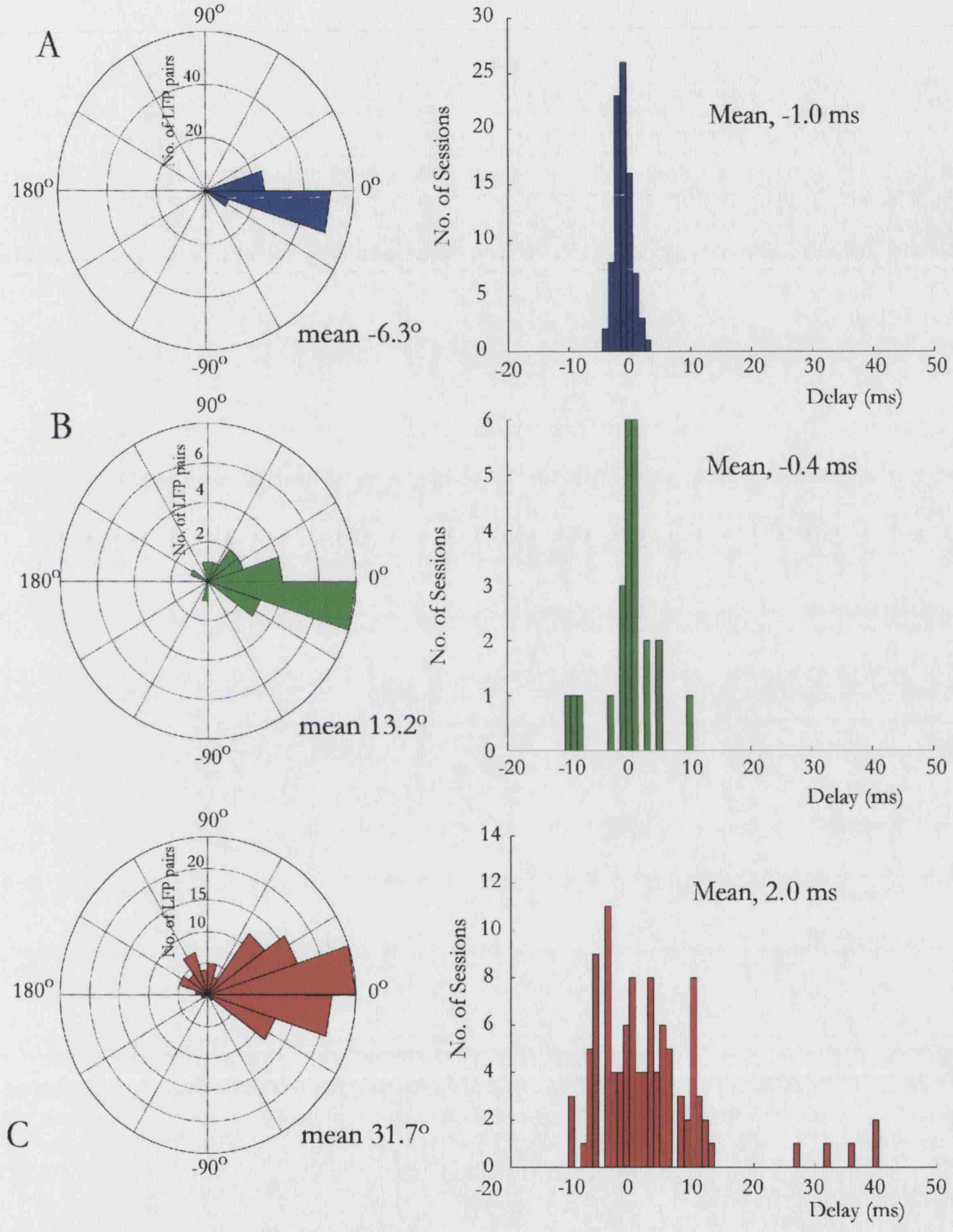

Figure 6.10 Phase shifts and time delays for the object grasp epoch. A. M1-M1, **B.** F5-F5, and **C.** M1-F5.

Fig. 6.10A and B show the phase shifts and time delay for M1-M1 and F5-F5 pairings of LFPs.

As in the observation epoch, values for the intra-area phase shifts clustered around 0°, as did the time delays. Again, F5-F5 pairings showed a wider distribution of values than M1-M1, with a few anti-phase LFPs having been recorded.

The inter-area pairings showed a clearer pattern than for the observation epoch. A majority of LFPs showed positive values for the phase delays, indicating that the M1 LFP led the F5 LFP. The average phase shift was 31.7°, with a resultant time delay of 2 ms. However, there were also instances of negative phase shifts and time delays, suggesting that as with the observation epoch, the LFP coherence was bi-directional, albeit principally in an M1 to F5 direction during this epoch of the task.

6.5.4 Conclusions

It has been established that there is clear coherence between the M1 and F5 areas of the cortex during a reach-to-grasp task, and that this coherence varies with parameters of the task, including the stage of the task (object observation in preparation for movement versus the active grasping and holding of the object) and also the physical properties of the object which lead to differences in the amount of beta power in the spectra of the LFPs. The phase and delay data suggest that the coherence observed may also have varied in its derivation during the two epochs of the task.

During object observation, neither area clearly led the other, with pairs of LFPs that apparently showed both directions of information transfer recorded. This is consistent with the theory that F5 is involved in setting up the upcoming grasp by processing the visual information concerning the physical properties of the object to be grasped, and transforming this information into an instruction for an appropriate grasp to be executed by M1. This would require the use of the reciprocal M1-F5 connection, and suggests that F5 as well as M1 is a source of oscillatory activity generation in the motor cortex.

During object grasp, the coherence suggests that M1 is the principal source of the oscillatory activity seen in the two areas, with a lesser contribution from the premotor cortex. During this period of action execution, M1 is the source of the principal output driving the musculature; the choice of grasp, and the hand pre-shaping required for the grasp has already been executed. M1 has been found to be the source of coherence between the motor cortex and the muscles during grasp, and it is likely that it is the main source of the oscillatory drive to both muscles and F5 during active grasp.

However, the anti-phase recordings which lead to the conclusion of bidiractionality during obsevation could be interpreted differently. It has been shown previously that the depth of a recording can affect its phase with repect to a fixed electrode (Murthy & Fetz, 1996a) with a 180° phase shift with a depth change of approximately 2 mm. Although no recordings with this degree of variation of depth were noted, there is always a possibility that depths may have been recorded somewhat inaccurately due to difficult penetration of the dura with the electrode, equipment malfunction etc., so this cannot be entirely ruled out. However, electrodes were not moved between epochs, so if this were the case, the same distribution might be expected during both epochs and this was not the case. It is therefore likely that for some LFPs, there is a genuine change in phase between the two epochs.

Chapter 7. Summary and Discussion

7.1 Summary

Chapters 2 and 3 described methodologies that have greatly enhanced the quality of intracortical recordings in this laboratory. The application of the MRI-derived techniques described in Chapter 2 has led to improved monkey head fixation, more accurate recordings and therefore to improved animal welfare. This in turn has led to better data yield and quality. Combined with the use of the antimitotic solution, 5-Fluorouracil, as described in Chapter 3, it has enabled the use of simultaneous dual-area multielectrode recording techniques to be developed, allowing high yield, stable data to be recorded during a visuomotor task. Dual area multielectrode recordings of local field potentials are a powerful way to study the interactions between two areas of the brain, as data can be assessed both within and across areas. This has allowed comparisons to be made during the performance of a complex, two-stage visuomotor task, leading to insights into the nature of the beta oscillations present in the motor cortex and their relationship to behaviour.

Chapters 4, 5 and 6 have described the background, methods and results of the current study investigating the roles of the beta oscillations present in local field potentials recorded in M1 and F5 in the macaque monkey during the visuomotor task. It has been demonstrated that the oscillations vary throughout the task, being most prevalent during the steady grasp of an object and secondarily during the observation of the object, and that the power of the oscillations varied with the object and grasp type. The two areas studied showed different proportions of tuned sites during the two epochs, and also different patterns of object-related tuning, indicating that the two areas had different

roles in the visuomotor grasp. The oscillations in the two areas were coherent in the beta frequency range, and showed a delay consistent with the conduction time between the two areas and a phase relationship that indicated that both may be sources of oscillatory activity. The relative contribution of these oscillators appears to vary during the two studied epochs of the task. When considered together, these results provide an insight into the relationship between M1 and F5, and suggest that the LFPs may not only be a useful tool in studying the basis of the functional circuitry of the brain, but that M1 and F5 LFPs could also be used clinically in the future, perhaps as the basis of a brain-machine interface, as they can carry significantly different signals for different objects, even during the observation phase of a reach-to-grasp task, i.e. without active movement. Results based on both the power spectra and the coherence also provide valuable evidence concerning the degree of independence of LFP recordings both within and across areas, suggesting that the information carried in the LFP can be specific to its location and it not identical to an LFP recorded at even a very small distance away.

7.2 Tuning of LFPs

The object-related tuning shown by the LFPs in M1 and F5 in this study has not previously been described. LFPs from areas involved in the visuomotor circuits have been shown to be tuned to other task parameters; for example, LFPs recorded from the lateral intraparietal area are spatially tuned in the gamma frequency band to the direction of a saccade (Pesaran *et al.*, 2002), and preliminary results have shown that PRR LFPs show a similar directional tuning during a delayed response reach task (Scherberger *et al.*, 2003). The tuning found in this study provides an insight into the function of the two areas in a reach-to-grasp task. All M1 LFPs were found to be tuned during the steady

grasp of an object, and usually with similar tuning – the LFPs were largely homogenous during actual execution of the motor task and tended to group objects more according to the physical properties of the object and grasp than to any visual similarity (although this has not been systematically confirmed). There are many reasons why this might be so. The location of the recordings were verified as being in the hand and arm area of M1 by ICMS, and the arm movement was largely similar for all objects, with only the hand posture varying (see Brochier *et al.*, 2004); the overall reaching movement required was therefore similar, requiring a largely similar descending motor output to the proximal muscles, with the variation required mostly for the more distal muscles of the hand for grasp. The possible groupings by grasp type are perhaps to be expected, owing to M1's major role in the execution of the grasp, rather than in any visual assessment of the object. In F5, a broader range of preferences was found, with the LFPs beta power possibly grouping the objects more by visual similarity than physical properties during observation and seemingly by grip type during steady grasp. This requires further rigorous assessment to clarify and statistically assess the objects and grasps in a more meaningful way, but would be consistent with previous findings on the role of F5 in selecting an appropriate action based on the higher order visuomotor input it receives from the parietal areas,

These findings of task-related tuning not only provide an insight into the motor and visuomotor properties of the LFPs in M1 and F5, but may also have important consequences in the clinical field.

7.3 Brain-Machine Interfaces

It has long been a goal of those studying the brain and spinal cord to provide theraputic aid to patients with spinal injuries who are left with limited or no motor function (see e.g. Humphrey *et al.*, 1970). As well as longer-term aims of restoring function through the regeneration of the damaged spinal cord, the intention to provide restorative function via an artificial pathway has been put forward. If signals from the brain could be decoded and routed to either the patient's own muscles or to an artificial prosthetic device, a paralysed patient could regain some motor function. The feasibility of using neural signals to control prosthetic appliances or machines became apparent with the advent of sophisticated electronics in the last 30 years and proposals of how to go about it started (Schmidt, 1980). Initially, research concentrated on spiking activity as a signal. Monkeys have been trained to move a cursor on a screen using only the activity of M1 neurons (Serruya *et al.*, 2002). Spikes have also been used to simultaneously decode grasp and trajectory in the macaque in real time; after training with a lever, the monkeys were still able to perform the task simply by using their neural signals (Carmena *et al.*, 2003). Three dimensional reaching with a 'virtual arm' can also be accomplished by monkeys with training (Taylor *et al.*, 2002). Human studies have confirmed that such techniques can also work in patients to allow them to produce on/off signals and later to control a cursor on a screen to allow communication through synthetic speech and typing (Kennedy & Bakay, 1998; Kennedy *et al.*, 2000). Although using spike signals as an output to a prosthetic device provides an immensely powerful tool, there are some drawbacks of using spikes as the signal. The long term recording of large numbers of single units is difficult to achieve, as scar tissue may form around the electrode tips, leading to a degradation of the signal (Szarowski *et al.*, 2003).

Another brain signal that has been used extensively is EEG (Wolpaw *et al.*, 2002). This has the advantage of being non-invasive and stable over extended periods of time, but as it derives from a large area of cortex, the signals are not very specific and may therefore limit the amount of variables that can be decoded. For example, a study to generate cursor control allowed patients to move a cursor in only one or possibly two dimensions (Fabiani *et al.*, 2004) – a poorer function than has been demonstrated in the monkey using single unit activity.

A third brain signal is currently the subject of many investigations and trials – the local field potential. The comparative benefits of the different signals have been much debated (Andersen *et al.*, 2004). LFPs, like single unit activity may only be recorded invasively; however, it has the advantage over single units in that LFPs may be recorded stably over a long period of time as it is less affected by the encapsulation of the electrode tips, and the advantage over EEG that it can provide highly specific information.

Pesaran *et al.* (2002) found that decoding the LFP activity on a single trial basis provided at least as good an indicator of the direction of the upcoming movement as spiking activity at the same location, and predicted the timing with more accuracy. A similar finding was made by Mehring *et al.* in 2003 who found that motor cortical LFPs could be used to decode the target location and hand velocity in a centre-out reaching task, even before movement onset. These parameters could be inferred from multiple LFPs at least as accurately as from unit activity, reinforcing the theory that LFPs could provide as much information about movement parameters as neurons.

Studies in F5 have shown that object-related activity is present in neuronal recordings and can be specific for either a grasp type or an object or group of objects (Murata *et al.*, 1997). 67% of neurons showed object selectivity. This thesis has presented data that

shows similarly specific object-related activity is also present in the local field potentials. 21.7% of F5 LFPs showed significant object tuning during the observation epoch, and 84.8% during steady object grasp. In M1, the figures were 13.9% and 100%. Again, this clearly demonstrates that LFPs can contain at least as specific information on the object to be grasped or being grasped as the single unit data. Trial-by-trial decoding of the object was beyond the scope of this thesis, but would prove an interesting challenge. It may prove that not only can information about the direction of reaching movements and force levels be decoded from LFP signals, but even specific information about the grasp of an object. The grouping analysis described in section 5.6 also showed that M1 and F5 LFPs could potentially be used to decode both the physical properties of the object to be grasped, and the desired hand posture to be used for the grasp. If this were possible, it could provide a strong input signal to contribute the control of a prosthetic device for reaching and grasping.

7.4 The Functional Relationship between M1 and F5

The significant coherence between the LFPs in M1 and F5 in the beta frequency range implies that these oscillations may have a functional relationship.

It is believed that the oscillatory drive in the motor cortex may arise from a network including pyramidal tract neurons (Baker *et al.*, 1997; Jackson *et al.*, 2002), and M1 has been suggested as the main source of the oscillatory drive (Conway *et al.*, 1995; Salenius *et al.*, 1997, Kilner *et al.*, 2000). PTNs have been shown to be phase locked to M1 LFPs which were coherent with EMG recorded in the hand muscles during a precision grip task (Baker *et al.*, 1999a) suggesting that part of this coherence is mediated by corticospinal fibres. The results shown in chapter 6 demonstrate that there

is significant coherence between M1 and F5 in the beta frequency range, even when a bipolar recording is made to limit the cortical volume from which the LFP signal was recorded. The range of significant coherence between the bipolar LFPs was narrower than the range of frequencies at which signifcant power was seen. This suggests that the coherent bipolar signal was limited to a narrow frequency range, despite both areas having oscillations at a broader range of frequencies. This coherence proves that the oscillatory signal in the two areas does not arise simply by volume conduction from a common and remote source; if this were the case, it would have been abolished in the bipolar recordings. A large part of the coherence was removed, indicating that there was a large common oscillatory drive to both areas, as well as the smaller remaining signal. This is suggestive that the ongoing beta oscillation may contain multiple independent components, only some of which may include the PTNs (Jackson *et al.*, 2002), i.e. that there may be multiple oscillators. The phase and delay results presented here suggest that both M1 and F5 could contain such a source. During the two epochs of the task, the phases of the coherence were found to have a bimodal distribution, indicating that for some inter-area pairs of LFPs, M1 was leading the oscillations, and for others, F5 was leading. During observation, F5 is showing a higher degree of object-related activity than M1 and is likely to be involved in the selection of an appropriate hand shape for the upcoming grasp, whereas during grasp, M1 may be expected to be dominant. The results showed that during both epochs, there was a bidirectional relationship, with M1 dominating, but that F5 led M1 more often during observation than grasp. This is consistent with a main oscillatory drive from M1, involving the PTNs and the CST for motor output. However, it is also suggestive that there may also be a small oscillatory drive from F5 to M1.

During observation, the peak beta frequency of the oscillations was approximately 1-2 Hz lower than the peak frequency during steady object grasp. This change in oscillatory frequency within an area has not been demonstrated previously. The contributions of the M1 and F5 oscillatory sources were also different during the two epochs. One possibility is that two oscillators may operate at slightly different frequencies. If the F5-source of oscillatory drive had a lower frequency than that in M1, then during observation where the M1:F5 oscillatory drive ratio was lower, the average frequency for each of the two areas would be lower, whereas during grasp where the M1:F5 oscillatory drive ratio is higher, the resultant averaged frequency would be higher, leading to the results that were found here.

There is an alternative hypothesis for the increased frequency of the oscillations from observation to grasp. As has already been reviewed, the oscillatory drive in the motor cortex may arise from a network including pyramidal tract neurons (Baker *et al.*, 1997; Jackson *et al.*, 2002). It has been shown that PTNs are often phasically active, and fire more during movement than while the monkey is at rest (Baker *et al.*, 2001). One theory is that PTNs fire, and then a delayed inhibitory feedback leads them to fire synchronously for a second time, causing the oscillations that can be seen in the LFP (Jackson, 2002). During the grasp phase of the task, the PTNs are generally more active than during the observation phase (Umilta *et al.*, 2003). There is therefore likely to be more of an excitatory drive to the PTNs during grasp than during observation. This increased excitatory state could cause the PTNs to be closer to their firing threshold, such that the effect of the inhibitory feedback could be reduced, leading to the subsequent firing of the PTNs to be sooner than when less excitatory drive is present.

This would lead to shorter cycles of PTN firing (increasing firing rate) and therefore to a higher frequency of oscillation at times when the PTNs are more active, such as during grasp when compared to observation. This hypothesis would also therefore account for the change in oscillatory frequency.

These two hypotheses are not mutually exclusive. The results from the bipolar recordings showed that there is a localised, narrow band of coherence which is not attributable to a single large signal, but also that such a signal does account for the a large amount of the coherence between M1 and F5. A major PTN based network could drive the majority of coherence observed, and more intrinsic M1-F5 oscillators could operate at different frequencies to differing extents as was previously suggested. Either, or a combination of both mechanisms could lead to the observed results. In order to investigate this further, the stimulation of the PTNs during the two epochs via an implanted PT electrode could be used in much the same manner as it was used during the precision grip task by Jackson *et al.* in 2002, in order to ascertain whether the phase of the oscillations in both M1 and F5 can be reset by a stimulus – if the change in frequency were entirely due to the M1 based oscillator incorporating the PTNs, the phases would be reset in both areas and to the same new frequency. If F5 and M1 responded differently, and F5 was not fully reset but instead showed some degree of independence from the PT stimulation, this would argue for and F5 oscillator being significantly involved.

If there are indeed multiple beta oscillators present in the motor system, they may subserve a different function during the different epochs of the task. Coherent oscillations are thought to allow 'binding' of two cortical areas, and given the large reciprocal projection between M1 and F5 and the fact that F5 may exert its influence on

the motor output via M1, it is likely that the coherent oscillations allow F5 to influence the motor output from M1 perhaps by binding together the object properties and the desired grasp to account for them, and the descending motor output from M1 that is needed to enact the grasp accurately. This would account for the increased influence of F5 (and the higher proportion of tuned LFPs) during observation and the more dominant effect of M1 during active grasp, when the desired hand posture has been achieved and the grasp successfully completed.

Reference List

Abeles, M. (1991). *Corticonics: Neural Circuits of Cerebral Cortex.* Cambridge University Press, Cambridge.

Akali, A., Khan, U., Khaw, P. T., & McGrouther, A. D. (1999). Decrease in adhesion formation by a single application of 5-fluorouracil after flexor tendon injury. *Plast.Reconstr.Surg.* **103**, 151-158.

Andersen, P., Hagan, P. J., Phillips, C. G., & Powell, T. P. (1975). Mapping by microstimulation of overlapping projections from area 4 to motor units of the baboon's hand. *Proc.R.Soc.Lond B Biol.Sci.* **188**, 31-36.

Andersen, R. A., Musallam, S., & Pesaran, B. (2004). Selecting the signals for a brain-machine interface. *Curr.Opin.Neurobiol.* **14**, 720-726.

Andreo, L. K., Uyemura, M. J., & Enzenauer, R. W. (1997). 5-Fluorouracil reduces scarring after strabismus surgery. *J.Pediatr.Ophthalmol.Strabismus* **34**, 107-110.

Arbib, M.A., Iberall, T. & Lyons, D. (1985). In *Hand Function and the Neocortex.* Eds. Goodwin, A.W. and Darian-Smith, I.. Springer.

Arbib, M. A., Billard, A., Iacoboni, M., & Oztop, E. (2000). Synthetic brain imaging: grasping, mirror neurons and imitation. *Neural Netw.* **13**, 975-997.

Asanuma, H. & Sakata, H. (1967). Functional organisation of a cortical efferent system examined with focal depth stimulation in cats. *J.Neurophysiol.* **30**, 35-54.

Asaria, R. H., Kon, C. H., Bunce, C., Charteris, D. G., Wong, D., Khaw, P. T., & Aylward, G. W. (2001). Adjuvant 5-fluorouracil and heparin prevents proliferative vitreoretinopathy : Results from a randomized, double-blind, controlled clinical trial. *Ophthalmology* **108**, 1179-1183.

Baker, S. N., Kilner, J. M., Pinches, E. M., & Lemon, R. N. (1999a). The role of synchrony and oscillations in the motor output. *Exp.Brain Res.* **128**, 109-117.

Baker, S. N. & Lemon, R. N. (2000). Precise spatiotemporal repeating patterns in monkey primary and supplementary motor areas occur at chance levels. *J.Neurophysiol.* **84**, 1770-1780.

Baker, S. N., Olivier, E., & Lemon, R. N. (1997). Coherent oscillations in monkey motor cortex and hand muscle EMG show task-dependent modulation. *J.Physiol* **501 (Pt 1)**, 225-241.

Baker, S. N., Philbin, N., Spinks, R., Pinches, E. M., Wolpert, D. M., MacManus, D. G., Pauluis, Q., & Lemon, R. N. (1999b). Multiple single unit recording in the cortex of monkeys using independently moveable microelectrodes. *J.Neurosci.Methods* **94**, 5-17.

Baker, S. N., Pinches, E. M., & Lemon, R. N. (2003). Synchronization in monkey motor cortex during a precision grip task. II. effect of oscillatory activity on corticospinal output. *J.Neurophysiol.* **89**, 1941-1953.

Baker, S. N., Spinks, R., Jackson, A., & Lemon, R. N. (2001). Synchronization in monkey motor cortex during a precision grip task. I. Task-dependent modulation in single-unit synchrony. *J.Neurophysiol.* **85**, 869-885.

Batista, A. P. & Andersen, R. A. (2001). The parietal reach region codes the next planned movement in a sequential reach task. *J.Neurophysiol.* **85**, 539-544.

Batista, A. P., Buneo, C. A., Snyder, L. H., & Andersen, R. A. (1999). Reach plans in eye-centered coordinates. *Science* **285**, 257-260.

Bekisz, M. & Wrobel, A. (1993). 20 Hz rhythm of activity in visual system of perceiving cat. *Acta Neurobiol.Exp.(Wars.)* **53**, 175-182.

Bennett, K. M. & Lemon, R. N. (1994). The influence of single monkey cortico-motoneuronal cells at different levels of activity in target muscles. *J.Physiol* **477 (Pt 2)**, 291-307.

Bennett, K. M. & Lemon, R. N. (1996). Corticomotoneuronal contribution to the fractionation of muscle activity during precision grip in the monkey. *J.Neurophysiol.* **75**, 1826-1842.

Bonfield, W. (1988). Composites for bone replacement. *J.Biomed.Eng* **10**, 522-526.

Boussaoud, D., Ungerleider, L. G., & Desimone, R. (1990). Pathways for motion analysis: cortical connections of the medial superior temporal and fundus of the superior temporal visual areas in the macaque. *J.Comp Neurol.* **296**, 462-495.

Bremmer, F., Duhamel, J. R., Ben Hamed, S., & Graf, W. (1997). The representation of movement in near extra-personal space in the macaque ventral intraparietal are (VIP). In *Parietal Lobe Contributions to Orientation in 3D Space*, eds. Their, P. & Karnath, H. O., pp. 255-270. Springer, Heidelberg.

Bremmer, F., Klam, F., Duhamel, J. R., Ben Hamed, S., & Graf, W. (2002). Visual-vestibular interactive responses in the macaque ventral intraparietal area (VIP). *Eur.J.Neurosci.* **16**, 1569-1586.

Brinkman, J. & Kuypers, H. G. (1972). Splitbrain monkeys: cerebral control of ipsilateral and contralateral arm, hand, and finger movements. *Science* **176**, 536-539.

Brinkman, J. & Kuypers, H. G. (1973). Cerebral control of contralateral and ipsilateral arm, hand and finger movements in the split-brain rhesus monkey. *Brain* **96**, 653-674.

Brochier, T., Spinks, R. L., Umilta, M. A., & Lemon, R. N. (2004). Patterns of muscle activity underlying object-specific grasp by the macaque monkey. *J.Neurophysiol.* **92**, 1770-1782.

Brown, P. & Marsden, C. D. (1998). What do the basal ganglia do? *Lancet* **351**, 1801-1804.

Buzsaki, G. (2002). Theta oscillations in the hippocampus. *Neuron* **33**, 325-340.

Caminiti, R., Ferraina, S., & Johnson, P. B. (1996). The sources of visual information to the primate frontal lobe: a novel role for the superior parietal lobule. *Cereb.Cortex* **6**, 319-328.

Caminiti, R., Genovesio, A., Marconi, B., Mayer, A. B., Onorati, P., Ferraina, S., Mitsuda, T., Giannetti, S., Squatrito, S., Maioli, M. G., & Molinari, M. (1999). Early coding of reaching: frontal and parietal association connections of parieto-occipital cortex. *Eur.J.Neurosci.* **11**, 3339-3345.

Carmena, J. M., Lebedev, M. A., Crist, R. E., O'Doherty, J. E., Santucci, D. M., Dimitrov, D. F., Patil, P. G., Henriquez, C. S., & Nicolelis, M. A. (2003). Learning to control a brain-machine interface for reaching and grasping by primates. *PLoS.Biol.* **1**, E42.

Cerri, G., Shimazu, H., Maier, M. A., & Lemon, R. N. (2003). Facilitation from ventral premotor cortex of primary motor cortex outputs to macaque hand muscles. *J.Neurophysiol.* **90**, 832-842.

Challis, R. E. & Kitney, R. I. (1991). Biomedical Signal processing. Part 3: The power spectrum and coherence function. *Med Biol Eng Comput* **29**, 225-241.

Clarke, R. H. & Henderson, E. E. (1920). Part II: Atlas of photographs of the frontal sections of the cranium and brain of the rhesus monkey (Macacus rhesus). In *Investigation of the Central Nervous System*, ed. Clarke, R. H., Johns Hopkins Press, Baltimore.

Colby, C. L. & Duhamel, J. R. (1991). Heterogeneity of extrastriate visual areas and multiple parietal areas in the macaque monkey. *Neuropsychologia* **29**, 517-537.

Colby, C. L., Duhamel, J. R., & Goldberg, M. E. (1993). Ventral intraparietal area of the macaque: anatomic location and visual response properties. *J.Neurophysiol.* **69**, 902-914.

Conway, B. A., Halliday, D. M., Farmer, S. F., Shahani, U., Maas, P., Weir, A. I., & Rosenberg, J. R. (1995). Synchronization between motor cortex and spinal motoneuronal pool during the performance of a maintained motor task in man. *J.Physiol* **489 (Pt 3)**, 917-924.

Courtemanche, R., Fujii, N., & Graybiel, A. M. (2003). Synchronous, focally modulated beta-band oscillations characterize local field potential activity in the striatum of awake behaving monkeys. *J.Neurosci.* **23**, 11741-11752.

Courtemanche, R., Pellerin, J. P., & Lamarre, Y. (2002). Local field potential oscillations in primate cerebellar cortex: modulation during active and passive expectancy. *J.Neurophysiol.* **88**, 771-782.

Crammond, D. J. & Kalaska, J. F. (1994). Modulation of preparatory neuronal activity in dorsal premotor cortex due to stimulus-response compatibility. *J.Neurophysiol.* **71**, 1281-1284.

Crammond, D. J. & Kalaska, J. F. (1996). Differential relation of discharge in primary motor cortex and premotor cortex to movements versus actively maintained postures during a reaching task. *Exp.Brain Res.* **108**, 45-61.

Cunningham, D. & Coleman, R. (2001). New options for outpatient chemotherapy--the role of oral fluoropyrimidines. *Cancer Treat.Rev.* **27**, 211-220.

Donoghue, J. P., Leibovic, S., & Sanes, J. N. (1992). Organization of the forelimb area in squirrel monkey motor cortex: representation of digit, wrist, and elbow muscles. *Exp.Brain Res.* **89**, 1-19.

Donoghue, J. P., Sanes, J. N., Hatsopoulos, N. G., & Gaal, G. (1998). Neural discharge and local field potential oscillations in primate motor cortex during voluntary movements. *J.Neurophysiol.* **79**, 159-173.

Dum, R. P. & Strick, P. L. (1991). The origin of corticospinal projections from the premotor areas in the frontal lobe. *J.Neurosci.* **11**, 667-689.

Dum, R. P. & Strick, P. L. (2002). Motor areas in the frontal lobe of the primate. *Physiol Behav.* **77**, 677-682.

Dum, R. P. & Strick, P. L. (2005). Frontal lobe inputs to the digit representations of the motor areas on the lateral surface of the hemisphere. *J.Neurosci.* **25**, 1375-1386.

Eckhorn, R., Frien, A., Bauer, R., Woelbern, T., & Kehr, H. (1993). High frequency (60-90 Hz) oscillations in primary visual cortex of awake monkey. *Neuroreport* **4**, 243-246.

Eckhorn, R. & Thomas, U. (1993). A new method for the insertion of multiple microprobes into neural and muscular tissue, including fiber electrodes, fine wires, needles and microsensors. *J.Neurosci.Methods* **49**, 175-179.

Elliott, J.M. & Connelly, K.J.(1984). A classification of manipulative hand movements. *Dev. Med. & Child Neurol.* **26**, 283-296.

Evarts, E. V. (1968). Relation of pyramidal tract activity to force exerted during voluntary movement. *J.Neurophysiol.* **31**, 14-27.

Fabiani, G. E., McFarland, D. J., Wolpaw, J. R., & Pfurtscheller, G. (2004). Conversion of EEG activity into cursor movement by a brain-computer interface (BCI). *IEEE Trans.Neural Syst.Rehabil.Eng* **12**, 331-338.

Feige, B., Aertsen, A., & Kristeva-Feige, R. (2000). Dynamic synchronization between multiple cortical motor areas and muscle activity in phasic voluntary movements. *J.Neurophysiol.* **84**, 2622-2629.

Ferraina, S., Garasto, M. R., Battaglia-Mayer, A., Ferraresi, P., Johnson, P. B., Lacquaniti, F., & Caminiti, R. (1997). Visual control of hand-reaching movement: activity in parietal area 7m. *Eur.J.Neurosci.* **9**, 1090-1095.

Ferrari, P. F., Gallese, V., Rizzolatti, G., & Fogassi, L. (2003). Mirror neurons responding to the observation of ingestive and communicative mouth actions in the monkey ventral premotor cortex. *Eur.J.Neurosci.* **17**, 1703-1714.

Fetz, E. E., Finocchio, D. V., Baker, M. A., & Soso, M. J. (1980). Sensory and motor responses of precentral cortex cells during comparable passive and active joint movements. *J.Neurophysiol.* **43**, 1070-1089.

Fogassi, L., Gallese, V., Buccino, G., Craighero, L., Fadiga, L., & Rizzolatti, G. (2001). Cortical mechanism for the visual guidance of hand grasping movements in the monkey: A reversible inactivation study. *Brain* **124**, 571-586.

Fogassi, L., Gallese, V., Fadiga, L., Luppino, G., Matelli, M., & Rizzolatti, G. (1996). Coding of peripersonal space in inferior premotor cortex (area F4). *J.Neurophysiol.* **76**, 141-157.

Galea, M. P. & Darian-Smith, I. (1994). Multiple corticospinal neuron populations in the macaque monkey are specified by their unique cortical origins, spinal terminations, and connections. *Cereb.Cortex* **4**, 166-194.

Gallese, V., Fadiga, L., Fogassi, L., & Rizzolatti, G. (1996). Action recognition in the premotor cortex. *Brain* **119 (Pt 2)**, 593-609.

Gallese, V., Keysers, C., & Rizzolatti, G. (2004). A unifying view of the basis of social cognition. *Trends Cogn Sci.* **8**, 396-403.

Gallese, V., Murata, A., Kaseda, M., Niki, N., & Sakata, H. (1994). Deficit of hand preshaping after muscimol injection in monkey parietal cortex. *Neuroreport* **5**, 1525-1529.

Galvan, V. V., Chen, J., & Weinberger, N. M. (2001). Long-term frequency tuning of local field potentials in the auditory cortex of the waking guinea pig. *J.Assoc.Res.Otolaryngol.* **2**, 199-215.

Gentilucci, M., Fogassi, L., Luppino, G., Matelli, M., Camarda, R., & Rizzolatti, G. (1988). Functional organization of inferior area 6 in the macaque monkey. I. Somatotopy and the control of proximal movements. *Exp.Brain Res.* **71**, 475-490.

Gentilucci, M., Fogassi, L., Luppino, G., Matelli, M., Camarda, R., & Rizzolatti, G. (1989). Somatotopic representation in inferior area 6 of the macaque monkey. *Brain Behav.Evol.* **33**, 118-121.

Georgopoulos, A. P., Kalaska, J. F., Caminiti, R., & Massey, J. T. (1982). On the relations between the direction of two-dimensional arm movements and cell discharge in primate motor cortex. *J.Neurosci.* **2**, 1527-1537.

Ghosh, S., Brinkman, C., & Porter, R. (1987). A quantitative study of the distribution of neurons projecting to the precentral motor cortex in the monkey (M. fascicularis). *J.Comp Neurol.* **259**, 424-444.

Gloor, P. (1969). *Hans Berger On the Electroencephalogram of Man* Elsevier, Amsterdam.

Godschalk, M., Mitz, A. R., van Duin, B., & van der, B. H. (1995). Somatotopy of monkey premotor cortex examined with microstimulation. *Neurosci.Res.* **23**, 269-279.

Gray, C. M. & Singer, W. (1989). Stimulus-specific neuronal oscillations in orientation columns of cat visual cortex. *Proc.Natl.Acad.Sci.U.S.A* **86**, 1698-1702.

Graziano, M. S., Yap, G. S., & Gross, C. G. (1994). Coding of visual space by premotor neurons. *Science* **266**, 1054-1057.

Grezes, J., Armony, J. L., Rowe, J., & Passingham, R. E. (2003). Activations related to "mirror" and "canonical" neurones in the human brain: an fMRI study. *Neuroimage.* **18**, 928-937.

Gross, J., Tass, P. A., Salenius, S., Hari, R., Freund, H. J., & Schnitzler, A. (2000). Cortico-muscular synchronization during isometric muscle contraction in humans as revealed by magnetoencephalography. *J.Physiol* **527 Pt 3**, 623-631.

Halliday, D. M., Conway, B. A., Farmer, S. F., & Rosenberg, J. R. (1998). Using electroencephalography to study functional coupling between cortical activity and electromyograms during voluntary contractions in humans. *Neurosci.Lett.* **241**, 5-8.

Hari, R. & Salenius, S. (1999). Rhythmical corticomotor communication. *Neuroreport* **10**, R1-10.

He, S. Q., Dum, R. P., & Strick, P. L. (1993). Topographic organization of corticospinal projections from the frontal lobe: motor areas on the lateral surface of the hemisphere. *J.Neurosci.* **13**, 952-980.

Hepp-Reymond, M., Kirkpatrick-Tanner, M., Gabernet, L., Qi, H. X., & Weber, B. (1999). Context-dependent force coding in motor and premotor cortical areas. *Exp.Brain Res.* **128**, 123-133.

Hepp-Reymond, M. C., Husler, E. J., Maier, M. A., & Ql, H. X. (1994). Force-related neuronal activity in two regions of the primate ventral premotor cortex. *Can.J.Physiol Pharmacol.* **72**, 571-579.

Humphrey, D. R. & Corrie, W. S. (1978). Properties of pyramidal tract neuron system within a functionally defined subregion of primate motor cortex. *J.Neurophysiol.* **41**, 216-243.

Humphrey, D. R., Schmidt, E. M., & Thompson, W. D. (1970). Predicting measures of motor performance from multiple cortical spike trains. *Science* **170**, 758-762.

Iberall, T., Bingham, G., and Arbib, M.A. (1986). Opposition Space as a Structuring Concept for the Analysis of Skilled Hand Movements. In H. Heuer & C. Fromm (Eds) *Generation and Modulation of Action Patterns,* Berlin: Springer-Verlag, 158-173.

Jackson, A. Synchrony in the primate motor system. 2002. PhD Thesis

Jackson, A., Spinks, R. L., Freeman, T. C., Wolpert, D. M., & Lemon, R. N. (2002). Rhythm generation in monkey motor cortex explored using pyramidal tract stimulation. *J.Physiol* **541**, 685-699.

Jankowska, E., Padel, Y., & Tanaka, R. (1975). The mode of activation of pyramidal tract cells by intracortical stimuli. *J.Physiol* **249**, 617-636.

Jeannerod, M., Arbib, M. A., Rizzolatti, G., & Sakata, H. (1995). Grasping objects: the cortical mechanisms of visuomotor transformation. *Trends Neurosci.* **18**, 314-320.

Kalaska, J. F., Cohen, D. A., Hyde, M. L., & Prud'homme, M. (1989). A comparison of movement direction-related versus load direction-related activity in primate motor cortex, using a two-dimensional reaching task. *J.Neurosci.* **9**, 2080-2102.

Kawato, M., Furukawa, K., & Suzuki, R. (1987). A hierarchical neural-network model for control and learning of voluntary movement. *Biol.Cybern.* **57**, 169-185.

Kayser, C. & Konig, P. (2004). Stimulus locking and feature selectivity prevail in complementary frequency ranges of V1 local field potentials. *Eur.J.Neurosci.* **19**, 485-489.

Kennedy, P. R. & Bakay, R. A. (1998). Restoration of neural output from a paralyzed patient by a direct brain connection. *Neuroreport* **9**, 1707-1711.

Kennedy, P. R., Bakay, R. A., Moore, M. M., Adams, K., & Goldwaithe, J. (2000). Direct control of a computer from the human central nervous system. *IEEE Trans.Rehabil.Eng* **8**, 198-202.

Khan, U., Occleston, N. L., Khaw, P. T., & McGrouther, D. A. (1997). Single exposures to 5-fluorouracil: a possible mode of targeted therapy to reduce contractile scarring in the injured tendon. *Plast.Reconstr.Surg.* **99**, 465-471.

Khaw, P. T., Doyle, J. W., Sherwood, M. B., Grierson, I., Schultz, G., & McGorray, S. (1993a). Prolonged localized tissue effects from 5-minute exposures to fluorouracil and mitomycin C. *Arch.Ophthalmol.* **111**, 263-267.

Khaw, P. T., Doyle, J. W., Sherwood, M. B., Smith, M. F., & McGorray, S. (1993b). Effects of intraoperative 5-fluorouracil or mitomycin C on glaucoma filtration surgery in the rabbit. *Ophthalmology* **100**, 367-372.

Khaw, P. T. & Migdal, C. S. (1996). Current techniques in wound healing modulation in glaucoma surgery. *Curr.Opin.Ophthalmol.* **7**, 24-33.

Khaw, P. T., Sherwood, M. B., MacKay, S. L., Rossi, M. J., & Schultz, G. (1992a). Five-minute treatments with fluorouracil, floxuridine, and mitomycin have long-term effects on human Tenon's capsule fibroblasts. *Arch.Ophthalmol.* **110**, 1150-1154.

Khaw, P. T., Ward, S., Porter, A., Grierson, I., Hitchings, R. A., & Rice, N. S. (1992b). The long-term effects of 5-fluorouracil and sodium butyrate on human Tenon's fibroblasts. *Invest Ophthalmol.Vis.Sci.* **33**, 2043-2052.

Kilner, J. M., Baker, S. N., Salenius, S., Hari, R., & Lemon, R. N. (2000). Human cortical muscle coherence is directly related to specific motor parameters. *J.Neurosci.* **20**, 8838-8845.

Kilner, J. M., Baker, S. N., Salenius, S., Jousmaki, V., Hari, R., & Lemon, R. N. (1999). Task-dependent modulation of 15-30 Hz coherence between rectified EMGs from human hand and forearm muscles. *J.Physiol* **516 (Pt 2)**, 559-570.

Kohler, E., Keysers, C., Umilta, M. A., Fogassi, L., Gallese, V., & Rizzolatti, G. (2002). Hearing sounds, understanding actions: action representation in mirror neurons. *Science* **297**, 846-848.

Kon, C. H., Occleston, N. L., Foss, A., Sheridan, C., Aylward, G. W., & Khaw, P. T. (1998). Effects of single, short-term exposures of human retinal pigment epithelial cells to thiotepa or 5-fluorouracil: implications for the treatment of proliferative vitreoretinopathy. *Br.J.Ophthalmol.* **82**, 554-560.

Kristeva-Feige, R., Fritsch, C., Timmer, J., & Lucking, C. H. (2002). Effects of attention and precision of exerted force on beta range EEG-EMG synchronization during a maintained motor contraction task. *Clin.Neurophysiol.* **113**, 124-131.

Kurata, K. (1989). Distribution of neurons with set- and movement-related activity before hand and foot movements in the premotor cortex of rhesus monkeys. *Exp.Brain Res.* **77**, 245-256.

Lacquaniti, F., Guigon, E., Bianchi, L., Ferraina, S., & Caminiti, R. (1995). Representing spatial information for limb movement: role of area 5 in the monkey. *Cereb.Cortex* **5**, 391-409.

Lebedev, M. A. & Wise, S. P. (2000). Oscillations in the premotor cortex: single-unit activity from awake, behaving monkeys. *Exp.Brain Res.* **130**, 195-215.

Lemon, R. N. (1984). *Methods for Neuronal Recording in Conscious Animals*, IBRO Handbook Series: Methods in Neurosciences ed. Wiley, London.

Lemon, R. N. (1988). The output map of the primate motor cortex. *Trends In Neurosciences* **11**, 501-506.

Lemon, R. N., Kirkwood, P. A., Maier, M. A., Nakajima, K., & Nathan, P. (2004). Direct and indirect pathways for corticospinal control of upper limb motoneurons in the primate. *Prog.Brain Res.* **143**, 263-279.

Lemon, R. N., Muir, R. B., & Mantel, G. W. (1987). The effects upon the activity of hand and forearm muscles of intracortical stimulation in the vicinity of corticomotor neurones in the conscious monkey. *Exp.Brain Res.* **66**, 621-637.

Lewis, J. W. & Van Essen, D. C. (2000). Corticocortical connections of visual, sensorimotor, and multimodal processing areas in the parietal lobe of the macaque monkey. *J.Comp Neurol.* **428**, 112-137.

Lounasmaa, O. V., Hamalainen, M., Hari, R., & Salmelin, R. (1996). Information processing in the human brain: magnetoencephalographic approach. *Proc.Natl.Acad.Sci.U.S.A* **93**, 8809-8815.

Luppino, G., Matelli, M., Camarda, R., & Rizzolatti, G. (1993). Corticocortical connections of area F3 (SMA-proper) and area F6 (pre-SMA) in the macaque monkey. *J.Comp Neurol.* **338**, 114-140.

Luppino, G., Matelli, M., Camarda, R. M., Gallese, V., & Rizzolatti, G. (1991). Multiple representations of body movements in mesial area 6 and the adjacent cingulate cortex: an intracortical microstimulation study in the macaque monkey. *J.Comp Neurol.* **311**, 463-482.

Luppino, G., Murata, A., Govoni, P., & Matelli, M. (1999). Largely segregated parietofrontal connections linking rostral intraparietal cortex (areas AIP and VIP) and the ventral premotor cortex (areas F5 and F4). *Exp.Brain Res.* **128**, 181-187.

Luppino, G. & Rizzolatti, G. (2000). The Organization of the Frontal Motor Cortex. *News Physiol Sci.* **15**, 219-224.

Maier, M. A., Armand, J., Kirkwood, P. A., Yang, H. W., Davis, J. N., & Lemon, R. N. (2002). Differences in the corticospinal projection from primary motor cortex and supplementary motor area to macaque upper limb motoneurons: an anatomical and electrophysiological study. *Cereb.Cortex* **12**, 281-296.

Maier, M. A. & Hepp-Reymond, M. C. (1995). EMG activation patterns during force production in precision grip. I. Contribution of 15 finger muscles to isometric force. *Exp.Brain Res.* **103**, 108-122.

Martin, R. F. & Bowden, D. M. (2000). *Primate Brain Maps: Structure of ther Macaque Brain* Elsevier, Amsterdam.

Mason, C. R., Gomez, J. E., & Ebner, T. J. (2001). Hand synergies during reach-to-grasp. *J.Neurophysiol* **86**. 2896-2910.

Mason, C. R., Gomez, J. E., & Ebner, T. J. (2002). Primary motor cortex neuronal discharge during reach-to-grasp: controlling the hand as a unit. *Arch.Ital.Biol.* **140**, 229-236.

Matelli, M., Camarda, R., Glickstein, M., & Rizzolatti, G. (1986). Afferent and efferent projections of the inferior area 6 in the macaque monkey. *J.Comp Neurol.* **251**, 281-298.

Matelli, M., Govoni, P., Galletti, C., Kutz, D. F., & Luppino, G. (1998). Superior area 6 afferents from the superior parietal lobule in the macaque monkey. *J.Comp Neurol.* **402**, 327-352.

Matelli, M., Luppino, G., Murata, A., & Sakata, H. Independent anatomical circuits for reaching and grasping linking inferior parietal lobule and inferior area 6 in the monkey. Soc. Neurosci. Abstr. 20[404.4]. 1994.

Matelli, M., Luppino, G., & Rizzolatti, G. (1985). Patterns of cytochrome oxidase activity in the frontal agranular cortex of the macaque monkey. *Behav.Brain Res.* **18**, 125-136.

Matelli, M., Luppino, G., & Rizzolatti, G. (1991). Architecture of superior and mesial area 6 and the adjacent cingulate cortex in the macaque monkey. *J.Comp Neurol.* **311**, 445-462.

Mehring, C., Rickert, J., Vaadia, E., Cardosa, d. O., Aertsen, A., & Rotter, S. (2003). Inference of hand movements from local field potentials in monkey motor cortex. *Nat.Neurosci.* **6**, 1253-1254.

Merriman, M. B., Mora, J. S., Beaumont, B. W., & Merrilees, M. J. (2001). Effects of varying 5-fluorouracil exposure duration on tenon's capsule fibroblasts. *Clin.Experiment.Ophthalmol.* **29**, 248-252.

Milner, A. D. & Goodale, M. A. (1995). *The Visual Brain in Action* Oxford University Press.

Mima, T., Steger, J., Schulman, A. E., Gerloff, C., & Hallett, M. (2000). Electroencephalographic measurement of motor cortex control of muscle activity in humans. *Clin.Neurophysiol.* **111**, 326-337.

Moll, L. & Kuypers, H. G. (1977). Premotor cortical ablations in monkeys: contralateral changes in visually guided reaching behavior. *Science* **198**, 317-319.

Mora, J. S., Nguyen, N., Iwach, A. G., Gaffney, M. M., Hetherington, J., Jr., Hoskins, H. D., Jr., Wong, P. C., Tran, H., & Dickens, C. J. (1996). Trabeculectomy with intraoperative sponge 5-fluorouracil. *Ophthalmology* **103**, 963-970.

Moran, S. L., Ryan, C. K., Orlando, G. S., Pratt, C. E., & Michalko, K. B. (2000). Effects of 5-fluorouracil on flexor tendon repair. *J.Hand Surg.[Am.]* **25**, 242-251.

Muir, R. B. & Lemon, R. N. (1983). Corticospinal neurons with a special role in precision grip. *Brain Res.* **261**, 312-316.

Murata, A., Fadiga, L., Fogassi, L., Gallese, V., Raos, V., & Rizzolatti, G. (1997). Object representation in the ventral premotor cortex (area F5) of the monkey. *J.Neurophysiol.* **78**, 2226-2230.

Murata, A., Gallese, V., Kaseda, M., & Sakata, H. (1996). Parietal neurons related to memory-guided hand manipulation. *J.Neurophysiol.* **75**, 2180-2186.

Murata, A., Gallese, V., Luppino, G., Kaseda, M., & Sakata, H. (2000). Selectivity for the shape, size, and orientation of objects for grasping in neurons of monkey parietal area AIP. *J.Neurophysiol.* **83**, 2580-2601.

Murray, E. A. & Coulter, J. D. (1981). Supplementary Sensory Area. In *Cortical Sensory Organization, Vol. 1: Multiple Somatic Areas*, ed. Woolsey, C. N., pp. 167-195. Humana, Clifton, NJ.

Murthy, V. N. & Fetz, E. E. (1992). Coherent 25- to 35-Hz oscillations in the sensorimotor cortex of awake behaving monkeys. *Proc.Natl.Acad.Sci.U.S.A* **89**, 5670-5674.

Murthy, V. N. & Fetz, E. E. (1996a). Oscillatory activity in sensorimotor cortex of awake monkeys: synchronization of local field potentials and relation to behavior. *J.Neurophysiol.* **76**, 3949-3967.

Murthy, V. N. & Fetz, E. E. (1996b). Synchronization of neurons during local field potential oscillations in sensorimotor cortex of awake monkeys. *J.Neurophysiol.* **76**, 3968-3982.

Mushiake, H., Inase, M., & Tanji, J. (1991). Neuronal activity in the primate premotor, supplementary, and precentral motor cortex during visually guided and internally determined sequential movements. *J.Neurophysiol.* **66**, 705-718.

Napier, J.R. (1956) The prehensile movements of the human hand. *J. Bone Joint Surg.* 38B: 902-913, 1956.

Nguyen, T. H. & Ho, D. Q. (2002). Nonmelanoma skin cancer. *Curr.Treat.Options.Oncol.* **3**, 193-203.

Occleston, N. L., Alexander, R. A., Mazure, A., Larkin, G., & Khaw, P. T. (1994). Effects of single exposures to antiproliferative agents on ocular fibroblast-mediated collagen contraction. *Invest Ophthalmol.Vis.Sci.* **35**, 3681-3690.

Olszewski, J. (1952). The Thalamus of the Macaca mulatta. In *An Atlas for Use with the Stereotaxic Instrument* S. Karger, Base, Switzerland.

Pandya, D. N. & Kuypers, H. G. (1969). Cortico-cortical connections in the rhesus monkey. *Brain Res.* **13**, 13-36.

Pandya, D. N. & Seltzer, B. (1982). Intrinsic connections and architectonics of posterior parietal cortex in the rhesus monkey. *J.Comp Neurol.* **204**, 196-210.

Passingham, R. E. (1982). *The Human Primate* Freeman, Oxford.

Pellerin, J. P. & Lamarre, Y. (1997). Local field potential oscillations in primate cerebellar cortex during voluntary movement. *J.Neurophysiol.* **78**, 3502-3507.

Penfield, W. & Rasmussen, T. (1952). *The cerebral cortex of man* Macmillan, New York.

Pesaran, B., Pezaris, J. S., Sahani, M., Mitra, P. P., & Andersen, R. A. (2002). Temporal structure in neuronal activity during working memory in macaque parietal cortex. *Nat.Neurosci.* **5**, 805-811.

Pfurtscheller, G., Stancak, A., Jr., & Neuper, C. (1996). Post-movement beta synchronization. A correlate of an idling motor area? *Electroencephalogr.Clin.Neurophysiol.* **98**, 281-293.

Pfurtscheller, G., Woertz, M., Muller, G., Wriessnegger, S., & Pfurtscheller, K. (2002). Contrasting behavior of beta event-related synchronization and somatosensory evoked potential after median nerve stimulation during finger manipulation in man. *Neurosci.Lett.* **323**, 113-116.

Porter, R. & Lemon, R. N. (1993). *Corticospinal Function and Voluntary Movement* Clarendon Press, Oxford.

Rizzolatti, G., Camarda, R., Fogassi, L., Gentilucci, M., Luppino, G., & Matelli, M. (1988). Functional organization of inferior area 6 in the macaque monkey. II. Area F5 and the control of distal movements. *Exp.Brain Res.* **71**, 491-507.

Rizzolatti, G. & Craighero, L. (2004). The mirror-neuron system. *Annu.Rev.Neurosci.* **27**, 169-192.

Rizzolatti, G. & Gentilucci, M. (1988). Motor and visual-motor functions of the premotor cortex. In *Neurobiology of Neocortex*, eds. Rakic, P. & Singer, W., pp. 269-284. Wiley, Chichester.

Rizzolatti, G., Luppino, G., & Matelli, M. (1996). The classic supplementary motor area is formed by two independent areas. *Adv.Neurol.* **70**, 45-56.

Rizzolatti, G., Luppino, G., & Matelli, M. (1998). The organization of the cortical motor system: new concepts. *Electroencephalogr.Clin.Neurophysiol.* **106**, 283-296.

Rosenberg, J. R., Amjad, A. M., Breeze, P., Brillinger, D. R., & Halliday, D. M. (1989). The Fourier approach to the identification of functional coupling between neuronal spike trains. *Prog.Biophys.Mol.Biol.* **53**, 1-31.

Roy,A.C., Paulignan,Y., Farne,A., Jouffrais,C. & Boussaoud, D. (2000) Hand kinematics during reaching and grasping in the macaque monkey. *Behav.Brain Res.***117**, 75-82.

Roy,A.C., Paulignan,Y., Meunier,M., & Boussaoud, D. (2002) Prehension movements in the macaque monkey: effects of object size and location. *J.Neurophysiol.* **88**, 1491-1499.

Sakata, H., Taira, M., Murata, A., & Mine, S. (1995). Neural mechanisms of visual guidance of hand action in the parietal cortex of the monkey. *Cereb.Cortex* **5**, 429-438.

Salenius, S., Portin, K., Kajola, M., Salmelin, R., & Hari, R. (1997a). Cortical control of human motoneuron firing during isometric contraction. *J.Neurophysiol.* **77**, 3401-3405.

Salenius, S., Schnitzler, A., Salmelin, R., Jousmaki, V., & Hari, R. (1997b). Modulation of human cortical rolandic rhythms during natural sensorimotor tasks. *Neuroimage.* **5**, 221-228.

Salmelin, R. & Hari, R. (1994). Spatiotemporal characteristics of sensorimotor neuromagnetic rhythms related to thumb movement. *Neuroscience* **60**, 537-550.

Sanes, J. N. & Donoghue, J. P. (1993). Oscillations in local field potentials of the primate motor cortex during voluntary movement. *Proc.Natl.Acad.Sci.U.S.A* **90**, 4470-4474.

Santello, M., Flanders, M., & Soechting, J.F. (1998). Postural hand synergies for tool use. *J.Neurosci.* **18,** 10105-10115.

Santello, M. & Soechting, J.F. (1998). Gradual molding of the hand to object contours. *J.Neurophysiol.* **79,** 1307-1320.

Scherberger, H., Buneo, C. A., Jarvis, M. R., & Andersen, R. A. Local Field Potential Tuning in the Macaque Posterior Parietal Cortex during Arm-Reaching Movements. Soc. Neurosci. Abstr.[279.16]. 2003. Washington, DC.

Schieber, M. H. (2001). Constraints on somatotopic organization in the primary motor cortex. *J.Neurophysiol.* **86,** 2125-2143.

Schmidt, E. M. (1980). Single neuron recording from motor cortex as a possible source of signals for control of external devices. *Ann.Biomed.Eng* **8,** 339-349.

Scott, S. H. & Kalaska, J. F. (1997). Reaching movements with similar hand paths but different arm orientations. I. Activity of individual cells in motor cortex. *J.Neurophysiol.* **77,** 826-852.

Seltzer, B. & Pandya, D. N. (1986). Posterior parietal projections to the intraparietal sulcus of the rhesus monkey. *Exp.Brain Res.* **62,** 459-469.

Serruya,M.D., Hatsopoulos,N.G., Paninski,L., Fellows,M.R., & Donoghue,J.P. (2002) Instant neural control of a movement signal. *Nature* **416(6877),** 141-142.

Shima, K. & Tanji, J. (2000). Neuronal activity in the supplementary and presupplementary motor areas for temporal organization of multiple movements. *J.Neurophysiol.* **84,** 2148-2160.

Shimazu, H., Maier, M. A., Cerri, G., Kirkwood, P. A., & Lemon, R. N. (2004). Macaque ventral premotor cortex exerts powerful facilitation of motor cortex outputs to upper limb motoneurons. *J.Neurosci.* **24,** 1200-1211.

Shinoda, Y., Yokota, J., & Futami, T. (1981). Divergent projection of individual corticospinal axons to motoneurons of multiple muscles in the monkey. *Neurosci.Lett.* **23,** 7-12.

Smith, A. M., Hepp-Reymond, M. C., & Wyss, U. R. (1975). Relation of activity in precentral cortical neurons to force and rate of force change during isometric contractions of finger muscles. *Exp.Brain Res.* **23**, 315-332.

Smith, M. F., Sherwood, M. B., Doyle, J. W., & Khaw, P. T. (1992). Results of intraoperative 5-fluorouracil supplementation on trabeculectomy for open-angle glaucoma. *Am.J.Ophthalmol.* **114**, 737-741.

Snider, R. S. & Lee, J. C. (1961). *A Stereotaxic Atlas of the Monkey Brain (Macaca mulatta).* University of Chicago Press, Chicago.

Snyder, L. H., Batista, A. P., & Andersen, R. A. (1997). Coding of intention in the posterior parietal cortex. *Nature* **386**, 167-170.

Spinks, R. L., Baker, S. N., Jackson, A., Khaw, P. T., & Lemon, R. N. (2003). Problem of dural scarring in recording from awake, behaving monkeys: a solution using 5-fluorouracil. *J.Neurophysiol.* **90**, 1324-1332.

Stancak, A., Jr., Riml, A., & Pfurtscheller, G. (1997). The effects of external load on movement-related changes of the sensorimotor EEG rhythms. *Electroencephalogr.Clin.Neurophysiol.* **102**, 495-504.

Stoney, S. D., Jr., Thompson, W. D., & Asanuma, H. (1968). Excitation of pyramidal tract cells by intracortical microstimulation: effective extent of stimulating current. *J.Neurophysiol.* **31**, 659-669.

Szarowski, D. H., Andersen, M. D., Retterer, S., Spence, A. J., Isaacson, M., Craighead, H. G., Turner, J. N., & Shain, W. (2003). Brain responses to micro-machined silicon devices. *Brain Res.* **983**, 23-35.

Taira, M., Mine, S., Georgopoulos, A. P., Murata, A., & Sakata, H. (1990). Parietal cortex neurons of the monkey related to the visual guidance of hand movement. *Exp.Brain Res.* **83**, 29-36.

Tanji, J. & Shima, K. (1994). Role for supplementary motor area cells in planning several movements ahead. *Nature* **371**, 413-416.

Tanji, J. & Shima, K. (1996). Supplementary motor cortex in organization of movement. *Eur.Neurol.* **36 Suppl 1**, 13-19.

Tanner, K. E., Doyle, C., & Bonfield, W. (1990). The Strength of the Interface Developed between Biomaterials and Bone. In *Clinical Implant Materials*, eds. Heimke, G., Soltesz, U., & Lee, A. J. C., pp. 149-154. Elsevier.

Taylor, D. M., Tillery, S. I., & Schwartz, A. B. (2002). Direct cortical control of 3D neuroprosthetic devices. *Science* **296**, 1829-1832.

Todorov, E. (2000). Direct cortical control of muscle activation in voluntary arm movements: a model. *Nat.Neurosci.* **3**, 391-398.

Umilta, M. A., Brochier, T., Spinks, R. L., & Lemon, R. N. Grip specification in primary motor cortex and premotor area F5 of the macaque monkey: Results from simultaneous multiple recordings in both areas. Society for Neuroscience [918.7]. 2003.

Umilta, M. A., Kohler, E., Gallese, V., Fogassi, L., Fadiga, L., Keysers, C., & Rizzolatti, G. (2001). I know what you are doing. a neurophysiological study. *Neuron* **31**, 155-165.

Ungerleider, L. G. & Mishkin, M. (1982). Two Cortical Visual Systems. In *Analysis of Visual Behavior*, eds. Ingle, D. J., Goodale, M. A., Mantel, G. W., & Mansfield, R. J. W., pp. 549-586. MIT Press, Cambridge, MA.

Wannier, T. M., Maier, M. A., & Hepp-Reymond, M. C. (1989). Responses of motor cortex neurons to visual stimulation in the alert monkey. *Neurosci.Lett.* **98**, 63-68.

Wilkins, M. R., Occleston, N. L., Kotecha, A., Waters, L., & Khaw, P. T. (2000). Sponge delivery variables and tissue levels of 5-fluorouracil. *Br.J.Ophthalmol.* **84**, 92-97.

Williamson, S. J. & Kaufman, L. (1981). Biomagnetism. *J Magn Magn Mat* **22**, 129-201.

Wolff, H. G. (1963). *Headache and Other Head Pain* Oxford University Press, New York.

Wolpaw, J. R., Birbaumer, N., McFarland, D. J., Pfurtscheller, G., & Vaughan, T. M. (2002). Brain-computer interfaces for communication and control. *Clin.Neurophysiol.* **113**, 767-791.

Wolpert, D. M., Ghahramani, Z., & Jordan, M. I. (1995). An internal model for sensorimotor integration. *Science* **269**, 1880-1882.

Wrobel, A., Bekisz, M., Kublik, E., & Waleszczyk, W. (1994). 20 Hz bursting beta activity in the cortico-thalamic system of visually attending cats. *Acta Neurobiol.Exp.(Wars.)* **54**, 95-107.